Table des matières

Liste des tableaux

Liste des figures

Liste des symboles

Symboles		Unité
E	Champ électrique	V/m
H	Champ magnétique	A/m
f_r	Fréquence de résonance	GHz
Δf	Décalage fréquentiel	GHz
H ou RH%	Pourcentage d'humidité relative	%
P	Pression de Gaz	mmHg ou Psi
P_s	Pression de saturation	
S	Sensibilité	KHz/%RH
T	Température	K ou °C
ε_r	Permittivité relative	
$\varepsilon_r(H)$	Permittivité relative en fonction de l'humidité	

Chapitre 1 - Introduction

Les capteurs environnementaux sont des éléments essentiels pour mesurer des grandeurs physiques variées. Récemment, le besoin de capteurs pour le contrôle de la qualité de l'air (gaz, humidité, poussière ...) dans les maisons et la sécurité dans les véhicules modernes a suscité beaucoup d'intérêt [1-4]. Il existe aussi différentes applications industrielles et résidentielles dans lesquelles il est essentiel de détecter des gaz tels que COx, SOx, NOx ou des gaz à effet de Serre tels que CO2, CH4, N2O etc. La disponibilité des capteurs performants, fiables et à faibles coûts est essentielle pour faciliter l'évolution de ces applications à grande échelle et en toute sécurité [5]. Actuellement, il existe un écart important entre les spécifications requises des technologies de capteurs et les produits disponibles sur le marché [6].

En conséquence, de nouveaux travaux s'orientent vers l'utilisation de technologies RF pour la réalisation de capteurs innovants. Par exemple, la détection de gaz est possible en utilisant des lignes de transmission micro-ondes [7-9]. Dans ces dispositifs, la variation de la permittivité du diélectrique sous l'application d'un signal micro-ondes et en présence d'un gaz est utilisée comme transducteur micro-ondes. D'autres structures micro-ondes ont été utilisées pour la détection de gaz tels que des guides d'ondes, des circuits imprimés LC (inductance-capacité) et des filtres à base de résonateurs diélectriques [20, 21]. Des matériaux sensibles dont leurs propriétés diélectriques varient avec la composition de

l'atmosphère gazeuse sont disponibles pour différents gaz [22-24]. Par exemple, la réponse diélectrique des nanotubes de carbone a été utilisée pour indiquer la présence de gaz à l'aide d'un résonateur micro-ondes inductif-capacitif [10]. Cette réponse affecte le spectre du dispositif qui peut être suivi afin d'identifier les concentrations des espèces à détecter. Récemment, une nouvelle génération de dispositifs électromagnétiques basée sur la technologie substrat intégré SIW (substrate integrated waveguide) a été présentée [10-13]. Cette technologie a rendu possible la réalisation de structures tridimensionnelles non-planaires à l'aide d'un substrat diélectrique planaire, ce qui facilite leur intégration avec d'autres composants ou dispositifs planaires [11, 14-17]. Par ailleurs, les composants à substrat intégré ont montré un excellent facteur de qualité qui pourrait être utilisable pour la réalisation de capteurs.

Ce projet de recherche s'intègre dans le domaine de la conception et de la réalisation d'une nouvelle solution applicable à la détection environnementale. Il présente une façon originale de produire des capteurs de gaz basés sur un composant micro-ondes SIW. Tout d'abord, les objectifs scientifiques et l'originalité du sujet seront présentés, suivis par des résultats de modélisation, de simulation et des mesures. Le document détaille la méthodologie de recherche ainsi que les étapes requises pour l'intégration des éléments du capteur proposé. Les différentes contributions scientifiques apportées ainsi que les contributions envisagées terminent ce rapport.

Dans ce travail une architecture de capteur pour le domaine de détection de gaz est proposée. L'objectif de ce travail est de fournir une solution de fabrication PCB et

d'intégration basée sur la fonctionnalisation d'un résonateur SIW pour favoriser la détection environnementale.

La solution présentée est compatible avec la technologie RF (active et passive) y compris l'identification, cela facilite son intégration aux réseaux de détection sans fil. D'autres solutions filaires sont également envisageables avec cette technologie de capteur SIW proposée.

Voici les points innovants apportés par le capteur intégré au substrat :

- Fabrication à l'aide de technologies matures
- Intégration simplifiée dans un système de monitoring filaire et/ou sans fil
- Principe de détection innovant basé sur les propriétés électromagnétiques des matériaux diélectriques intégrés dans la structure du capteur
- Sensibilité accrue (facteur de qualité élevé)
- Possibilité de capteurs différents sur une même fabrication
- Possibilité d'opération sans fil avec adressage pour les applications en milieux hostiles
- Fabrication monolithique avec la réalisation du circuit de monitoring, n'exige pas d'empaquetage et d'assemblage additionnel

Les nouvelles structures de détection basées sur des cavités SIW résonantes opèrent aux fréquences 3.6 et 4.15 GHz. La structure du capteur est réalisée en introduisant des

trous dans une région à l'intérieur du résonateur SIW et la fonctionnaliser avec un matériau diélectrique sensible au gaz. En présence d'une variation environnementale (gaz, l'humidité, etc...), la permittivité de la région fonctionnalisée change ce qui provoque un décalage fréquentiel dans le spectre de fréquence de résonance du résonateur micro-ondes. Ce changement de fréquence peut être détecté et utilisé comme principe de détection du capteur. Le décalage fréquentiel a été estimé en utilisant la méthode analytique de perturbation diélectrique. Les prototypes ont été testés au laboratoire dans une chambre d'essai à environnement contrôlé pour la détection de l'hydrogène et de l'humidité.

La mise en œuvre d'un nouveau capteur exige un progrès technologique et une méthodologie de l'exploitation des connaissances dans des domaines tels que les matériaux et les dispositifs micro-ondes. Figure 1-1 représente la vision générale de conception du capteur micro-ondes.

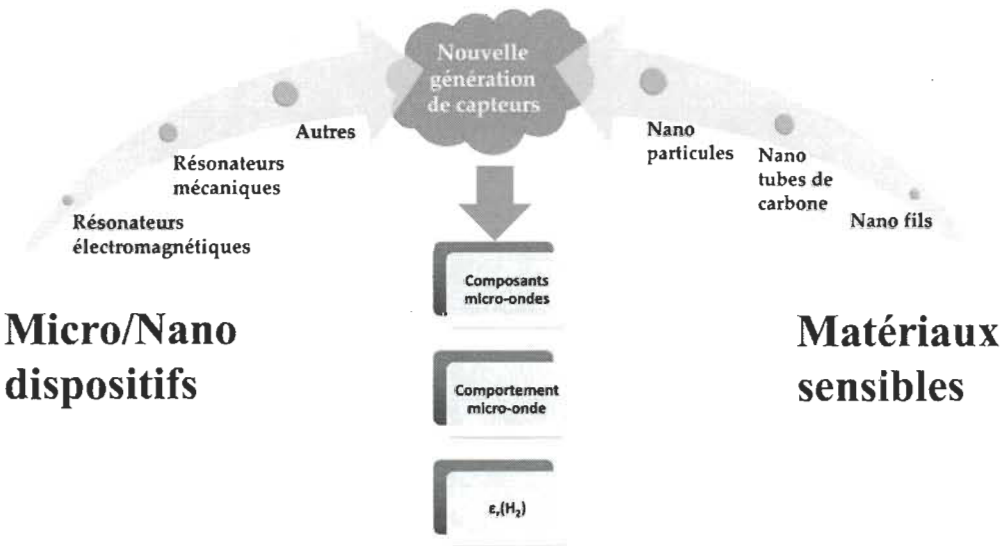

Figure 1-1 La vision générale de conception du capteur micro-ondes.

Ensuite, une vérification de la viabilité de ce nouveau capteur sera effectuée en utilisant des outils de simulation 3D, puis la fabrication de ce nouveau dispositif sera effectuée par des équipements de prototypges. Enfin, les prototypes réalisés seront caractérisés afin de les valider expérimentalement. Une caractérisation micro-ondes sera effectuée pour vérifier ses performances en détection de gaz et en communication sans fil en forme de tag RFID.

La technologie de fabrication de capteurs intégrés au substrat est bien établie avec des coûts inférieurs à ceux des technologies de fabrication de capteurs commerciaux. Une estimation du coût de production des capteurs de gaz basée sur la technologie a été effectuée. À ce stade, deux solutions limites ont été considérées afin de définir une plage réaliste de prix (Figure.1-2). Ce prix serait applicable après la maturation de la technologie pour des volumes relativement faibles. Le coût anticipé de production de la solution proposée est réduite puisque l'empaquetage et l'assemblage hybride sont éliminés comparativement aux technologies de détection courantes.

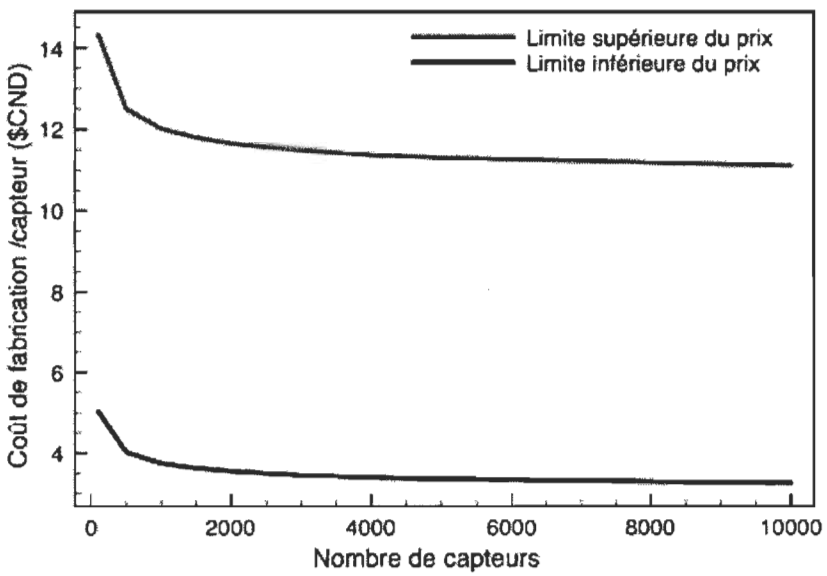

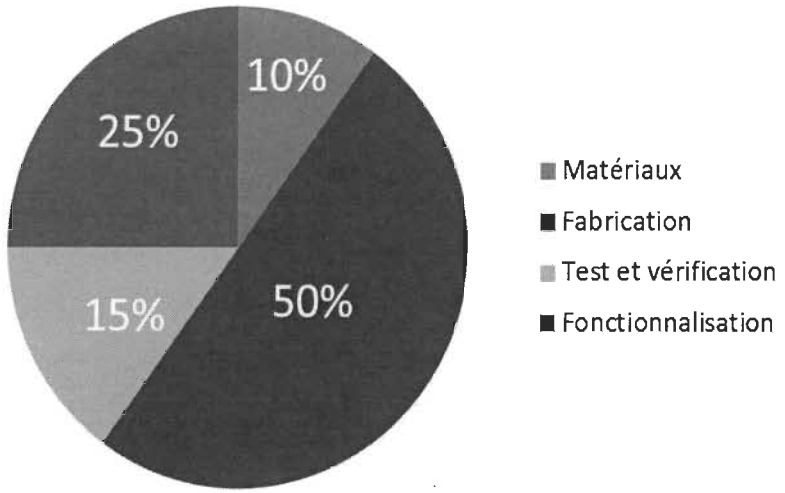

Figure 1-2 Estimation du coût par capteur en fonction du volume de production et répartition du coût de production estimée pour les capteurs.

Cette première évaluation inclut les matériaux, la fabrication, le test, la validation et la fonctionnalisation. Le coût de la fabrication et des matériaux est basé sur des fournisseurs canadiens habituels. Évidemment, une optimisation des coûts reste possible, mais la répartition finale du coût (Fig.1-2) suit les tendances publiées pour les technologies de production exploitées.

Cette thèse, sous forme d'article, présente plusieurs contributions. En premier lieu une revue bibliographique des capteurs et une mise en contexte a été faite (**voir contributionI**), cela détermine les technologies actuelles, le choix de matériaux et la géométrie du composant (SIW). Les problématiques sont présentées à travers une étude expérimentale sur les éléments de détection micro-machinés commerciaux et une comparaison des résultats aux systèmes de détection traditionnels (**voir contribution II**). La première implémentation est présentée en forme des tags RFID micro-ondes basés sur des

résonateurs SIW où chaque résonateur est connecté à une antenne (**voir contribution III**). Les données sont codées par l'introduction d'un nombre variable de trous d'air à l'intérieur de la cavité; ce qui donne une signature unique et identifiable au niveau de la fréquence spectrale. Ensuite, le résonateur SIW est présenté comme un capteur d'humidité. Dans ce travail une vérification de la viabilité sera mise en place par des outils de simulation ainsi que le développement d'un modèle analytique basé sur la méthode de perturbation de cavité résonante pour la région fonctionnalisée de résonateur. Ce modèle permet d'étudier l'effet de la taille de la région fonctionnalisée sur la sensibilité (**voir contribution IV et contribution V**). Enfin, les prototypes des tags réalisés seront caractérisés afin de les valider expérimentalement. Une caractérisation micro-ondes sera effectuée ainsi que sa performance en détection. Les tests expérimentaux ont été effectués sur les prototypes fabriqués pour deux cas : l'humidité et l'hydrogène. Puis une comparaison des résultats entre le modèle analytique et la simulation du dispositif a été réalisée. La thèse a mis en place un canal de communication sans fil pour les tags RFID micro-ondes. Ce canal permet de étudier la communication avec les capteurs SIW. Le canal de communication est modélisé en utilisant un modèle de matrice à deux ports du résonateur et les représentations mathématiques d'antennes. Les tags sont fabriqués et testés expérimentalement et des paramètres tels que la distance entre les tags et le lecteur et l'antenne du lecteur ont été étudiées et leurs effets sur l'interrogatoire ont été comparés au modèle **(voir contribution VI)**.

Chapitre 2 - Mise en contexte du projet

L'importance des capteurs de gaz touche plusieurs domaines comme l'environnement, la santé, l'alimentation et les secteurs résidentiels et industriels. Le marché des capteurs est en pleine croissance due aux demandes des applications actuelles ainsi que des applications émergeantes. Cette croissance est poussée par l'exigence de certaines industries qui requière de meilleures performances de sensibilité, de temps de réponse et aussi accéder aux progrès technologiques dans le domaine des micro-nano/dispositifs et l'avancement de matériaux sensibles. La Figure 2-1 montre l'évolution du marché des capteurs.

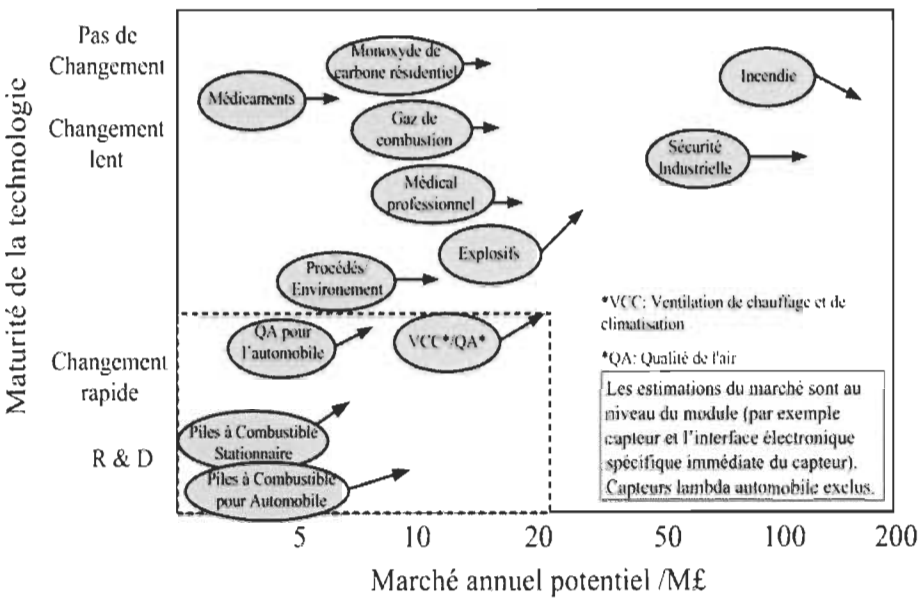

Figure 2-1 L'évolution du marché des capteurs pour plusieurs secteurs.

La majorité des capteurs de gaz commerciaux (catalytique, thermique, oxyde métalliques semi-conducteurs, et optique) souffrent de deux inconvénients majeurs, la

consommation énergétique élevée et ils reposent sur des processus de fabrication dispendieux. La limitation de leur autonomie énergétique est due aux types de transducteurs utilisés pour convertir le pourcentage de gaz en signal électrique qui nécessite une alimentation électrique. Par exemple, dans le cas des capteurs à oxyde métalliques semi-conducteurs, des capteurs catalytiques et des capteurs à conductivité thermique, il faut y ajouter un élément chauffant qui consomme de l'énergie pour faciliter l'absorption et la désorption du gaz (**voir contribution I**). Par ailleurs, l'intégration des capteurs commerciaux dans un réseau de capteurs sans fil avec la technologie RFID augmente la consommation énergétique et la complexité du système ainsi que le coût. Le réseau de capteurs sans fils contient un grand nombre de nœuds qui sont des capteurs capables de récolter, analyser et de transmettre des données environnementales d'une manière autonome. Pour transformer les capteurs de gaz commerciaux en nœud il faut attacher une unité (transmetteur - récepteur) à chaque capteur dans le réseau ceci peut être considérablement couteux en terme de matériels.

La complexité du processus de fabrication des capteurs est due au fait que la technologie de fabrication de l'élément sensible pour les capteurs de gaz n'est pas compatible avec la technologie (Si) utilisée pour la micro-fabrication de circuits intégrés. Récemment des éléments sensibles réalisés à l'aide des techniques de micro-fabrication ont été proposés. Ces capteurs ont été analysés et testés et les résultats ont été publiés dans une revue (**voir contribution II**).

En résumé, les performances attendues pour la solution proposée dans cette thèse sont répertoriées dans le tableau 2-1 où les performances d'exemples de capteurs commerciaux sont également présentées.

Tableau 2-1 Les performances de capteurs commerciaux et les performances ciblées par la technologie SIW.

Paramètres	**Capteurs commerciaux**		**Performances ciblées de la technologie SIW proposée**
Plage de mesure	Siemens (MOX)	0-2000 ppm	10 ppm
	SAW+polymère	<500 ppm	
	MOX	< 50 ppm	
	NDIR	0-5000 ppm	
Coûts	NDIR	100- 1000$	50 $
	Autres	200- 500$	
Consommation	NDIR	439 mW	1 mW
	Autres	150 mW	
Temps de réponse	NDIR	40 - 200 s	< 4 s

Un type de dispositif électromagnétique identifié comme un composant intégré au substrat (SIW) a été présenté et caractérisé [1,2]. Les composants SIW ont rendu possible la fabrication des structures non planaires tridimensionnelles sur un substrat diélectrique planaire ce qui facilite leur intégration avec d'autres composants ou dispositifs planaires [2]. Par ailleurs, les composants intégrés au substrat présentent de meilleurs facteurs de qualité et des faibles pertes que d'autres composants planaires. Les composants SIW sont

fabriqués en introduisant des trous métallisés ou par alternance de différentes couches de diélectrique. De plus, les structures intégrées au substrat ont été proposées sur des substrats flexibles tels que les papiers ou plastiques (PET) par l'impression jet d'encre.

Plusieurs dispositifs micro-ondes intégrés au substrat ont été conçus pour les applications de télécommunications. Par exemple, des guides d'ondes intégrés et des filtres à base de guide d'ondes intégrés ont été réalisés [3,4] avec de faibles pertes. Des antennes intégrées ont été fabriquées au complet sur un seul substrat [5,6] grâce à cette technique. Des circuits oscillateurs ont été construits avec des résonateurs intégrés au substrat [6]. Ces types d'oscillateurs présentent une meilleure résistance contre le bruit de phase dû au facteur de qualité élevé des résonateurs intégrés.

Malgré les avancements de cette technique d'intégration, les capteurs intégrés au substrat n'ont jamais été utilisés pour les applications de détections environnementales comme la surveillance la qualité de l'air. Selon une recherche effectuée à travers les bases de brevets, l'idée de concevoir un capteur intégré au substrat (SIW) n'a pas été brevetée. Cependant, il y a des brevets pour d'autres dispositifs intégrés au substrat conçus pour le domaine de télécommunications. Ceux-ci ne sont pas destinés au domaine de détection. Par exemple :

- Guide d'onde intégrée au substrat (Office européen des brevets) (CN101834339 (A))

- Guide multi mode intégré au substrat (Office européen des brevets) (CN101667682 (A))

Pour cela, une demande de brevet a été déposée («Microwave resonator sensor and associated methods of sensing», (Ref: 05015656-85USPR))pour protéger et valoriser le travail présenté dans cette thèse. Étant donné que cette technique est compatible avec la technologie RF, les capteurs intégrés au substrat pourraient être intégrés dans les réseaux de détection sans fil ainsi que la détection filaire. Une solution proposée dans cette thèse basée sur la technologie SIW en utilisant la transduction micro-ondes [18, 19].

Chapitre 3 - Modélisation des capteurs intégrés au substrat

3.1 Théorie des composants SIW

Les guides d'ondes intégrés au substrat sont des guides d'ondes rectangulaires formés par deux conducteurs plats séparés d'un substrat diélectrique. La géométrie du guide est déterminée par des parois conductrices verticales, construites par des trous métallisés appelés vias. La structure SIW est conçue en choisissant la période spatiale et le diamètre de vias prévus pour guider la propagation des ondes avec un minimum de pertes par rayonnement. L'espacement entre les vias contrôle la quantité de fuites électromagnétiques du guide d'ondes. La largeur du guide d'ondes est déterminée par la fréquence de coupure désirée (résonance du mode dominant). La Figure 3-1 présente les paramètres géométriques influants comme le diamètre (D) des vias, l'espacement entre les vias (b), la largeur (W_{eff}) et la longueur du guide d'ondes (L_{eff}).

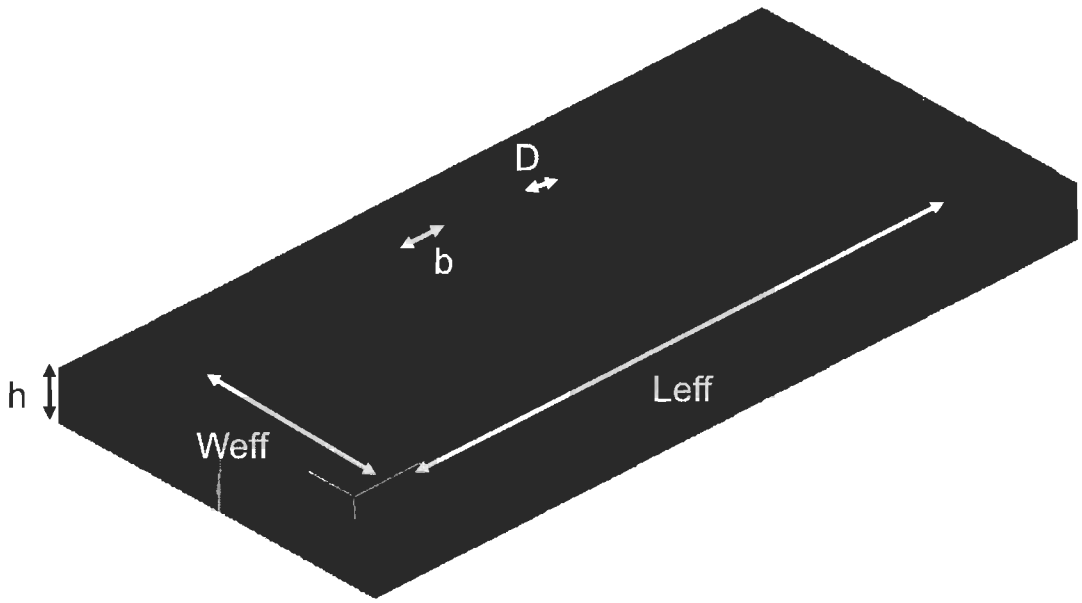

Figure 3-1 La structure générale d'un guide d'ondes intégré au substrat.

Un résonateur intégré au substrat peut être construit à partir du guide d'ondes présenté à la Figure 3-1 en fixant des conditions limites favorisant la résonnance. Figure 3-2 illustre la structure d'un résonateur intégré au substrat.

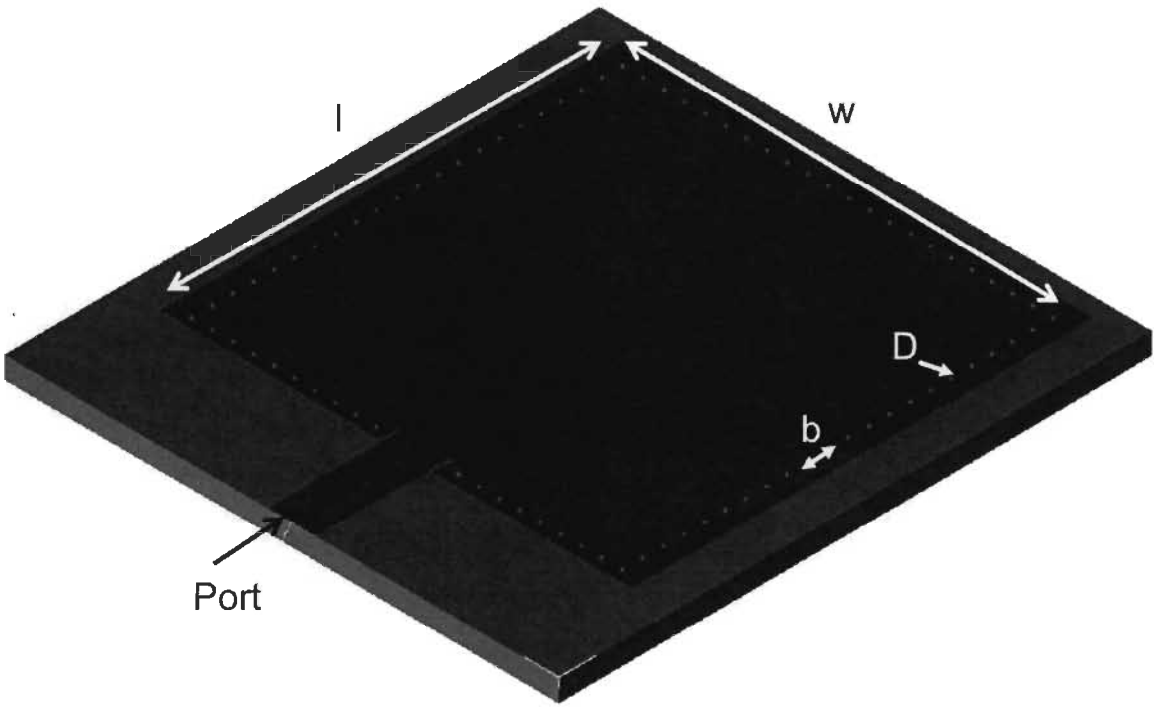

Figure 3-2 La structure générale d'un résonateur intégré au substrat.

Le rapport entre ces paramètres géométriques (dimensions du résonateur) et la fréquence de résonance du résonateur SIW est défini par :

$$f_r = \frac{c}{2\sqrt{\varepsilon_r}}\sqrt{\left(\frac{n}{w}\right)^2 + \left(\frac{m}{l}\right)^2} \qquad (1)$$

où c est la vitesse de l'onde électromagnétique dans le vide, n et m sont l'indice du mode de résonance, ε_r est la permittivité relative du substrat, w et l sont respectivement la largeur et la longueur effective du résonateur, qui sont déterminées par le placement des vias

d'interconnexion. Les dimensions l et w sont déterminées par le diamètre et la période de vias en utilisant l'équation

$$w = w_i - \frac{D^2}{0.95b} \tag{2}$$

où D est le diamètre des trous, b est l'espacement entre les vias et w_i est la largeur du guide d'onde [35, 36].

3.2 Les matériaux sensibles et la fonctionnalisation d'un SIW

Pour réaliser un capteur, le dispositif SIW présenté en Figure 3-2 doit être fonctionnalisé de manière à lui permettre de changer son comportement (fréquence de résonance) en présence d'une grandeur physique à détecter. Pour ce faire, des régions vides sont introduites à l'intérieur de la cavité résonante SIW. Ces régions sont ensuite remplies d'un matériau diélectrique sensible à la présence de gaz. La figure 3-3 présente le résonateur intégré proposé avec la région fonctionnalisée.

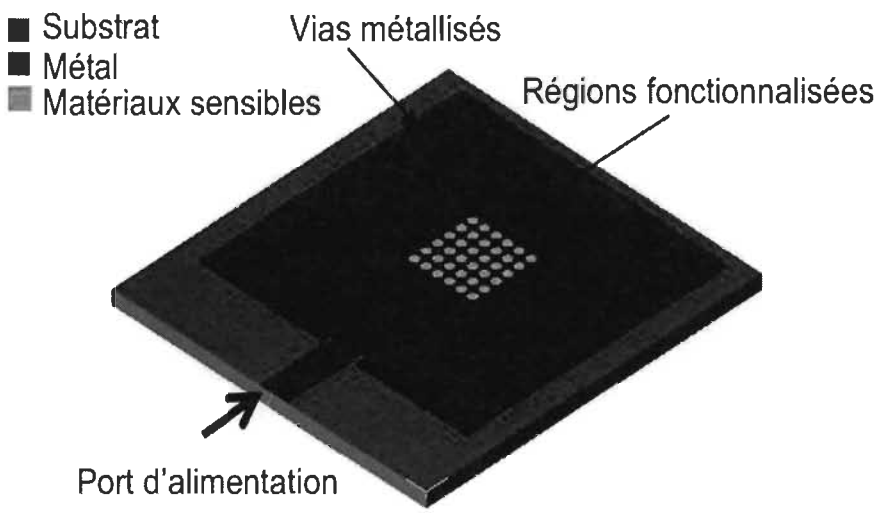

Figure 3-3 Le capteur intégré au substrat à base d'un résonateur SIW.

Les matériaux diélectriques potentiels pour la détection de gaz sont énumérés dans le tableau 3-1

Tableau 3-1 Matériaux de détection de gaz pour les capteurs proposés

Gaz à détecter	Matériaux diélectriques sensibles au gaz
H_2	SnO_2 , Fe_2O_3
O_2	TiO_2
O_3	In_2O_3 , ZnO
Formaldéhyde	Structure Pérovskite oxyde: $La_{1-x}Sr_xFeO_3$ (x = 0, 0.2, 0.5); polymère conducteurs PPy/EBSA
CO	WO_3, In_2O_3, MoO_3, V_2O_5 ,Ga_2O_3 ,TiO_2

Le tableau 3-2 liste les matériaux diélectriques sensibles à d'autres grandeurs physiques comme la température et l'humidité.

Tableau 3-2 Matériaux des autres grandeurs physiques

Gaz à détecter	Matériaux diélectriques sensibles au gaz
Humidité	Polymère Kapton 500HN

Les polymères fonctionnalisés peuvent être utilisés pour faciliter l'intégration des matériaux sensibles dans le capteur SIW en utilisant des procédés de fabrication de circuits imprimés (PCB) industriels (**voir contribution V**).

3.3 Modèle analytique du résonateur fonctionnalisé

Fonctionnaliser une cavité résonante SIW avec un diélectrique sensible implique une modification du substrat d'origine par un autre matériau diélectrique, ce qui perturbe la fréquence de résonance et le facteur de qualité composant. Pour analyser les modifications apportées par l'introduction d'un diélectrique externe, la méthode de perturbation d'une cavité résonante peut être utilisée pour estimer le décalage de fréquence. Une relation entre la taille de la région fonctionnalisée et le décalage de fréquentielle peut être mise en place analytiquement. Figure 3-4 montre un résonateur de SIW avec une région fonctionnalisée et les paramètres géométriques (**voir contribution IV**).

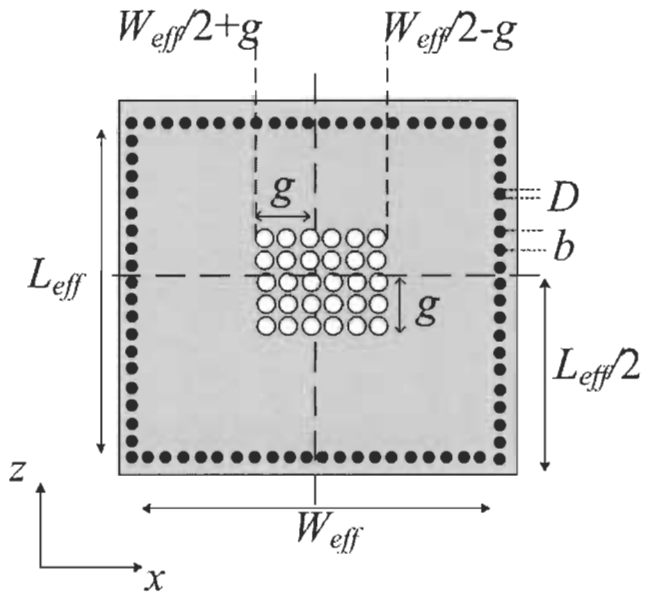

Figure 3-4 Les paramètres géométriques pour le capteur SIW.

La fréquence de résonance d'un résonateur non perturbé est donnée par

$$f_r = \frac{c}{2\sqrt{\varepsilon_r}}\sqrt{\left(\frac{m}{W_{eff}}\right)^2+\left(\frac{n}{L_{eff}}\right)^2} \tag{3}$$

où

$$L_{eff} = L - \frac{D^2}{0.95b}, W_{eff} = W - \frac{D^2}{0.95b} \tag{4}$$

Les conditions D <λ_g / 5 et b < 2D pour les vias métallisés où λ_g est la longueur d'ondes guidée assurent que la perte de rayonnement est maintenue à un niveau négligeable.

Dans ce cas, le résonateur intégré au substrat peut être modélisé en utilisant le guide d'ondes rectangulaire classique où les équations de conception et le cadre théorique du guide rectangulaire sont applicables. Pour cette raison, la variation relative de la fréquence de résonance due à une perturbation diélectrique $\Delta\varepsilon$ est donnée par

$$\frac{\omega - \omega_r}{\omega_r} \approx \frac{-\int_{V_0} \Delta\varepsilon \left|\vec{E}_0\right|^2 dV}{\int_{V_0} \left(\varepsilon \left|\vec{E}_0\right|^2 + \mu \left|\vec{H}_0\right|^2\right) dV} \tag{5}$$

E_0 et H_0 sont les champs électrique et magnétique non perturbés à l'intérieur du résonateur. Il est important de noter que la perturbation ne s'applique qu'à la constante diélectrique car il n'y a pas de perturbation due au matériau magnétique, par conséquent, $\Delta\mu = 0$. Pour le mode TE101 le champ électrique à l'intérieur du résonateur est donné par[1]

$$E_y = A \sin\frac{\pi x}{L} \sin\frac{\pi z}{W} \tag{6}$$

En utilisant la géométrie présentée dans la figure 3-4, les intégrales dans le numérateur et dénominateur peuvent être résolues donnant l'expression suivante :

---

[1] D. M. Pozar, "Microwave Engineering". John Wiley & Sons, Inc.

$$\frac{-\int_{V_0}\Delta\varepsilon\left|\vec{E}_0\right|^2 dV}{\int_{V_0}\left(\varepsilon\left|\vec{E}_0\right|^2+\mu\left|\vec{H}_0\right|^2\right)dV}=\frac{-\int_0^{\delta}\int_0^{h}\int_0^{\delta}\left(\Delta\varepsilon E^2{}_y\right)dzdydx}{-2\int_0^{L}\int_0^{h}\int_0^{W}\left(\varepsilon E^2{}_y\right)dzdydx}=-\frac{\Delta\varepsilon\left(2\pi\delta+L\sin\frac{2\pi\delta}{L}\right)\left(2\pi\delta+W\sin\frac{2\pi\delta}{W}\right)}{8WL\pi^2\varepsilon} \tag{7}$$

Dans le cas où $W = L$ la fraction de changement de la fréquence de résonance peut prendre la forme

$$\frac{\omega-\omega_r}{\omega_r}\approx-\frac{\Delta\varepsilon\left(2\pi g+W\sin\frac{2\pi g}{W}\right)^2}{8W^2\pi^2\varepsilon} \tag{8}$$

Augmenter la distance g c'est à dire augmenter la région fonctionnalisée à l'intérieur du résonateur SIW aura une influence sur la sensibilité. L'équation (8) donne une estimation du décalage de fréquence dû à la variation de la constante diélectrique Δε. La variation Δε est la différence entre la permittivité du substrat et la permittivité de la région fonctionnalisée. Étant donné que la région fonctionnalisée est un mélange entre le diélectrique de substrat et diélectrique sensible, il est préférable d'utiliser une permittivité effective ε_{eff} de la région. Il y a différentes théories pour les milieux composites qui contiennent plus d'un diélectrique. Elles sont utilisées pour la modélisation des propriétés électromagnétiques des matériaux composites. L'un d'eux est le modèle de Maxwell Garnett, qui est simple et commode pour la modélisation en raison de sa linéarité. Le modèle est valide Maxwell Garnett (**voir contribution IV**) qui est simple et commode pour la modélisation en raison de sa linéarité. Dans ce cas, $\Delta\varepsilon = \varepsilon_{eff} - \varepsilon_r$ où ε_{eff} est donné par Maxwell-Garnett (MG) règle des mélanges de diélectriques (**voir contribution IV**)

$$\varepsilon_{eff}=\varepsilon_r+3f\varepsilon_r\frac{\varepsilon_{mat}-\varepsilon_r}{\varepsilon_{mat}+2\varepsilon_r-f(\varepsilon_{mat}-\varepsilon_r)} \tag{9}$$

La permittivité ε_{mat} est la permittivité du matériau dans les trous, f est la fraction volumique de ε_{mat} en ε_r.

3.4 Conception d'un tag SIW et d'une chaîne de communication

Dans le cas de capteur sans-fil une plateforme d'interrogation avec les capteurs intégrés est utilisée. Les capteurs SIW doivent dans ce cas-ci avoir une adresse pour l'identifier dans un réseau sans-fil. L'interrogateur est responsable d'analyser les données qui viennent de chaque capteur dans le réseau sans-fil.

La structure du résonateur SIW présentée dans la section d'avant peut servir comme une structure RFID pour l'identification micro-ondes. En changeant le nombre de trous dans la région fonctionnalisée, la permittivité effective change ce qui entraine un décalage fréquentiel donné par

$$\frac{\partial f_r}{\partial \varepsilon_{eff}} \propto \frac{-1}{\varepsilon_{eff}^{3/2}} \tag{9}$$

Ce décalage donne une signature différente dans la bande spectrale allouée à l'opération du résonateur SIW ce qui rend le résonateur identifiable dans cette bande. En introduisant une antenne, le résonateur SIW peut être interrogé à distance. Le système d'interrogation est illustré en figure 3-5 (**voir contribution VI**).

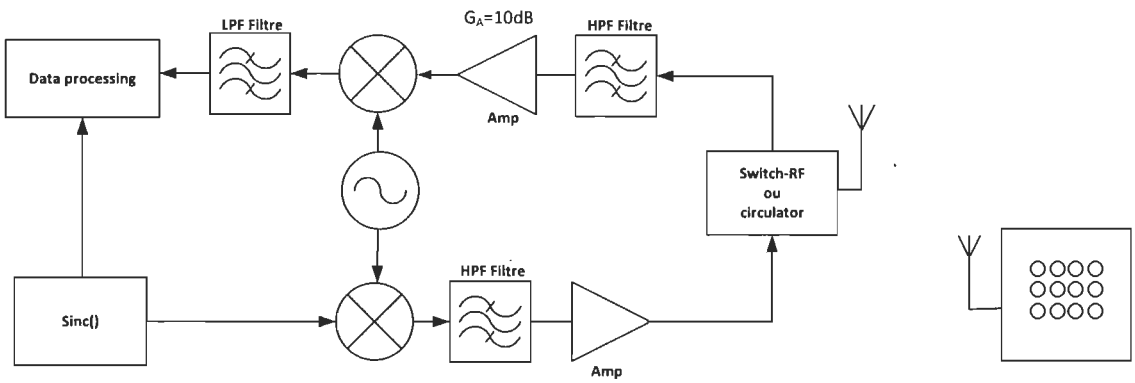

Figure 3-5 Le système de lecture RFID pour les tags SIW.

Le système de lecture RFID a été implémenté en utilisant National Instrument PXI-1075 avec des modules différents. Une interface utilisateur a été construite dans laquelle le niveau de puissance du signal transmis, la fréquence centrale et la bande de fréquence émise peuvent être ajustés.

Chapitre 4 - Les résultats des travaux obtenus

Dans cette section, les résultats de tests et de prototypage sont présentés. Cette section contient aussi une description de l'infrastructure utilisée qui ont permis d'obtenir ces résultats selon le type de test effectué. Les prototypes de résonateurs conçus ont pour dimensions 31 mm × 31 mm, ce qui fixe la fréquence centrale de la bande d'opération à 3.56 GHz pour le mode fondamental TE_{101}. Les dimensions du capteur SIW peuvent être modifiées pour changer la bande de fréquence utilisée par le capteur. Les prototypes ont été fabriqués en utilisant une technique de fabrication de PCB standard.

4.1 Évaluation des capteurs d'hydrogène commerciaux micro-fabriqués

Une évaluation des capteurs d'hydrogène commerciaux micro-fabriqués a été faite dans le cadre d'une collaboration internationale (IEA HIA-tâche 31) avec « Institute for Energy and Transport Cleaner Energy Unit» (IE-JRC) au Pays-Bas, « The National Renewable Energy Laboratory» (NREL) aux U.S.A et l'IRH sur la sûreté de l'hydrogène pour les nouvelles technologies commerciales de capteurs d'hydrogène.

Une revue de la littérature des systèmes de détection d'hydrogène micro-fabriqués montre que les capteurs TC (conductivité thermique), MOX (oxyde métallique), et catalytiques (CAT) sont les plus fréquemment utilisés pour les capteurs d'hydrogène dans le secteur de la sécurité. En particulier, la structure du dispositif sensible est souvent fabriquée par « bulk micro-machining », tandis que les électrodes et les connexions électriques sont typiquement conçues par des techniques de traitement de surface. La

Figure 4-1 montre la micro-structure de l'élément sensible micro-fabriqué pour un capteur de H2.

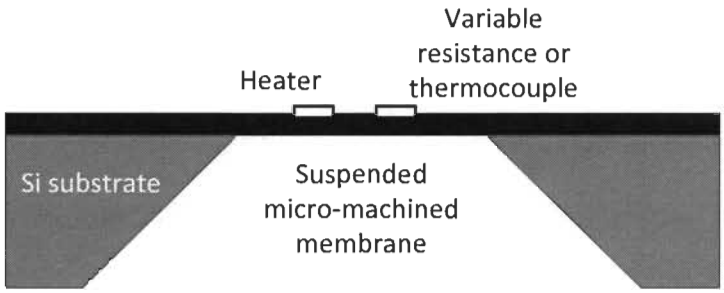

Figure 4-1 La micro-structure du capteur H2 commercial micro-fabriqué.

Une étude de marché a été réalisée pour identifier des capteurs d'hydrogène et des systèmes de détection disponibles dans les deux formats micro-usinés et conventionnels. Des capteurs TC ainsi que des systèmes de détection conventionnels et micro-usinés ont été achetés et testés (**voir contribution II**).

Les capteurs TC commerciaux indiquent la concentration d'hydrogène, permettant ainsi d'augmenter la précision de la mesure. D'autre part, les dispositifs de détection MOX sans circuit de commande commerciaux ont été achetés et testés. Les éléments de détection MOX indiquent la sortie sous forme résistive qui peut être retraduite en utilisant des circuits électriques conçus selon les recommandations du fabricant. Cette étude avait le but suivant :

- Caractériser des capteurs d'hydrogène micro-fabriqués disponibles sur le marché et les comparer avec la technologie de fabrication traditionnelle pour les applications industrielles.

- Acquérir la connaissance nécessaire pour évaluer et tester les capteurs de gaz. Cette connaissance aura permis de concevoir le banc de test pour les gaz ayant les protocoles de tests qui sont analogues aux recommandations des normes internationales.

- Situer le sujet de recherche sur les capteurs micro-ondes dans un contexte industriel et orienter les solutions autour des techniques micro-ondes actuelles.

Tous les capteurs et dispositifs de détection ont été opérés en suivant les recommandations fournies par le fabricant et dans leurs conditions de fonctionnement spécifiées. Typiquement, les évaluations de capteurs ont été réalisées à 25 °C, une pression ambiante et 50% d'humidité relative. Les concentrations de gaz de test varient de 0 à 2% en volume de H2 dans l'air, avec des concentrations spécifiques et des séquences d'exposition indiquées dans l'article II. La caractérisation porte sur les points suivants :

- Caractérisation du temps de réponse et du temps de recouvrement des capteurs TC et MOX micro-fabriqués et comparaison avec les capteurs TC et MOX traditionnels.

- L'impact du débit de gaz sur la performance des capteurs.

- Caractérisation de la linéarité et la précision des capteurs.

4.2 Prototype d'un capteur d'humidité SIW et résultats de tests

Les dispositifs SIW sont conçus en utilisant le logiciel électromagnétique pour développer la structure 3D du résonateur et pour effectuer une analyse de propagation. Cette simulation permet d'estimer les caractéristiques du résonateur SIW telles que la fréquence de résonance, la distribution du champ électrique à l'intérieur de la cavité résonante SIW et la phase. L'effet de la forme que la région fonctionnalisée introduit à l'intérieur du résonateur SIW a été examiné. Les conditions limites absorbantes ont été appliquées le long des parois entourant la structure du résonateur SIW. Le design utilise le substrat Roger RO3004C (ε_r = 3.55 d'épaisseur 1.524 mm , tanδ = 0.002) et une couche de cuivre d' épaisseur 17 µm)(**voir contribution IV**).

Une preuve de concept et des prototypes ont été réalisés pour vérifier la faisabilité des capteurs intégrés au substrat. La structure du capteur a d'abord été simulée afin d'optimiser ses fonctionnalités et de choisir la bande d'opération. Le tableau 4-1 énumère les paramètres de conception de la structure illustrée à la Figure 4-2. Le principe de détection est basé sur une variation de la constante diélectrique due à la présence d'air humide dans les trous. La présence d'humidité modifie la permittivité de l'air en fonction de la valeur relative de l'humidité H selon [37] :

$$\varepsilon_r(H) = 1 + \frac{211}{T}\left(P + \frac{48 P_s}{T} H\right) \times 10^{-6} \qquad (10)$$

où T est la température absolue (en K), P est la pression de l'air humide (en mm Hg), Ps est la pression de vapeur d'eau saturée (en mm Hg), H est l'humidité relative (en%).

L'équation montre que la constante diélectrique de l'air humide est proportionnelle au pourcentage d'humidité relative. Étant donné que la fréquence de résonance du résonateur est inversement proportionnelle à la constante diélectrique efficace [38], le changement de l'humidité relative H dû à la présence d'humidité affectera la fréquence de résonance. Ce changement fréquentiel peut être exploité comme une indication de la présence d'humidité (**voir contribution IV**).

Tableau 4-1 Paramètres de design de résonateur SIW

Paramètre	w_{eff}	L_{eff}	s	t	d_{metal}	d_{air}	p
Valeur	31 mm	31 mm	0,37 mm	9,7mm	0,4 mm	0,8mm	1,5mm

Ces paramètres ont été utilisés pour fabriquer la structure du résonateur sur un substrat RO4003C Roger à partir du masque (voir figure 4-2).

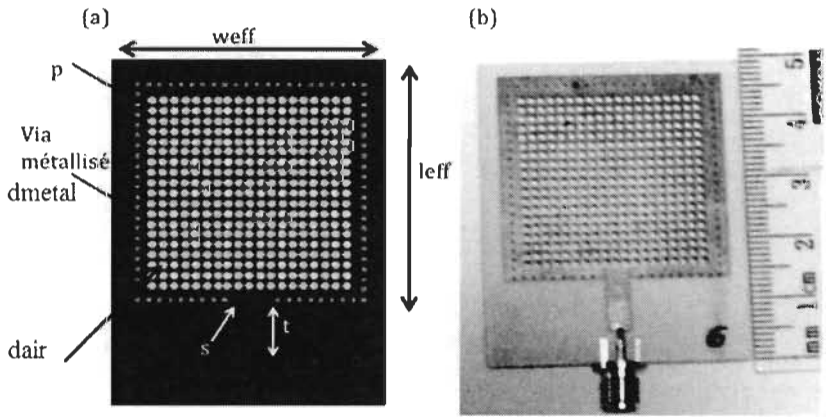

Figure 4-2 (a) Masque de fabrication avec les paramètres de design (b) prototype d'un capteur fabriqué.

Le banc de test (voir Figure 4-3 a and b) a été utilisé pour tester la capacité du capteur à détecter l'humidité. En augmentant le pourcentage d'humidité relative de 0% à 80%, le décalage fréquentiel a été mesuré pour deux résonateurs SIW1 qui a une région sensible

plus large que SIW2 (voir figure 4-4) ou la région sensible est juste au centre de la cavité résonante.

(a)

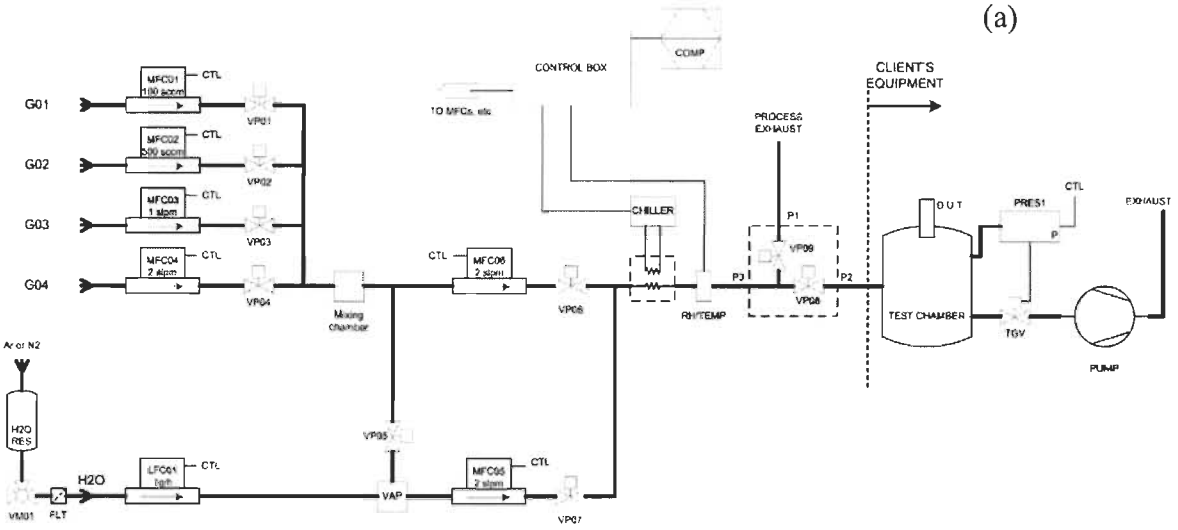

(b)

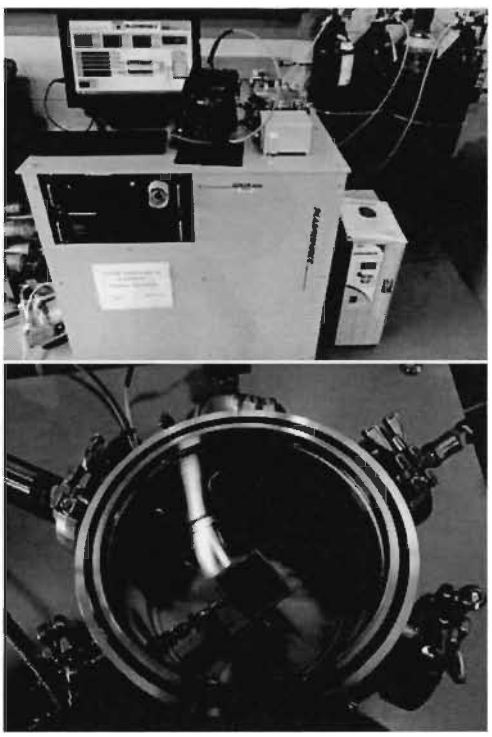

Figure 4-3 (a) Schéma de système de mélangeur de gaz. (b) Banc de test du capteur d'humidité.

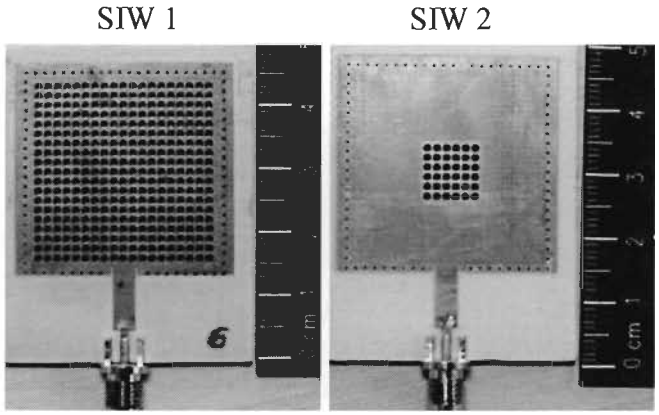

Figure 4-4 Deux résonateurs SIW1 et SIW2 avec deux régions fonctionnalisées différentes.

La figure 4-5 (a) et (b) montre le décalage fréquentiel simulé et mesuré pour le mode TE_{101}, ainsi que la variation de la fréquence (axe de gauche) du résonateur fabriqué. Les résultats ont été obtenus en variant le taux d'humidité de 0 à 80%.

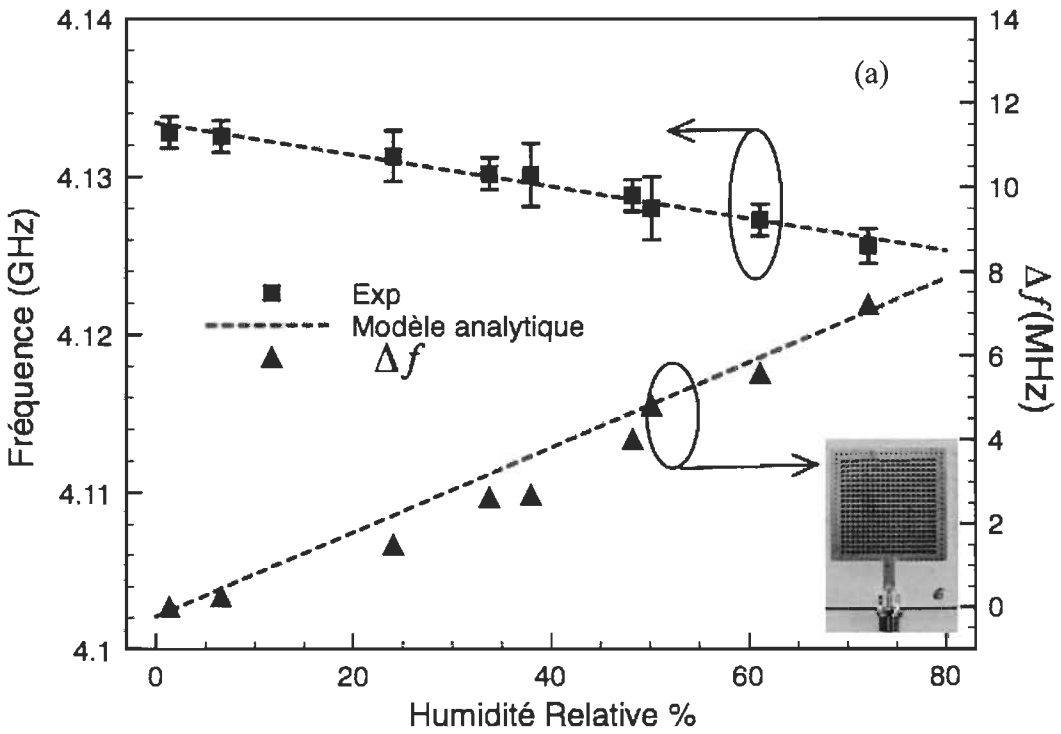

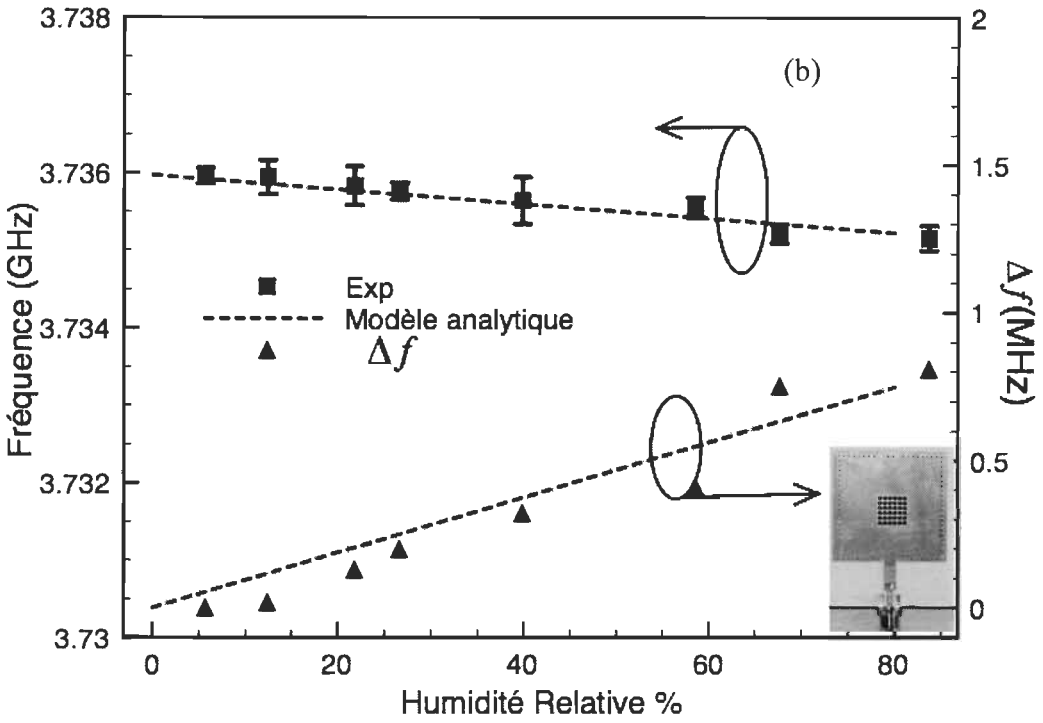

Figure 4-5 (a) Décalage fréquentiel du mode TE_{101} pour SIW1 (b) décalage fréquentiel du mode TE_{101}pour SIW2.

Le mode TE_{101} de résonance présente une variation maximale de fréquence de 9 MHz à 80% d'humidité relative. Pour qualifier la performance des capteurs, une mesure de sensibilité est nécessaire. La sensibilité d'un capteur est définie comme étant la variation de la sortie du capteur par unité de changement dans le paramètre mesuré. Elle est donnée par l'expression [17]:

$$S = \left| \frac{\Delta f_r}{\Delta \%RH} \right| \tag{11}$$

où Δf_r est la variation de la fréquence de résonance et Δ% RH est la variation correspondante à l'humidité relative. La sensibilité mesurée pour SIW1 s'avère être 101 kHz / RH%. La même mesure a été effectuée sur le second résonateur, SIW2, pour le même mode de résonance. Le deuxième résonateur présente un décalage de fréquence maximum de 0,8 MHz à 80% d'humidité relative et une sensibilité de 9,35 kHz / RH%. Les sensibilités ont été calculées par régression linéaire de la fréquence de résonance mesurée (**voir contribution IV**).

4.3 Résultats de test pour le tag RFID

Les applications sans fil voient une croissance rapide au cours des dernières années, d'où l'augmentation de la nécessité de l'identification par radiofréquence (RFID). Dans le cas des capteurs sans-fil, il est nécessaire d'avoir un moyen de distinguer chaque capteur dans le réseau. Les tags RFID passifs offrent l'avantage de l'identification à distance avec zéro consommation d'énergie et une durée de vie illimitée. Dans le contexte de réseau de capteurs sans fil, cette section démontre le concept et le prototypage d'une nouvelle structure de SIW pour l'identification des micro-ondes. La proposition de structure de tag sans-fil est basée sur un résonateur intégré au substrat qui encode les données dans le spectre du signal en utilisant des trous d'air à l'intérieur de la structure de résonateur. Étant donné que le diélectrique change en fonction du nombre de trous, la structure proposée a l'avantage de codage sans augmenter la taille du résonateur.

Une preuve de concept et des prototypes ont été réalisés pour vérifier la méthode d'adressage sans-fil pour les capteurs intégrés au substrat (**voir contribution III**). La méthode d'adressage est basée sur des résonateurs intégrés au substrat où l'adresse est identifiée par un nombre variable des trous d'air dans les résonateurs. Quatre configurations représentant quatre différentes adresses dans le spectre de fréquence ont été proposées (voir figure 4-6).

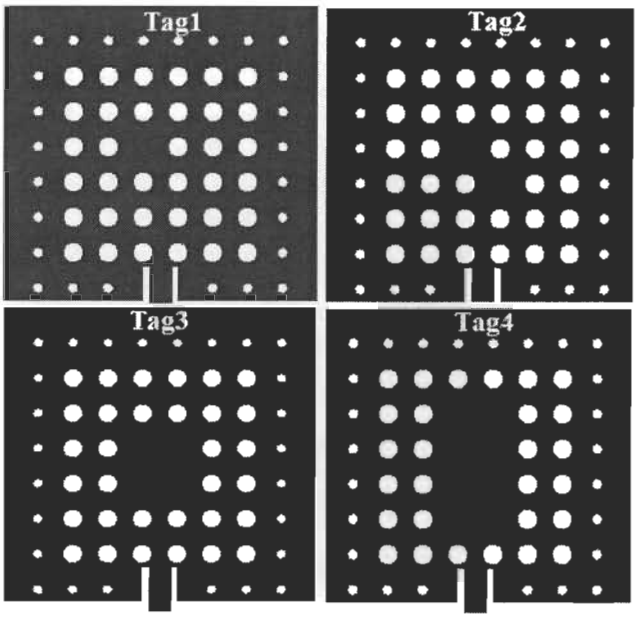

Figure 4-6 Quatre résonateurs avec des adresses différentes.

Les quatre configurations ont été simulées, fabriquées et testées expérimentalement. Les résultats de simulations et de tests sont présentés dans la figure 4-7.

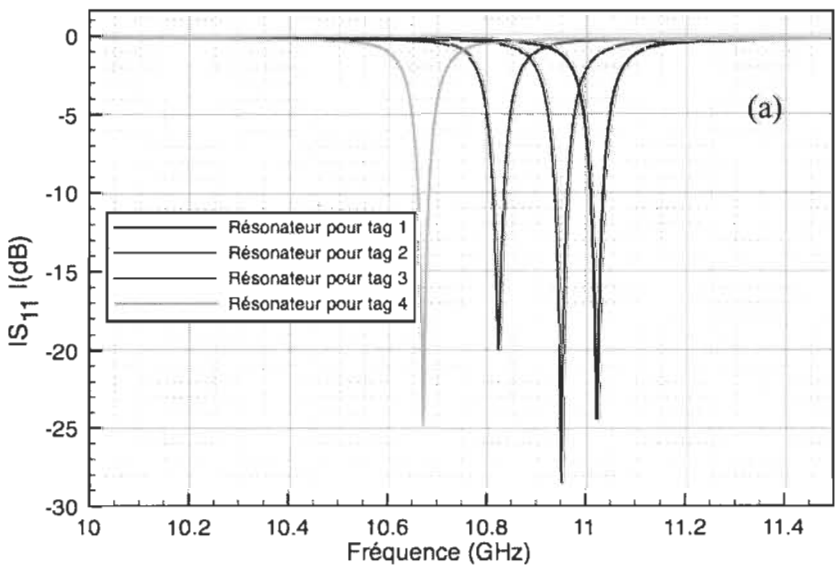

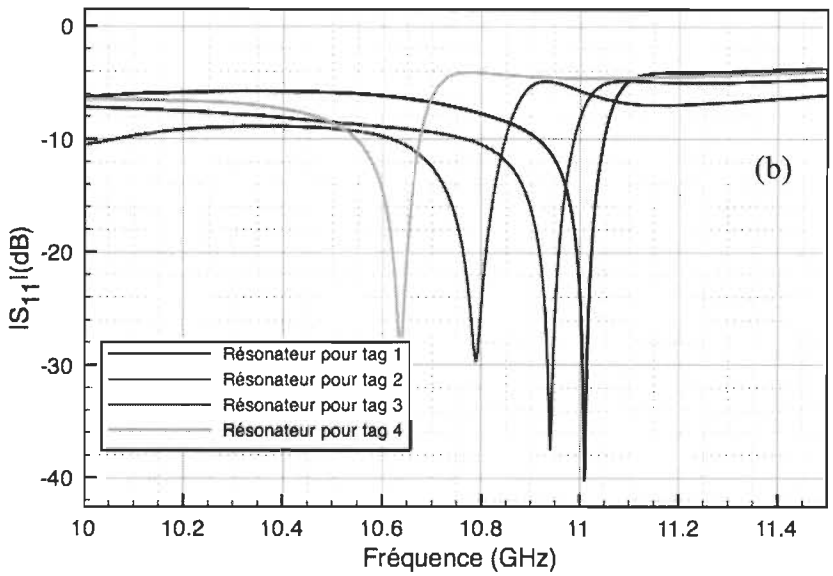

Figure 4-7 (a) Résultats de simulation (b) résultats expérimentaux d'adressage.

Les fréquences de résonance sont dans la bande de fréquence de 10.5 à 11.1 GHz. Ce mode présente un facteur de qualité (Q) de 373,3 et la fréquence diminue de 0,1 GHz pour chaque trou d'air manquant à l'intérieur du résonateur intégré au substrat. Pour les tests sans-fil, une antenne résonant à une fréquence centrale de la bande d'adressage à 10,7 GHz en plaque circulaire a été conçue. Les prototypes des unités d'adressage intégrées au substrat avec les antennes d'interrogation sont représentés en figure 4-8.

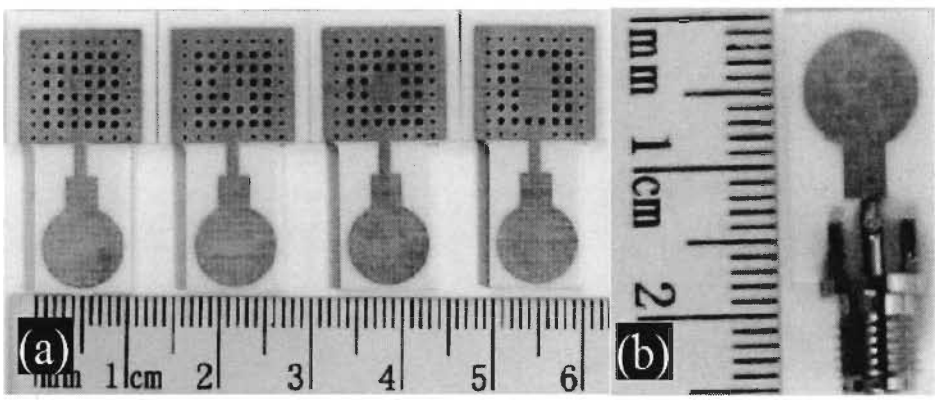

Figure 4-8 (a) quatre résonateurs représentant les quatre adresses d'identification (b) antenne d'interrogation.

Chaque unité d'adressage a été interrogée séparément pour identifier sa signature. L'antenne interrogatrice et les unités d'adressage sont séparées par une distance de 1 cm. Les résultats montrent que la signature de chaque unité d'adressage correspond à sa fréquence de résonance et peut être détectée à partir du niveau du signal. La Figure 4-9 montre les résultats de l'essai mené sans fil sur chaque point séparément. Le paramètre S11 de l'antenne est représenté par la courbe en pointillés. Lorsque l'antenne interrogatrice est approchée de l'une de ces unités, la fréquence de résonance de cette unité apparaît comme un pic distinct dans la signature de fréquence.

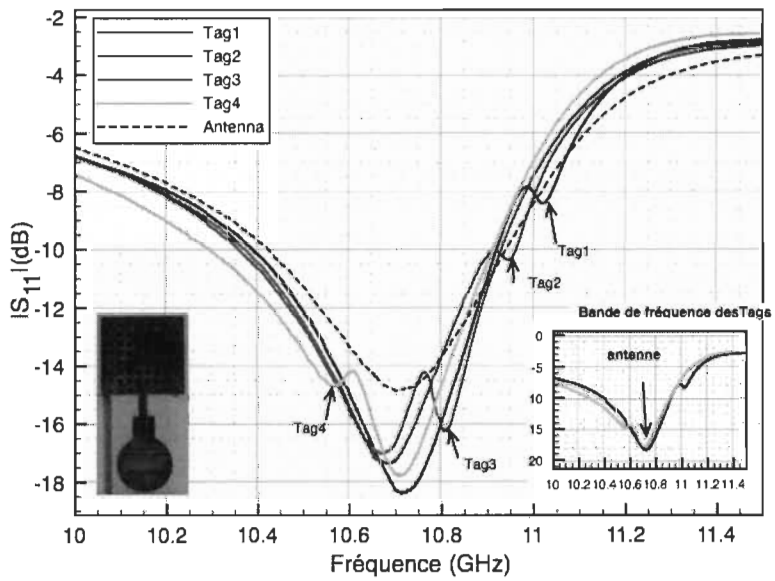

Figure 4-9 Test sans fil pour les unités d'adressage.

4.4 Preuve de concept et prototype pour le capteur d'hydrogène

4.4.1 Résultats de détection à 100% H2 pour le capteur SIW

Cette section présente une preuve de concept et des prototypes pour vérifier la faisabilité du capteur intégré au substrat pour la détection de gaz. La structure du capteur a

été simulée pour optimiser ses fonctionnalités et pour choisir sa bande d'opération. Le prototype de capteur d'hydrogène a été fabriqué avec une région sensible au milieu de la cavité résonante comme illustré à la figure 4-3. Le dioxyde d'étain SnO2 a été choisi pour fonctionnaliser le résonateur et le rendre sensible à la présence d'hydrogène.

La région fonctionnalisée est choisie pour qu'elle soit au milieu de la cavité SIW (figure 4-3) car le champ électrique est maximal dans cette position, et donc augmente l'effet du champ sur le diélectrique. Un test a été effectué pour mesurer le décalage de fréquence du capteur intégré en mettant le capteur SIW dans une chambre avec un débit de gaz d'hydrogène constant et une concentration de 100%. Le premier mode de fréquence de résonance du capteur SIW a été mesuré avec un analyseur de réseau vectoriel (VNA). Le décalage fréquentiel observé pour ce mode en présence d'hydrogène gazeux était de 30 MHz qui est la différence entre la fréquence de résonance à l'air et la fréquence de résonance en présence de 100% H2. Ce décalage fréquentiel est dû à la variation de la constante diélectrique de la région de SnO2 fonctionnalisée. Étant donné que la fréquence de résonance du résonateur SIW est liée à la constante diélectrique de substrat par ε_{eff} qui est la permittivité efficace du substrat diélectrique, la variation de ε_{eff} va induire un changement dans la fréquence de résonance indiquant la présence du gaz d'hydrogène. La figure 4-10 présente les résultats des essais expérimentaux avec et sans gaz d'hydrogène, montrant ainsi l'effet de l'introduction du gaz sur la fréquence de résonance du résonateur SIW fonctionnalisé avec SnO2.

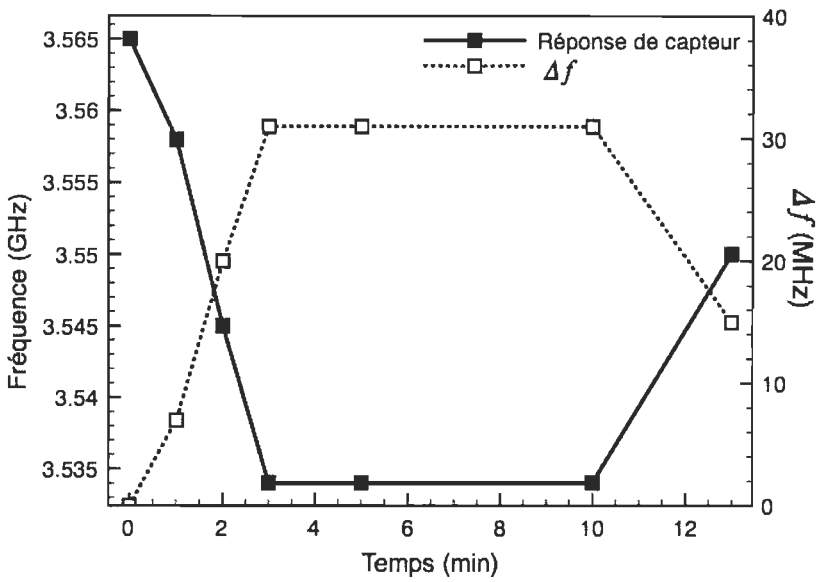

Figure 4-10 Résultats de la variation de la fréquence de résonance pour un capteur H2 intégré au substrat pour une concentration de gaz fixée à 100%.

4.4.2 Résultats de détection à 2% H2 pour le capteur SIW

Le capteur d'hydrogène étant un capteur à basse concentration (2% d'H2), le banc de test utilisé pour caractériser le résonateur SIW est présenté à la figure 4-3. Dans ce cas-ci, la condition à l'intérieur de la chambre pendant les tests est présentée en figure 4-11. La chambre a été mise sous vide avant de remplacer le gaz interne par 2% de H2. Les mesures de fréquences ont été prises à l'air et à l'hydrogène.

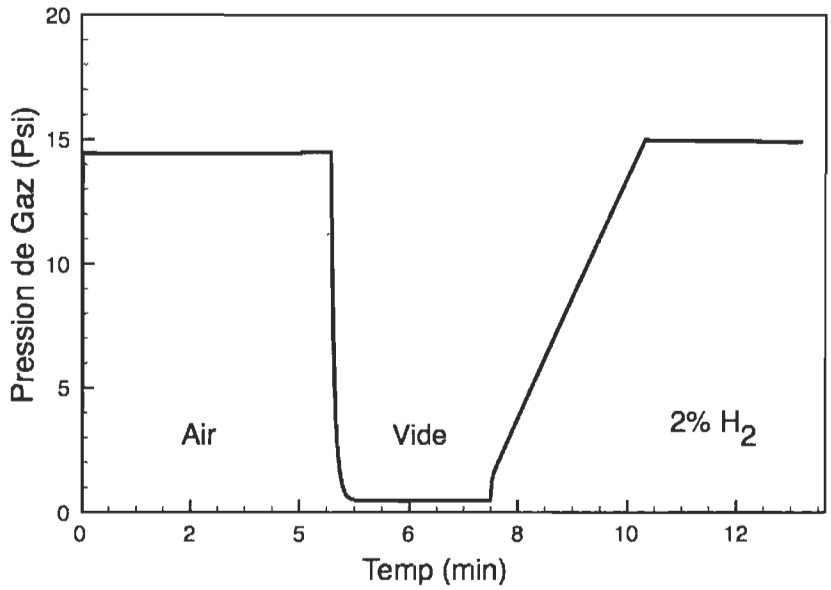

Figure 4-11 Condition cyclique entre air et 2% H2 dans la chambre de test.

Les résultats de mesures de la fréquence de résonance sont présentés dans le tableau 4-2. La permittivité du SnO2 a été extraite (à l'air et à 2% H2) en utilisant la méthode de perturbation décrite dans le quatrième article. En réorganisant l'équation (7) dans (**contribution IV**), on peut avoir le changement de permittivité :

$$\frac{\omega-\omega_r}{\omega_r} \approx -\frac{\Delta\varepsilon\left(2\pi g + W\sin\frac{2\pi g}{W}\right)^2}{2W^2\pi^2\varepsilon_r} \Rightarrow \Delta\varepsilon \approx \frac{2W^2\pi^2\varepsilon_r(\omega-\omega_r)}{\omega_r\left(2\pi g + W\sin\frac{2\pi g}{W}\right)^2} \tag{12}$$

Où ω_r est la fréquence de résonance non perturbée du résonateur SIW utilisé.

ε_r est la permittivité de substrat et $\Delta\varepsilon = \varepsilon_{mat}-\varepsilon_r$.

Les valeurs de permittivité extraites sont des valeurs approximatives parce que la perturbation métallique n'a pas été considérée.

Tableau 4-2 Résultats de mesure de la fréquence de résonance

Simulation EMPro	f_r **(GHz)**
air (ε_{mat} =1)	3,7
ε_{mat} =2	3,64
ε_{mat} =3,84 (de SnO2 extrait de perturbation)	3,529
ε_{mat} =3,88 (à 2%H2 extrait de perturbation)	3,526
Model Analytique	f_r**(GHz)**
air (ε_{mat} =1)	3,905
ε_{mat} =2	3,803
ε_{mat} =3,84	3,615
ε_{mat} =3,88 (à 2%H2 extrait de perturbation)	3,612
Résultats de mesure Pratique	f_r**(GHz)**
air (ε_{mat} =1)	3,694
résonateur avec SnO2 à l'air	3,615
résonateur avec SnO2 à 2%H2	3,612

La structure fonctionnalisée du résonateur SIW a été simulée pour valider les résultats obtenus du modèle analytique et comparés avec les résultats pratiques. Le décalage fréquentiel entre la réponse du résonateur à l'air et à l'hydrogène a été calculé dans les trois cas (simulation, analytiquement et mesure). Le tableau 4-3 résume les valeurs calculées.

Tableau 4-3 Comparaison entre les décalages fréquentiels

	Δf (simulation)	Δf (modèle analytique)	Δf (pratique)
Valeur en (GHz)	0.003	0.0031	0.003

Un test de répétabilité a ensuite été effectué sur 4 échantillons de poudre de SnO2 broyée pendant 60min sous air et H2 à 2%. La moyenne des quatre mesures a été évaluée. Les résultats sont présentés dans le tableau 4-4.

Tableau 4-4 Test de répétabilité pour la fréquence de résonance

	fr GHz P1	*fr*GHz P2	*fr*GHz P3	*fr*GHz P4	*fr*(GHz) moyenne
trous air	3,694	3,694	3,694	3,694	3,694
SnO2 air	3,611	3,612	3,627	3,611	3,61525
SnO2H2 2%	3,607	3,608	3,624	3,608	3,61175

En utilisant la valeur moyenne des fréquences de résonance montrées dans le tableau VI, la différence entre la fréquence de résonance de résonateur SIW fonctionnalisé à l'air et à 2% H2 et Δf_r(moyenne) = 0.0035 GHz. Elle est du même ordre de grandeur que le Δf évalué au tableau 4-3.

4.4.3 Étude comparative des variations de fréquences de résonance en présence de poudre de SnO2 et SnO2 dopé avec Palladium dans la plage de 0 à 2% de H2

Cette étude comparative est effectuée pour deux cas de figure : l'une en présence de SnO2 dans la région fonctionnalisée du dispositif, et l'autre en présence de SnO2+1%Pd.

La nano poudre de Palladium qui est un bon catalyseur pour l'hydrogène a été utilisée pour doper la nano poudre de SnO2 présentée précédemment. De plus, le Palladium est un métal dont on s'attend à avoir plus de perte dans la région fonctionnalisée. Pour cette raison, la quantité de Palladium doit être choisie de sorte à ne pas trop dégrader la

fréquence de résonance. Un échantillon de nano poudre SnO2 a été préparé en la broyant pendant 60 min. La poudre de Palladium utilisée contient 99,99% de particules de Palladium de haute pureté ayant une taille comprise entre 0,25 µm - 0,55 µm. Une dose d'un pourcentage de nano poudre de Palladium a été mélangée avec la nano poudre de SnO2 pour faire le dopage. Le mélange a ensuite été utilisé pour fonctionnaliser le résonateur SIW.

Le but est d'évaluer les variations de la fréquence de résonance du dispositif entre le vide ou l'air et en présence d'une concentration contrôlée de gaz d'hydrogène (0.5%, 1% et 2%). Pour une variation de la concentration du gaz à détecter, l'hydrogène à 2% a été dilué avec l'azote pour avoir de faibles concentrations. Pour chaque condition de test, la réponse du capteur sera considérée comme la variation de la fréquence de résonance du résonateur SIW fonctionnalisé. Les concentrations de gaz d'essai vont être variées en fonction du pourcentage de volume d'hydrogène dans l'air pour des concentrations spécifiques et des séquences d'exposition cycliques. La figure 4-12 traduit les résultats de cette étude comparative pour un résonateur SIW fonctionnalisé avec SnO2. Δf est la différence entre le résonateur fonctionnalisé exposé successivement à l'air et à H2 puis un second cas avec une variation entre le vide et H2 :

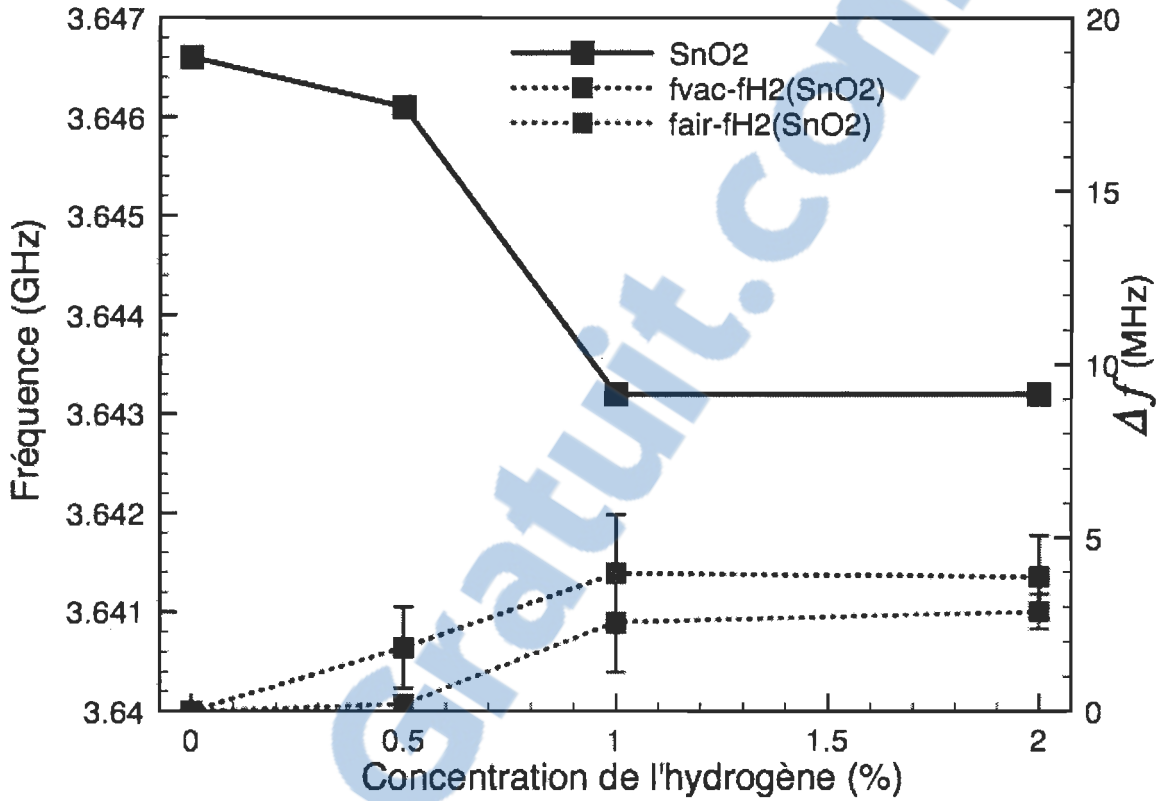

Figure 4-12 Décalage fréquentiel du mode TE_{101} pour une région sensible de SnO2.

La figure 4-13 traduit les résultats de cette étude comparative pour un résonateur SIW fonctionnalisé avec SnO2 dopé avec 1% Pd. Δf est la différence entre le résonateur fonctionnalisé exposé successivement à l'air et à l'H2, puis un second cas avec une variation entre le vide et l'H2 :

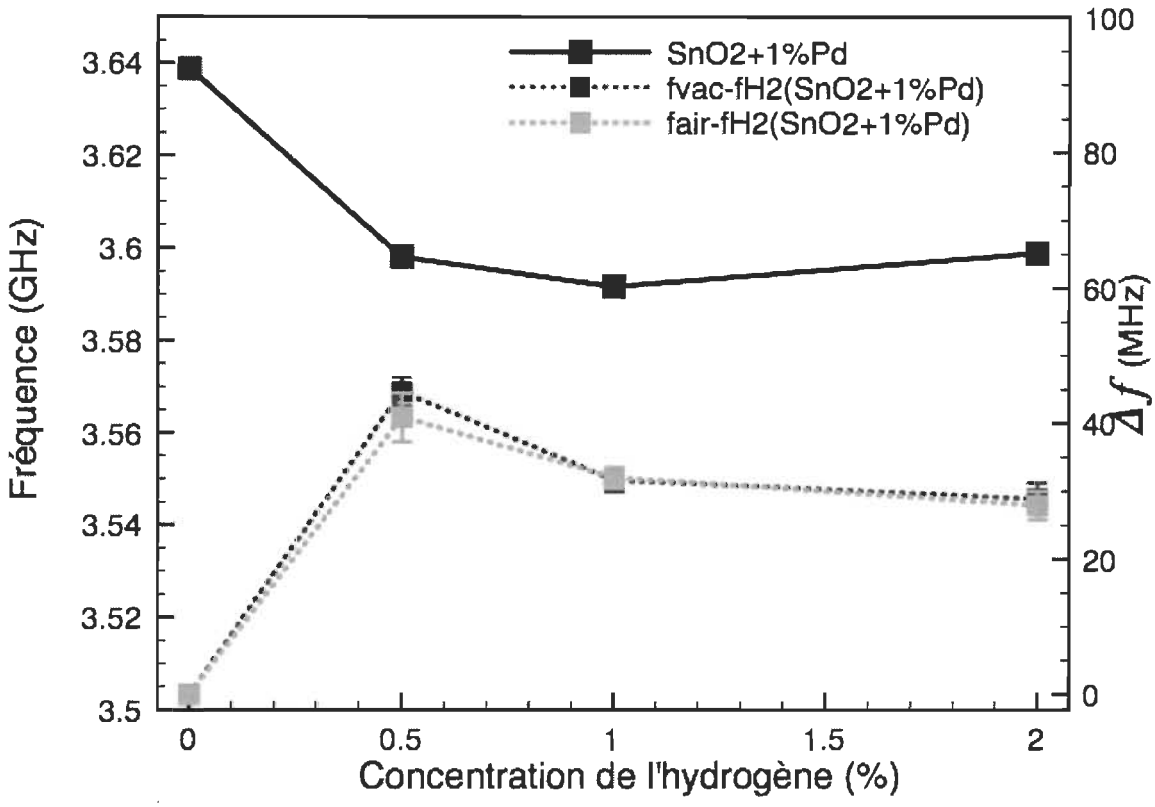

Figure 4-13 Décalage fréquentiel du mode TE_{101} pour une région sensible de SnO2+1%Pd.

Les courbes de résultats ci-dessus illustrent que la variation de la permittivité des nano-poudres (SnO2) dopées avec les nanoparticules de palladium permet d'atteindre de meilleures performances en sensibilité du dispositif de détection de gaz. Le décalage de fréquence est amélioré d'un facteur 10 dans le cas de SnO2 dopé de Pd.

4.5 Étude de tolérance dimensionnelle de fabrication et des paramètres diélectriques du substrat

Les capteurs intégrés au substrat sont fabriqués par la technique PCB. Cette technique a une certaine précision de fabrication associée à la machine et au substrat utilisé. Cette section présente une étude de tolérance de fabrication basée sur les spécifications des machines PCB et les paramètres du substrat utilisé pour fabriquer les capteurs SIW. Cela permet de déterminer l'effet de petites variations dans la géométrie du composant, et d'estimer son effet sur la fréquence de résonance dans le cas d'une production de masse. Les tolérances dues à la variation géométrique de fabrication et la variation de température sont étudiées pour la fréquence de résonance de la cavité SIW. La variation de la fréquence de résonance peut être prédite en utilisant les caractéristiques du substrat (tel que décrit dans le datasheet) et les paramètres utilisés dans le procédé de fabrication, à savoir la tolérance et la précision de la machine PCB. En utilisant la même approche proposée en (**contribution IV** voir équation (8)), on peut déduire la variation maximale, ou la stabilité de la fréquence de résonance d'une cavité.

$$\Delta f_{r(TE101)} = \left|\frac{\partial f_r}{\partial \varepsilon_r}\right|_{\varepsilon_r} T_{\varepsilon_r} + \left|\frac{\partial f_r}{\partial W_{eff}}\right|_{W} T_{W_{eff}} + \left|\frac{\partial f_r}{\partial L_{eff}}\right|_{L} T_{L_{eff}} + \left|\frac{\partial f_r}{\partial D}\right|_{D} T_D \tag{13}$$

où $\partial f_r/\partial \varepsilon r$, $\partial f_r/\partial W_{eff}$ et $\partial f_r/\partial L_{eff}$ sont les dérivées partielles de eq. (1) évaluées à la valeur nominale des εr, W_{eff} et L_{eff}, et $T_{\varepsilon r}$, T_{Weff} et T_{Leff} sont les tolérances totales sur les dimensions physiques de la cavité. T_D est la tolérance de la machine PCB utilisée pour la fabrication de la structure SIW. La tolérance de longueur a été calculée en utilisant la formule de dilatation linéaire

$$\Delta L = L \alpha \Delta T \tag{14}$$

où α est le coefficient de dilatation linéaire donné dans la fiche de données de Roger ($\alpha = 11 \times 10^{-6} / ^\circ C$) et ΔT est la variation de température. Le tableau 4-5 liste les paramètres avec ces tolérances.

Tableau 4-5 Les paramètres de substrat et ces tolérances

	Paramètre	Tolérance
Roger's substrat RO4003C	Permittivité = 3.55	±0.005
	Tolérance de W et L (-55°C -288°C)	0.342 μm
LPKF	Précision de Vias	±0.001 mm

En utilisant les valeurs indiquées dans le tableau 4-5, on peut obtenir la tolérance en fréquence de résonance Δf_r à partir de la tolérance en permittivité du substrat et de la tolérance en longueur. $\Delta f_r = \pm$ 2.6MHz pour une fréquence de résonance f_r = 3.64GHz. Si l'on considère seulement la variation de température, la tolérance en fréquence $\Delta f_r = \pm$ 40.47kHz est uniquement due à la tolérance en longueur.

Chapitre 5 - Contributions scientifiques et publications

Cette section présente au lecteur une vue d'ensemble des recherches et des travaux effectués sur le capteur SIW menés au cours de la période de doctorat. Premièrement, du fait de l'originalité de la solution et l'approche proposées, un dépôt d'une demande de brevet provisoire a été effectué en 2013. Il s'agit de valoriser le travail de doctorat et l'orienter vers les intérêts industriels tout en protégeant intellectuellement l'innovation. La référence de brevet est la suivante :

- Hatem El Matbouly, Frédéric Domingue, «Microwave resonator sensor and associated methods of sensing», (Ref: 05015656-85USPR) provisional patent application 2013.

Ensuite, dans le cadre de la collaboration internationale (IEA HIA-tâche 31) avec «Institute for Energy and Transport Cleaner Energy Unit» (IE-JRC) au Pays-Bas, «The National Renewable Energy Laboratory» (NREL) aux É.U et l'IRH sur la thématique sûreté de l'hydrogène des nouvelles technologies commerciales, des capteurs d'hydrogène ont été testés et comparés. Le but de ce stage de formation à (l'Institut for Energy Petten/Pays-Bas) était de caractériser des capteurs d'hydrogène micro-machinés disponibles sur le marché, et d'acquérir la connaissance nécessaire pour évaluer et tester les capteurs de gaz. Il a aussi servi à situer le sujet de recherche dans un contexte industriel et orienter les solutions afin de répondre aux besoins actuels. Cette collaboration a mené aux publications suivantes :

- (Chapitre de livre): H. El Matbouly, F. Domingue, V. Palmisano, L. Boon-Brett, «Hydrogen Gas Detection», Measurement, Instrumentation, and Sensors Handbook, 2ed Edition 2014.

- H. El Matbouly, F. Domingue, V. Palmisano, L. Boon-Brett, M. B. Post, C. Rivkin, R. Burgess, and W. J. Buttner «Assessment of Commercial Micro-Machined Hydrogen Sensors Performance Metrics for Safety Sensing Applications», International Journal of Hydrogen Energy 2013. (Soumis)

Une contribution dans le domaine d'identification radiofréquence a été publiée dans le revue «IEEE Microwave and Wireless Components Letters» portant sur l'idée d'utiliser le résonateur SIW comme un tag passif

- Hatem El Matbouly, Naimi Boubekeur, Frédéric Domingue, «A Novel Chipless Identification Tag Based on a Substrate Integrated Cavity Resonator», IEEE Microwave and Wireless Components Letters Volume: 23, Issue: 1   Page(s): 52 – 54, 2013.

9.3. Publications de conférences

(Conference invited special session): Hatem EL MATBOULY, Guy AYISSI EYEBE, Frédéric DOMINGUE, «Modeling and Characterization of a Substrate Integrated Chip-less Tag Communication System » Proc. ICECom2013 in Dubrovnik, 14 – 16 October 2013.

N. Boubekeur, H. El Matbouly, F. Domingue, «Dielectric Powder Characterization by Radio Frequency Measurements Technique for Hydrogen Sensor Applications: Application to Iron Oxide», Proceeding of IEEE Sensors Conference, 3-6 November (2013) Baltimore, Maryland (USA).

Guy AYISSI EYEBE, Hatem EL MATBOULY, Frédéric DOMINGUE, «Dual-Band Antenna for Sensing Applications in ISM Bands», Proceeding of IARIA SENSORDEVICES 2013.

Kevin Dionne, Hatem El Matbouly, Frédéric Domingue, Loïc Boulon, «A General Purpose Inductively Coupled Voltage Sensor», IEEE International Conference on RFID - Technologies and Applications (RFID - TA) – Sensing, Nice, France 2012.

Kevin Dionne, Hatem El Matbouly, Frédéric Domingue, Loïc Boulon,« A Chipless HF RFID Tag with Signature as a Voltage Sensor» IEEE International Conference on Wireless Information Technology and Systems, Hawaï, 2012.

Issam Kerroum, Hatem El Matbouly, Frédéric Domingue. «Survey of commercial sensors and emerging miniaturized technologies for safety applications in hydrogen vehicles» IEEE Sensor Application Symposium, Italie, 2012.

5.1 Contribution I : Chapitre de livre «Hydrogen Gas Sensors»

Le chapitre de livre publié dans «Measurement, Instrumentation, and Sensors Handbook, 2nd Edition 2014» présente une revue des technologies commerciales de capteurs d'hydrogène qui sont disponibles et leurs principes d'opération. Le chapitre présente les caractéristiques de performance de ces types de capteurs, comme la plage de mesure, la sensibilité, la sélectivité et le temps de réponse/ recouvrement. Les technologies émergentes disponibles et leurs impacts sur l'amélioration de la détection de gaz d'hydrogène sont également présentés dans ce chapitre.

Les capteurs d'hydrogène sont des dispositifs transducteurs qui détectent l'hydrogène en état gazeux et ensuite produise un signal électrique qui a une amplitude proportionnelle à la concentration du gaz d'hydrogène. Il existe plusieurs types de capteurs d'hydrogène, les plus courants sont les capteurs catalytiques (CAT), électrochimiques (EC), à conductivité thermique (TCD), les capteurs métal-oxyde (MOX), et les capteurs métal-oxyde-semi-conducteur (MOS). Un bilan des principaux types des capteurs disponibles sur le marché est détaillé dans ce chapitre.

L'objectif de cette publication est de présenter une étude bibliographique détaillée des technologies courantes de détection de l'hydrogène et démontrer le principe de détection de chacune de ces technologies ainsi que leurs performances de détection. Cela est primordial pour mener une recherche sur un nouveau principe de détection et un dispositif à structure innovante dans le domaine de la détection de gaz.

12

Hydrogen Gas Sensors: Flow

H. El Matbouly
LMST-Université du Québec à Trois-Rivières

F. Domingue
LMST-Université du Québec à Trois-Rivières

V. Palmisano
European Commission-JRC Institute for Energy

L. Boon-Brett
European Commission-JRC Institute for Energy

12.1 Introduction

The demand for hydrogen as a process gas and as a renewable energy carrier to reduce dependence on fossil fuels and to mitigate the problems associated with greenhouse gas emissions is increasing [1,2].

Hydrogen has a very low density (0.0899 kg/m^3) and boiling point (20.39 K) and high diffusion coefficient (0.61 cm^2/s in air). It has a low minimum ignition energy (0.017 mJ), high heat of combustion (142 kJ/g H_2), and wide flammable range (4–75 vol% in air), as well as a high burning velocity and an ignition temperature of 560 °C. Hydrogen also acts as a strong reducing agent for many elements and has a high permeability through many materials [3]. In addition, hydrogen is a colorless, odorless, and tasteless flammable gas that makes it undetectable by human senses.

Due to the unique physical and chemical properties of hydrogen, hydrogen-based applications require rigorous safety precautions in comparison to other industrial gases. Since the use of odorants in many hydrogen applications is not possible, dedicated detection devices or sensors are essential to warn of the presence of unwanted hydrogen leaks. Hydrogen sensors play an essential role in ensuring the safety of hydrogen-based applications. As such, sensors boost end user confidence and therefore facilitate the safe use and commercialization of hydrogen as an alternative fuel. Some applications require not only detecting the presence of hydrogen but also measuring the concentration of the gas in the ambient [3].

This chapter reviews the available commercial hydrogen-sensing technologies and their operating principles. The chapter discusses the performance characteristics of these sensor types, such as measuring range, sensitivity, selectivity, and response time. Available emergent technologies and their impact on improved hydrogen gas sensing are also presented.

Hydrogen sensors are transducer devices that detect hydrogen gas and produce an electric signal with a magnitude proportional to the hydrogen gas concentration.

There are several different types of hydrogen sensors and the most common commercial types are catalytic (CAT), electrochemical (EC), thermal conductivity (TCD), semiconductive metal–oxide (MOX), and metal–oxide–semiconductor (MOS) sensors. The following section presents an overview of the main sensor types available on the market.

12.2 Commercial Sensor Technologies and Their Detection Principles of Catalytic Hydrogen Gas Sensor

The detection principle of CAT hydrogen gas sensors is based on heat generation due to hydrogen reaction with oxygen on the surface of a CAT material. There are two types of CAT hydrogen sensors: pellistor type and thermoelectric type.

A pellistor-type sensor is made of two platinum wires embedded in separate beads: a sensing bead and a reference bead. The sensing bead is impregnated with catalyst (usually palladium) to accelerate the oxidation of hydrogen. The reference bead compensates for environmental effects such as changes in humidity or temperature. These two beads are mounted in a Wheatstone bridge as shown in Figure 12.1.

When the target gas is introduced, CAT combustion of the gas occurs on the surface of the sensing bead, releasing heat and causing the temperature of the bead to rise. As a result, the resistance of the embedded platinum wire changes, which imbalances the Wheatstone bridge and provides an output signal that varies with target gas concentration. CAT-type sensors were first suggested by Jonson in 1923 and used in mines for methane detection [4,5]. CAT pellistor-type sensors are well-developed and widely available.

On the other hand, thermoelectric-type CAT sensors use the thermoelectric Seebeck effect to transform the heat generated from the exothermic hydrogen oxidation reaction into an electric signal. The thermoelectric voltage generated is related to the temperature difference by the following expression:

$$U = S\Delta T \tag{12.1}$$

where

U is the thermoelectric voltage generated

S is the Seebeck coefficient

ΔT is the temperature difference due to heat generation

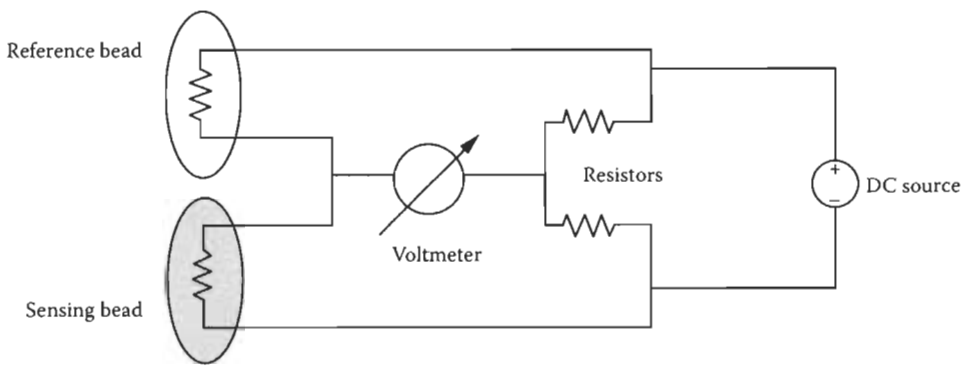

FIGURE 12.1 Wheatstone bridge circuit connected to a CAT hydrogen sensor. The sensing bead represents the variable resistor that imbalances the bridge in the presence of hydrogen.

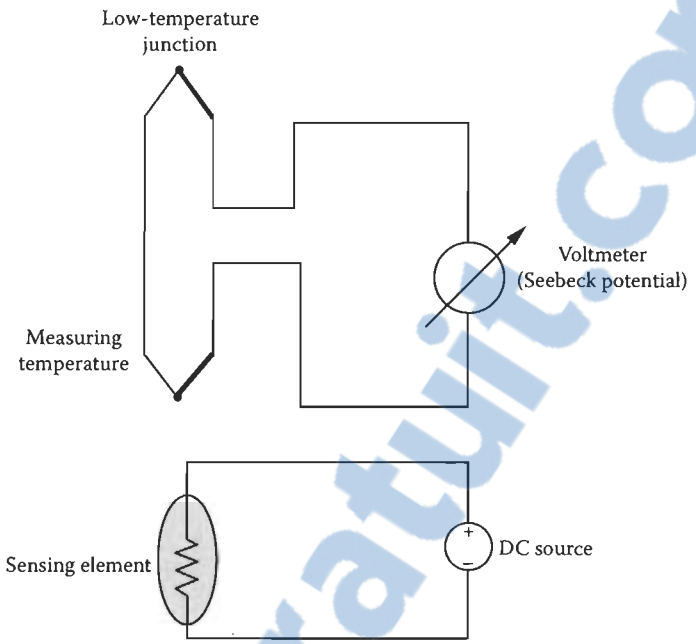

FIGURE 12.2 Schematic diagram representing hydrogen sensing by thermoelectric effect.

Thermoelectric hydrogen gas sensors are fabricated as a film of a thermoelectric material deposited on an insulating substrate material. One-half of the thermoelectric material is coated with a catalyst, and oxidation of hydrogen on the catalyst surface generates heat. This generates a temperature gradient over the thermoelectric film that produces a voltage signal measurable by an electric circuit. One advantage of thermoelectric hydrogen sensors over pellistor sensors is that they can operate at room temperature or slightly elevated temperatures (<100 °C) [6]. Figure 12.2 represents the CAT thermoelectric gas sensor. The thermoelectric effect was first used in sensing application in 1985 and reported by McAleer et al. [7].

12.2.1 Thermal Conductivity Hydrogen Gas Sensor

TCD hydrogen sensors exploit the exceptionally high TCD of hydrogen (0.168 W/m·K at 25 °C), seven times higher than air (0.024 W/m·K at 25 °C). The hydrogen concentration is inferred by the rate at which a sensing thermal element releases heat compared to a reference element. In the classical configuration the two elements are placed into two separate cells connected in a Wheatstone bridge circuit: when the gas is introduced at the sensing element, the difference in thermal conduction from the hot to the cold elements leads to a change in temperature that affects the resistance of the sensor and thus imbalances the bridge. This imbalance can be measured and can be used to indicate the hydrogen concentration. The main difference between the CAT bead sensor and the TCD sensor is the absence of a chemical reaction [8]. Figure 12.3 represents the circuit diagram of the TCD sensor.

12.2.2 Electrochemical Hydrogen Gas Sensor

EC sensors detect the change in charge transport or electrical properties due to EC reactions of hydrogen gas at the sensing electrode. The sensor structure consists of three electrodes stacked parallel and separate by an electrolytic solution as shown in Figure 12.4. There are two types of EC gas detection: amperometric and potentiometric [4].

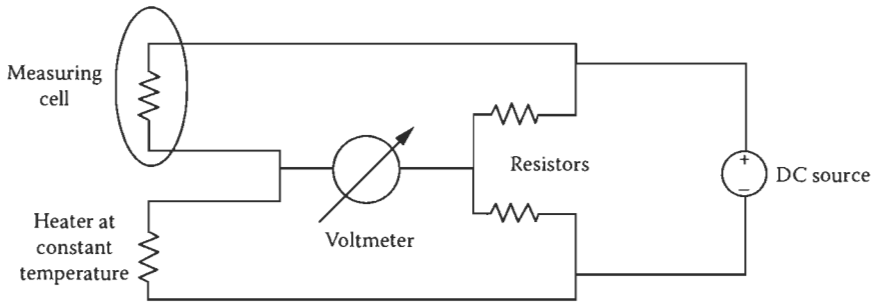

FIGURE 12.3 TCD sensor measuring circuit using a Wheatstone bridge. The measuring cell represents the variable resistor that imbalances the bridge in the presence of hydrogen.

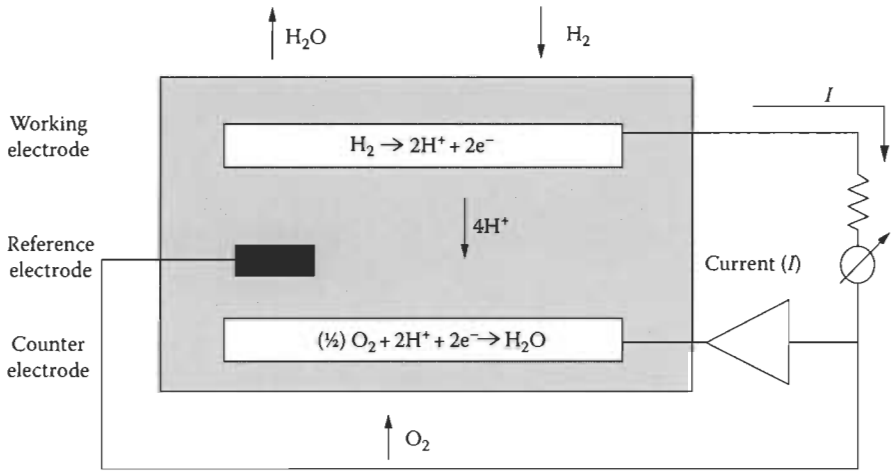

FIGURE 12.4 EC cell for hydrogen detection.

Amperometric sensors work at a constant applied voltage where the sensor signal is a diffusion-limited current. When hydrogen penetrates the gas diffusion barrier, it reaches the surface of the working electrode (anode) where the following oxidation reaction takes place:

$$H_2 \rightarrow 2H^+ + 2e^-$$

The electrons released in this reaction flow to the cathode (counter electrode) via an external circuit; this electric current constitutes the sensor signal. Protons released from the oxidation reaction cross the electrolyte and reach the counter electrode where the reduction of oxygen takes place as follows:

$$(1/2)O_2 + 2H^+ + 2e^- \rightarrow H_2O$$

The flow of electric current is proportional to the hydrogen gas concentration according to Faraday's law:

$$i = zQF$$

where

F is the Faraday constant, 96486.7 A · s/mol
z is the number of exchanged electrons per molecule
Q is the conversion rate of hydrogen in mol/s

The reference electrode maintains a constant voltage at the working electrode.

Potentiometric sensors have the same structure but work at zero current, and the measured quantity is the potential difference or electromotive force between the sensing electrode and the reference electrode. The electrode potential is related to the hydrogen gas concentration and can be written according to the Nernst equation as follows:

$$E = E^0 + \frac{RT}{zF} \ln\left(\frac{a}{a_0}\right) \tag{12.2}$$

where

E is the electrode potential
E^0 is the standard electrode potential
R is the universal gas constant
T is the absolute temperature
F is the Faraday constant
z is the number of electrons taking part in the reaction
a is the chemical activity of the analytes (proportional to hydrogen concentration)
a_0 is the activity of the reference

The processes of diffusion and chemical reaction must be at equilibrium before an accurate signal can be obtained from these sensors [6,9].

12.2.3 Semiconductive Metal–Oxide Hydrogen Sensors

MOX sensors consist of two metal electrodes connected to an active material. The electrodes allow the measurement of the resistance change of the active layer that depends on the target gas concentration. The active material is a semiconducting MOX, such as SnO_2, ZnO, TiO_2, FeO, Fe_2O_3, NiO, Ga_2O_3, In_2O_3, Sb_2O_5, MoO_3, and WO_3, whose electric resistance varies in the presence of hydrogen gas.

When the sensor reaches its operating temperature (generally between 180 °C and 450 °C), oxygen chemisorbs on the surface of the MOX material and forms negatively charged adsorbed oxygen ions that create a surface potential that acts as a barrier to electron flow. Thus, oxygen is necessary to operate this type of sensor. The electric resistance of the active layer is attributed to this barrier potential. In the presence of hydrogen, the surface density of negatively charged oxygen and, consequently, the barrier potential decrease, thus reducing the electric resistance of the active layer. The resistance change can be related to the hydrogen concentration. Typically the MOX film is heated using a resistive metal film [9,10]. Figure 12.5 represents MOX sensor structure.

12.2.4 Metal–Oxide–Semiconductor Hydrogen Sensors

MOS gas sensors are characterized by a three-layer structure: a CAT metal layer is deposited over an oxide layer on a semiconductor substrate. Their operation is based on work function (measured in electron volts) variation due to the presence of hydrogen. For hydrogen detection a hydrogen-sensitive CAT metal, such as platinum or palladium (the gate metal), is deposited on the oxide layer. In the presence of hydrogen, the current–voltage (I–V) characteristics of the MOS transistor change [11]; this change can be detected indicating the presence of the gas as Figure 12.6 illustrates.

In addition to MOS transistor hydrogen sensors, there are metal–semiconductor (MS) Schottky diodes and MOS capacitors structures that can be also used to detect the hydrogen.

In Schottky diodes the CAT metal, typically palladium or platinum for hydrogen detection, is directly in contact with a semiconductive material (Figure 12.7). Hydrogen molecules adsorb onto the surface of the CAT metal and dissociate into hydrogen atoms inducing a change in the work function of the metal

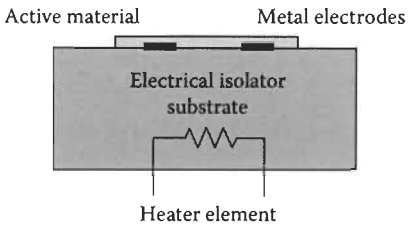

FIGURE 12.5 Typical MOX hydrogen gas sensor structure.

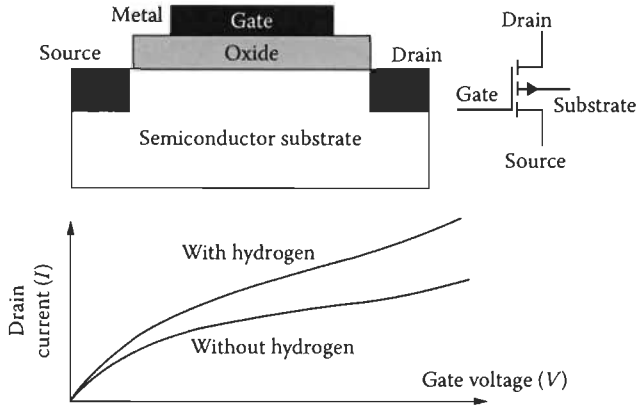

FIGURE 12.6 MOS transistor structure and the *I–V* for hydrogen detection.

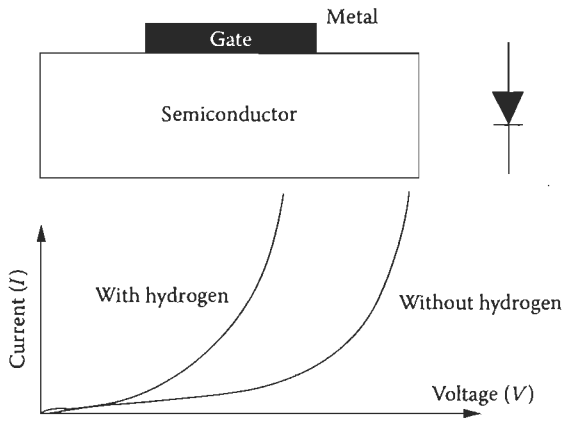

FIGURE 12.7 Schottky diode hydrogen gas sensor structure and the *I–V* curve presenting its principle of operation.

and hence the Schottky barrier height. This change in the Schottky barrier height causes a shift in the *I–V* characteristics. The response can be measured as the change in voltage when the diode is operated at constant bias current [6].

A MOS capacitor is the simplest MOS device and a cross-sectional view of a typical MOS capacitor is shown in Figure 12.8. A thin oxide layer is sandwiched between a metal layer (palladium or platinum) and a silicon substrate layer. The absorption of hydrogen and the chemical reactions at the MOX interface cause a change in the *C–V* characteristics of the capacitor and shift the flat band voltage by an amount proportional to the hydrogen gas concentration [9]. The first MOS capacitor hydrogen sensor was reported by Steele et al. in 1976 [12].

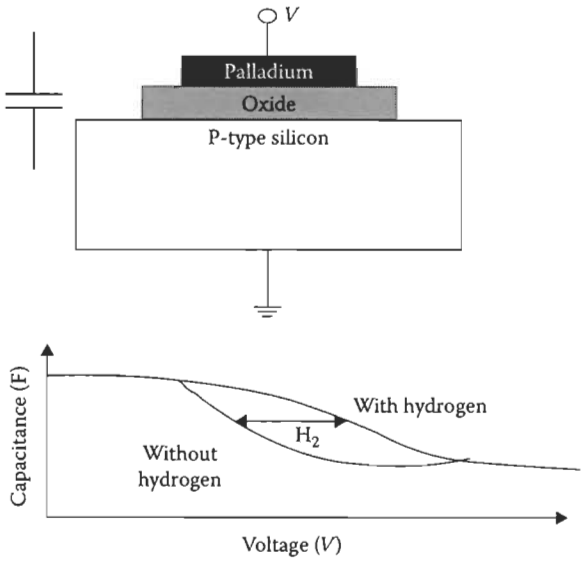

FIGURE 12.8 Typical MOS capacitor for hydrogen detection.

12.2.5 Pd-Based Hydrogen Sensors

Another class of hydrogen sensor is based on the interaction of palladium with hydrogen: the hydrogen molecule is split at the thin palladium film interface and atomic hydrogen can be accommodated in the metal lattice resulting in a change of its physical properties. The hydrogen concentration can be related to the change in the electric resistance (resistance-based sensors), to the change in metal lattice expansion (mechanical sensors), or to the change in dielectric function (optical sensors) of the sensing material. For a review of those sensors, see [6].

12.3 Hydrogen Sensor Specifications

The performance of commercial hydrogen sensors has been evaluated [6,9,13]. Table 12.1 compares the performance specifications of the most common commercial sensor types discussed in the previous sections.

12.3.1 Partial List of Hydrogen Sensor Suppliers and Manufacturers

Tables 12.2 through 12.5 list some known hydrogen sensor suppliers and manufacturers, with links to their websites.

TABLE 12.1 Performance Specifications of Commercial Hydrogen Sensor Types

	Temperature Range (°C)		Humidity (RH%)		Measuring Range (vol%)	Pressure (kPa)		Response	Recovery	Power	Life Time
Sensor	Min	Max	Min	Max	Max	Min	Max	Time (s)	Time (s)	(mW)	(Years)
CAT	−20	70	5	95	4	70	130	<30	10	1000	5
TCD	0	50	0	95	100	80	120	<10	7.5	<500	5
EC	−20	55	5	95	4	80	110	<90	2	2–700	2
MOS	−40	110	5	95	4.4	70	130	<2	10	700	10
MOX	−20	70	10	95	2	80	120	<20	10	<800	>2

Source: Hubert, T. et al., *Sens. Actuators B Chem.*, 2011.

TABLE 12.2 Partial List of Hydrogen CAT Sensor Suppliers

Sensor Supplier or Manufacturers	Websites
Neodym	http://www.neodymsystems.com/
Applied Nanotech	www.appliednanotech.net
ACME Engineering Prod.	http://www.acmeprod.com
RKI Instruments	http://rkinstruments.com/
General Monitors	http://www.generalmonitors.com/
City Technology Ltd	http://www.citytech.com/

TABLE 12.3 Partial List of Hydrogen TCD Sensor Suppliers

Sensor Supplier or Manufacturers	Websites
J. Dittrich	http://www.dittrich-systeme.de/
Neroxis	http://www.neroxis.ch/
BlueSens	http://www.bluesens.com
Advanced Gasmitter	http://www.sensors-inc.com/
MST IT	http://www.mst-it.com/
AppliedSensor	http://www.appliedsensor.com/

TABLE 12.4 Partial List of Hydrogen EC Sensor Suppliers

Sensor Supplier or Manufacturers	Websites
City Technology Ltd	http://www.citytech.com/
Solid Sense	http://www.solidsense.de/
Nemoto & Co., Ltd	http://www.nemoto.co.jp
Euro-Gas	http://www.euro-gasman.com/Sensors_intro.htm
Membrapor	http://www.membrapor.ch/
Hanwei Electronics Co., Ltd	http://english.hwsensor.com/
Synkera Technologies	http://www.synkera.com/

TABLE 12.5 Partial List of MOS and MOX Hydrogen Sensor Suppliers

Sensor Supplier or Manufacturers	Websites
Hanwei Electronics Co., Ltd	http://english.hwsensor.com/
Figaro Engineering	http://www.figarosensor.com/
e2v Technologies	http://www.e2v.com/products-and-services/instrumentation-solutions/gas-sensors/our-gas-sensor-technology/
Winsen	http://www.winsensor.com/english/news.asp
AppliedSensor	http://www.appliedsensor.com/
UST Umweltsensortechnik GmbH	http://www.umweltsensortechnik.de/index3.htm
Synkera Technologies	http://www.synkera.com/

12.4 Requirements of Hydrogen Gas Sensors

To use hydrogen gas sensors in industrial applications, general requirements described in EN IEC 60079-29-1 have to be followed [14]. The previously discussed hydrogen sensors were developed to meet these requirements as it is shown in Table 12.6, and they are suitable for applications such as the production of ammonia or methanol or for safety monitoring in nuclear power plants, where hydrogen is produced via the thermochemical splitting of water as well as stationary systems.

TABLE 12.6 Performance Requirements for Industrial Applications

Parameters	Performance Requirements
Measuring range	Up to 1 vol% H_2 in air
Lower detection limit	<0.1 vol%
Response time	<30 s
Recover time	<30 s
Life time	3–5 years

Source: Boon-Brett, L. et al., *Int. J. Hydrogen Energy*, 35, 371, 2010.

TABLE 12.7 Performance Requirements for Automotive Applications

Parameters	Performance Requirements
Measuring range	0%–4% H_2 in air
Response time	<3 s
Recovery time	<3 s
Ambient temperature	−40 °C to +125 °C
Humidity	0%–100% Relative humidity

Source: Boon-Brett, L. et al., *Int. J. Hydrogen Energy*, 35, 371, 2010.

However, for new hydrogen-based applications, the development of new technologies for the detection and measurement of hydrogen concentration requires new performance specifications for which some standards already exist [15].

The use of hydrogen as an automotive fuel represents a new application for which stringent performance specifications have been cited [16]. Table 12.7 reports the requirements for automotive applications in terms of measuring range, response time, recovery time, and operating range of temperature and humidity.

Other requirements for hydrogen sensors in automotive applications are high reliability, long lifetime, high selectivity, and adaptability to the application interface. Low-cost, small dimensions, and

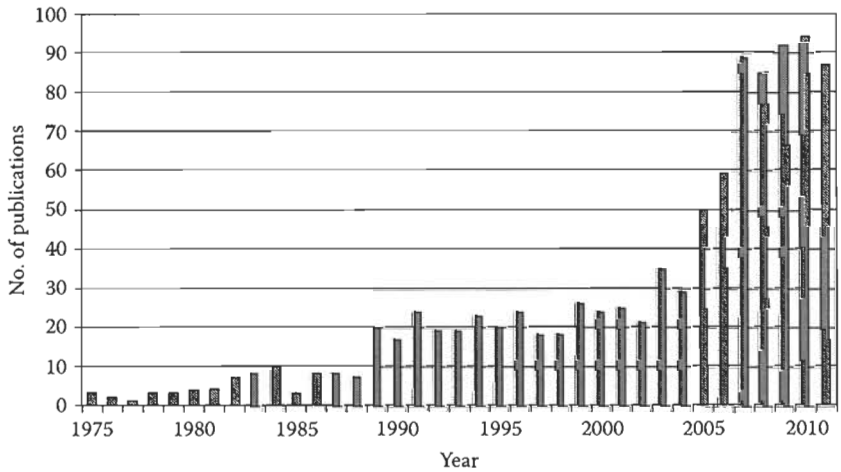

FIGURE 12.9 The number of publications in the area of hydrogen sensing according to an inquiry (June 2012) in SciVerse Scopus (www.scopus.com).

low power consumption are also important concerns for the automotive industry. From the analysis of the performance of hydrogen sensors available on the market (see Table 12.1), it is possible to conclude that there are some weaknesses concerning the performance requirements for automotive industry: although some of the automotive requirements are satisfied by the reported MOS sensor, dimensions, power consumption, and lower detection limit still need to be improved. The use of innovative technologies may enhance hydrogen sensor performance and add extra specifications allowing for integration with different systems/applications [6,7]. In fact research on novel approaches for hydrogen detection is increasing as reflected in the growing number of relevant publications in this area. Figure 12.9 shows the number of publications from 1975 until 2011.

12.5 Emerging Technologies in Hydrogen Gas Sensors

Emerging nanofabrication technologies enable the fabrication of submicron and nanometric devices working according to new hydrogen detection principles that add further performance improvements for gas sensing [17,18].

This section reviews and analyzes various emerging hydrogen-sensing techniques and discusses their advantages and weaknesses. Research and development work being performed to compensate these weaknesses is also presented.

12.5.1 Acoustic Hydrogen Gas Sensors

Acoustic technology offers a novel way of hydrogen sensing since it has the potential for passive wireless gas sensing that facilities the integration in sensor network applications. An acoustic sensor is constructed from two transducers on a piezoelectric substrate such as $LiNbO_3$ or $LiTaO_3$: one of these transducers is responsible to convert the input signal into an acoustic wave, while the second converts the acoustic wave back into an electric output signal as shown in Figure 12.10. This technique claims more robustness under different environment conditions [6].

The operating principle of acoustic gas sensor is based on the propagation of an elastic wave in the device by piezoelectric effect. The gas detection layer (usually palladium) is placed in the path of the acoustic wave between the input and the output transducers. When the sensitive layer absorbs hydrogen, a change in its mechanical (mass density), electrical properties (electric conductivity), or both will occur that produces a detectable change in the frequency of the acoustic wave. The resonant frequency at which the elastic wave propagates depends on the width of the transducer, while the mode of operation depends on elastic wave propagation mode, device geometry, and adopted technology [9]. Figure 12.10 shows a top view of the acoustic gas sensor structure.

Surface acoustic wave (SAW) mode is the most commonly used mode in hydrogen gas detection [19]. In this mode, the use of palladium or a polymer as the gas detection layer permits a mass density change (mass loading) due to the absorption of hydrogen. In this mode, the mass-loading effect dominates since the conductivity of the sensing material is too low to modify the propagation of the

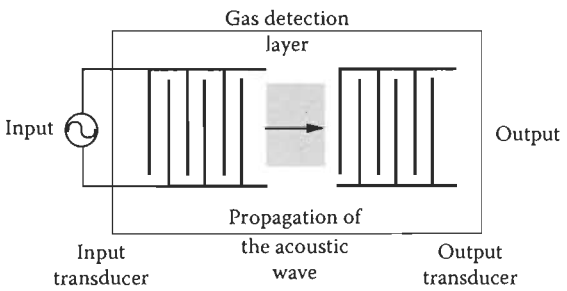

FIGURE 12.10 Top view of an acoustic gas sensor with the input and output transducer.

acoustic wave [20]. To modify the propagation of SAW by changing the electric conductivity, semiconducting MOXs such as WO_3 [21], InO_x [22], and SiN_x [23] are used. In order to improve the sensitivity of the sensitive layer in SAW devices, the gas detection layer is nanostructured to increase the surface-to-volume ratio and hence having more surface contact with the hydrogen that permits a fast response to the gas [24]. Nanostructured ZnO as well as palladium nanowires have been investigated [25,26] showing an enhancement in the sensitivity compared to film structures of the same materials. To improve the selectivity to hydrogen, SAW sensors incorporating a hydrogen catalyst with the semiconducting MOXs have been reported [27].

However, this propagation mode shows some weaknesses, especially a poor stability for temperature and humidity [8]. Therefore, the other propagation modes must be exploited for automotive industry requirements. For example, use of shear horizontal SAW (SH-SAW) sensors instead of SAW sensors reduces the effect of humidity thanks to the absence of vertical component of the wave in the first mode. Other wave propagation modes can be investigated for robustness as well as to facilitate their generation by the transducers [9].

12.5.2 Micromachined Hydrogen Gas Sensors

The advances in the field of microfabrication have permitted fabrication of three dimensional structures from a silicon substrate using micromachining techniques such as bulk micromachining, surface micromachining, dissolved wafer process, LIGA, and electrodischarge machining (EDM) [28]. The available commercial micromachined hydrogen sensors apply the same detection principles discussed previously but with microfabricated sensing elements. MOX, TCD, and CAT micromachined sensors have the advantage of improved performance compared with their conventionally fabricated counterparts.

Silicon wafers coated with silicon dioxide (SiO_2) and silicon nitride (Si_2N_3) are usually used for integration with other components or for micromachining as a sacrificial layer. The structure of the micromachined sensor is almost the same for all these detection principles, which consists of a suspended membrane on which the sensing elements are placed. The membrane is fabricated by either bulk or surface micromachining. Figure 12.11 shows the structure of the micromachined (TCD) gas sensor.

In case of CAT micromachined gas sensor, there are two suspended membranes: one for the active element and the other for the reference element that replace the beads. This can be considered as miniaturization of the classical bead structure that is usually in the order of centimeters [29]. Figure 12.12 is a cross section of a micromachined CAT sensor.

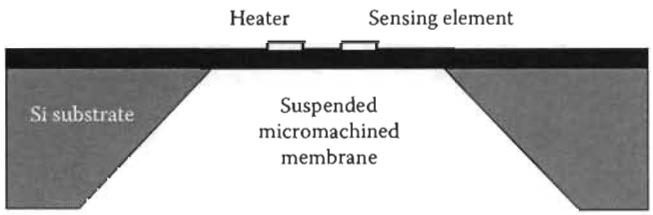

FIGURE 12.11 Micromachined structures for TCD H_2 commercial sensors.

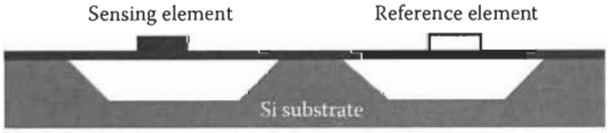

FIGURE 12.12 The structure of micromachined CAT gas sensor on Si substrate.

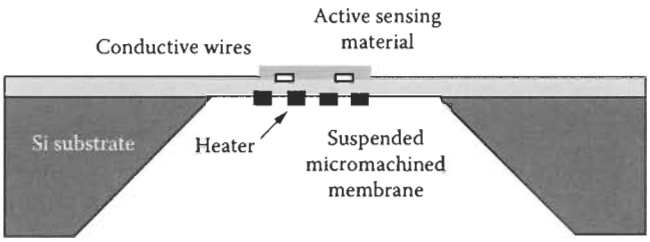

FIGURE 12.13 Micromachined structure of MOX hydrogen gas sensor.

Semiconductive MOX hydrogen sensors can also be fabricated using micromachining techniques whereby the MOX material is deposited on the micromachined suspended membrane. Some MOX structures have the heating element on the same surface as the active material [30], but it is also possible for the heater to be deposited on the underside of the membrane (Figure 12.13).

Micromachined hydrogen sensors show improved performance over conventionally designed and manufactured hydrogen sensors. They are faster and more stable under different environmental conditions. Moreover, they are cheaper and smaller and consume less power. However, there are some challenges facing these sensors and their low cost can only be realized when mass produced.

12.5.3 Nano-/Microelectromechanical System Hydrogen Gas Sensors

Nanolithography allows fabricating nano-/microelectromechanical system (N-MEMS) with high surface-to-volume ratio and with dimensions in the order of a few atomic distances. N-MEMS devices are used in several applications such as mechanical resonators, RF switches, actuators, and sensors. N-MEMS resonators have a quality factor in the order of $\sim 10^3$ and an operation frequency in the MHz range. Their functionality is based on the mechanical motion of their components due to an external stimulus. Designing an N-MEMS resonator implies choosing the material and the geometry of the structure. For example, a double-clamped N-MEMS beam resonator has a resonant frequency f_0 given by [31–33]

$$f_0 = 1.03 \frac{w}{L^2} \sqrt{\frac{E}{\rho}} \tag{12.3}$$

where

w is the width

L is the length of the beam

E and ρ are the Young modulus and the density of the material, respectively

The N-MEMS resonator is usually actuated by an external source to reach its mechanical resonance frequency.

NEMS/MEMS resonator devices allow for gas detection by introducing a gas-sensitive layer. For example, N-MEMS can be used for hydrogen sensing in MHz range using gold–palladium alloy as detection material [31]. The sensing mechanism of this sensor is based on resonant frequency shift due to the presence of the hydrogen gas. Another N-MEMS hydrogen sensor has been presented [34], showing the advantage of low power consumption and high sensitivity under ambient conditions [35–37].

12.6 Conclusion

This chapter has reviewed commercially available hydrogen sensor technologies and has discussed the physical principles of hydrogen detection in each of these technologies. The chapter has summarized the performances and operating conditions of each sensor type and compared them to the current industrial

requirements and to the emergent hydrogen applications requirements. Gaps still exist between the sensor performance requirements for emerging applications and the actual performance of commercial hydrogen sensors. Novel hydrogen detection techniques have the potential to enhance hydrogen sensor performance in order to meet the needs of these emerging markets.

References

1. S. Blanchette Jr., A hydrogen economy and its impact on the world as we know it, *Energy Policy*, 36(4), 522–530, 2008.
2. ENEA-consulting, Application des systèmes Hydrogène pour les besoins du développement à horizon 2020–2025, Mai 2011, http://www.enea-consulting.com/wp-content/uploads/Rapport-H2-Dvlpmt-Final.pdf, accessed in August 2013.
3. W.M. Haynes (Ed.), *CRC Handbook of Chemistry and Physics*, 92th edn., 2011–2012.
4. J.G. Firth, A. Jones, T.A. Jones, The principles of the detection of flammable atmospheres by catalytic devices, *Combustion and Flame*, 20, 303–311, 1973.
5. E. Jones, The pellistor catalytic gas detection, in: P. Moseley, B.C. Tofield (Eds.), *Solid State Gas Sensors*, Adam Hilger, Bristol, England, pp. 17–31, 1987.
6. T. Hubert, L. Boon-Brett, G. Black, U. Banach, Hydrogen sensors—A review, *Sensors and Actuators B: Chemical*, B157, 329–352, 2011.
7. J.F. McAleer et al., Tin dioxide gas sensor: Use of the Seebeck effect, *Sensors and Actuators*, 8, 251–257, 1985.
8. M. Watanabe, R. Inoue, D. Ichikawa, K. Furusaki, Development of thermal conductivity type hydrogen sensor, *ECS Transactions*, 28(20), 31–42, 2010.
9. I. Kerroum, H. El Matbouly, F. Domingue, Survey of commercial sensors and emerging miniaturized technologies for safety applications in hydrogen vehicles, *IEEE Sensors Applications Symposium (SAS)*, Brescia, Italy, 2012.
10. B. Lutz, R. Wind, C. Kostelecky, D. Routkevitch, D. Deininger, Development of ultra-low power metal oxide sensors and arrays for embedded applications, *AIP Conference Proceedings*, New York, Vol. 1362, pp. 62–63, 2011.
11. T. Usagawa, Y. Kikuchi, Device characteristics for Pt–Ti–O gate Si–MISFETs hydrogen gas sensors, *Sensors and Actuators B*, 160, 105–114, 2011.
12. M.C. Steele, J.W. Hile, B.A. MacIver, Hydrogen-sensitive palladium gate MOS capacitors, *Journal of Applied Physics*, 47, 2537–2538, 1976.
13. L. Boon-Brett, J. Bousek, P. Moretto, Reliability of commercially available hydrogen sensors for detection of hydrogen at critical concentrations: Part II—Selected sensor test results, *International Journal of Hydrogen Energy*, 35, 562–571, 2009.
14. IEC 60079-29-1. Ed. 1.0, Explosive atmospheres—Part 29-1: Gas detectors—Performance requirements of detectors for flammable gases, 2007, http://webstore.iec.ch/preview/info_iec60079-29-1%7Bed1.0%7Db.pdf, accessed on August 9, 2013.
15. ISO 26142, Hydrogen detection apparatus, 2010, http://www.iso.org/iso/catalogue_detail.htm?csnumber=52319, accessed on August 8, 2013.
16. L. Boon-Brett, J. Bousek, G. Black, P. Moretto, P. Castello, T. Hübert, U. Banach, Identifying performance gaps in hydrogen safety sensor technology for automotive and stationary applications, *International Journal of Hydrogen Energy*, 35, 371–384, 2010.
17. M. Dragoman, A. Muller, D. Neculoiu, G. Konstantinidis, K. Grenier, D. Dubuc, L. Bary, R. Plana, H. Hartnagel, E. Fourn, E. Flahaut, Carbon nanotubes-based microwave and millimeter wave sensors, *Proceedings of the 37th European Microwave Conference*, Munich, Germany, October 2007.
18. P. Zhang, Design and fabrication of chemiresistor type micro/nano hydrogen gas sensors using integrated electrodes, PhD thesis, University of Central Florida, Orlando, FL, 2008.

19. A. D'Amico, A. Palma, E. Verona, Surface acoustic wave hydrogen sensor, *Sensors and Actuators*, 3, 31–39, 1982.
20. S.J. Ippolito, S. Kandasamy, K. Kalantar-Zadeh, W. Wlodarski, A. Holland, Comparison between conductometric and layered surface acoustic wave hydrogen gas sensors, *Smart Materials and Structures*, 15, 131–136, 2006.
21. W.P. Jakubik, Investigations of thin film structures of WO_3 and WO_3 with Pd for hydrogen detection in a surface acoustic wave sensor system, *Thin Solid Films*, 515, 8345–8350, 2007.
22. S.J. Ippolito, S. Kandasamy, K. Kalantar-Zadeh, W. Wlodarski, K. Galatsis, G. Kiriakidis, N. Katsarakis, M. Suchea, Highly sensitive layered ZnO/$LiNbO_3$ SAW device with InO_x selective layer for NO_2 and H_2 gas sensing, *Sensors and Actuators B*, 111–112, 207–212, 2005.
23. A.C. Fechete, W. Wlodarski, K. Kalantar-Zadeh, A.S. Holland, J. Antoszewski, S. Kaciulis, L. Pandolfi, SAW-based gas sensors with rf sputtered InO_x and PECVD SiN_x films: Response to H_2 and O_2 gases, *Sensors and Actuators B*, 118, 362–367, 2006.
24. C. Drake, S. Deshpande, D. Bera, S. Seal, Metallic nanostructured materials based sensors, *International Material Reviews*, 52, 259–317, 2007.
25. F.-C. Huang, Y.-Y. Chen, T.-T. Wu, A room temperature surface acoustic wave hydrogen sensor with Pt coated ZnO nanorods, *Nanotechnology*, 20, 065501, 2009.
26. C. Caliendo, I. Fratoddi, M.V. Russo, Nanostructured organometallic polymer and palladium/polymer hybrid: Surface investigation and sensitivity to relative humidity and hydrogen in surface acoustic wave sensors, *Nanotechnology*, 18, 125504, 2007.
27. P.J. Shaver, Activated tungsten oxide gas detector, *Applied Physics Letters*, 11, 255, 1997.
28. S.A. Tadigadapa, N. Najafi, Developments in microelectromechanical systems (MEMS): A manufacturing perspective, *Transactions of the ASME*, 125, 816–823, 2003.
29. E.-B. Lee, I.-S. Hwang, J.-H. Cha, H.-J. Lee, W.-B. Lee, J.J. Pak, J.-H. Lee, B.-K. Ju, Micromachined catalytic combustible hydrogen gas sensor, *Sensors and Actuators B*, 153, 392–397, 2011.
30. I. Simon, N. Bârsan, M. Bauer, U. Weimar, Micromachined metal oxide gas sensors: Opportunities to improve sensor performance, *Sensors and Actuators B*, 73, 1–26, 2001.
31. X.M.H. Huang et al., Nanomechanical hydrogen sensing, *Applied Physics Letters*, 86, 143104, 2005.
32. C. Durand, Développement de résonateurs électromécaniques en technologie Silicon On Nothing, à détection capacitive et amplifiée par transistor MOS, en vue d'une co-intégration permettant d'adresser une application de référence de temps, PhD thesis, Université des Sciences et Technologies de Lille, Lille, France, N d'ordre: 4337, janvier 2009.
33. N.V. Lavrik, M.J. Sepaniak, P.G. Datskos, Cantilever transducers as a platform for chemical and biological sensors, *Review of Scientific Instruments*, 75(7), 2229, 2004.
34. J. Henrriksson, L.G. Villanueva, and J. Brugger, Ultra-low power palladium-coated MEMS resonators for hydrogen detection under ambient conditions, *Transducers'11*, Beijing, China, June 5–9, 2011.
35. X.L. Feng, C.J. White, A. Hajimiri, M.L. Roukes, A self-sustaining ultrahigh-frequency nanoelectromechanical oscillator, *Nature*, 3, June 2008.
36. M. Dragoman et al., Carbon nanotubes-based microwave and millimeter wave sensors, *Proceedings of the 37th European Microwave Conference*, Munich, Germany, October 2007.
37. M. Li, B. Myers, X. Tang, S.J. Aldridge, C. McCaig, J.J. Whiting, R.J. Simonson, N.S. Lewis, M.L. Roukes, Nanoelectromechanical resonator arrays for ultrafast, gas-phase chromatographic chemical analysis, *Nanoletters*, 10, 3899–3903, 2010.
38. G. Tortissier, Étude et développement d'une plateforme de détection chimique à ondes acoustiques de surface pour environnement sévère haute température, PhD thesis, University Bordeaux 1, Bordeaux, France, 2009.
39. M. Kimura, N. Takashima, MEMS hydrogen gas sensor for the entire concentration range of hydrogen gas, *Sensors and Materials*, 23(7), 201, 2011.

5.2 Contribution II revue: «Assessment of commercial micro-machined hydrogen sensors performance metrics for safety sensing applications»

L'article présente une étude expérimentale sur les éléments de détection micro-machinés commerciaux et une comparaison des résultats aux systèmes de détection traditionnels. Bien que certaines améliorations de performances aient été observées pour les capteurs micro-machinés commerciaux par rapport à leurs homologues conventionnels, les résultats montrent aussi cependant que la majorité des capteurs micro-machinés souffrent d'une dégradation significative de certains aspects en termes de performances. Ce travail vérifie expérimentalement les métriques de détection pour les capteurs de type TC et MOX fabriqués via des techniques de conception micro-technologiques. Les objectifs spécifiques de cette étude sont les suivants:

- Étudier de nouveaux capteurs d'hydrogène commerciaux micro-fabriqués et mesurer leurs performances.

- Fournir aux utilisateurs finaux une ressource pour prendre des décisions éclairées sur la sélection d'une technologie de détection spécifique pour leurs applications.

- Informer et orienter les concepteurs et les développeurs de capteurs sur les types de modifications de conception pouvant certes améliorer certaines performances d'un dispositif de détection mais aussi par la même occasion, entrainer des dégradations involontaires et surtout non tolérables par rapports aux exigences du marché actuel.

Les procédures expérimentales et les courbes de performance sont présentées dans l'article. La performance de l'élément de détection TC micro-machiné est supérieure ou égale à son homologue traditionnel sur tous les paramètres analytiques critiques. Comparé au modèle traditionnel dont les performances de temps de réponse sont évaluées à 26.1±1.16 s, celles des systèmes de détection à technologie TC ont de meilleurs temps de réponse avoisinant 6.7±0.6 s. Ce qui n'est pas le cas pour la plupart des systèmes de détection MOX micro-machinés.

La réponse du capteur micro-machiné est linéaire dans la plage de 0-2% H2. Cela n'implique pas que la fabrication des éléments sensibles MOX (ou des systèmes de détection CAT) est fondamentalement incompatible avec la méthode de micro-usinage. Cependant, due à la complexité structurelle de tels dispositifs et des contraintes liées aux exigences de fabrication (par exemple, des structures en couches avec des revêtements catalytiques fonctionnant à des températures élevées), il est plus difficile de concevoir des dispositifs entièrement micro-usinés sans pour autant avoir des mesures compromises.

Ce travail a été effectué dans le cadre d'un stage sur la sûreté de l'hydrogène (IEA HIA-tâche 31) au centre «JRC-European Commission, Institute for Energy & Transort, Petten», aux Pays-Bas. Mes principales tâches consistaient :

- A effectuer des tests de performances de capteurs,
- A analyser les résultats expérimentaux obtenus,

- A échanger et valider les résultats dans le cadre de la collaboration avec (NREL aux É.U)

- Et finalement à rédiger l'article en assurant la coordination avec les auteurs afin de satisfaire et intégrer les idées et concepts intellectuels de chacun.

INTERNATIONAL JOURNAL OF HYDROGEN ENERGY 39 (2014) 4664–4673

Available online at www.sciencedirect.com

ScienceDirect

journal homepage: www.elsevier.com/locate/he

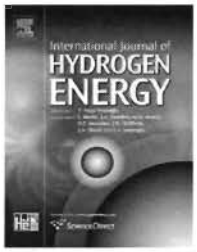

Assessment of commercial micro-machined hydrogen sensors performance metrics for safety sensing applications

H. El Matbouly [a,*], *F. Domingue* [a], *V. Palmisano* [b], *L. Boon-Brett* [b], *M.B. Post* [c], *C. Rivkin* [c], *R. Burgess* [c], *W.J. Buttner* [c]

[a] *Laboratoire de microsystèmes et télécommunications, Université du Québec à Trois-Rivières, Trois-Rivières, Québec, Canada*

[b] *European Commission, DG Joint Research Centre, Institute for Energy and Transport, PO. Box 2, 1755 ZG Petten, The Netherlands*

[c] *Transportation and Hydrogen Systems Center, National Renewable Energy Laboratory, 15013 Denver West Parkway, Golden, CO 80401-3305, USA*

ARTICLE INFO

Article history:
Received 14 November 2013
Received in revised form
7 January 2014
Accepted 8 January 2014
Available online 1 February 2014

Keywords:
Hydrogen sensors
Sensing element
Hydrogen safety applications
Thermal conductivity
Metal oxide
Micro-machine

ABSTRACT

Hydrogen sensors are increasingly recognized as safety enhancing components in applications where hydrogen is used as a clean energy carrier. The availability of low-cost, reliable, high performance hydrogen sensors is critical for facilitating the widespread and safe deployment of hydrogen systems. Accordingly, new sensing element designs based on advanced manufacturing techniques are being developed. Using micro-machining techniques, miniaturized versions of conventional hydrogen gas sensing elements have already been introduced in the market, with the promise of low-cost and high performance sensing metrics. An assessment of commercial micro-machined sensing elements relative to their conventional counterpart is presented in this paper. The results show that although some performance improvements were observed for commercial micro-machined sensors relative to their conventional counterparts, some models of micro-machined sensors were plagued with significant performance degradation. Furthermore, actual sensor performance, as determined by laboratory assessment often did not meet the manufacturer's published specifications. This work verifies the sensing metrics improvements brought by the micro-technology as well as its shortcomings for guiding the end-user safety applications.

* *Corresponding author.* Tel.: +1 8193765011.
E-mail addresses: hatem.el.matbouly@uqtr.ca, hatemelmatbouly@yahoo.ca (H. El Matbouly), frederic.domingue@uqtr.ca (F. Domingue), valerio.palmisano@ec.europa.eu (V. Palmisano), lois.brett@ec.europa.eu (L. Boon-Brett), matthew.post@nrel.gov (M.B. Post), carl.rivkin@nrel.gov (C. Rivkin), robert.burgess@nrel.gov (R. Burgess), william.buttner@nrel.gov (W.J. Buttner).

0360-3199/$ – see front matter
http://dx.doi.org/10.1016/j.ijhydene.2014.01.037

1. Introduction

Access to clean, affordable, and safe energy is essential to assure high quality of life, industrial growth, and economic development. Hydrogen has been identified as a viable alternative energy carrier [1], and its use is rapidly expanding in industries such as automotive [2], forklift [3], and back-up power systems [3]. When produced from renewable energy sources, hydrogen offers solutions to environmental and supply security problems associated with fossil fuels [4,5]. As a gas, hydrogen has physical and chemical properties that require special considerations to ensure its safe use. Because it is odorless and colorless, human senses will not directly respond to hydrogen; thus, sensors are used for its detection [6]. Markets for hydrogen sensors already exist, such as for monitoring battery back-up systems, and in the mining, petroleum, chemical and aerospace industries. However the demand for hydrogen sensors is growing rapidly as the hydrogen infrastructure expands to support the production, storage, distribution and dispensing of hydrogen as a fuel for automotive applications (including the 2015 projected release of commercial hydrogen-powered fuel cell electric vehicles) and stationary applications such as domestic combined heat and power applications and uninterrupted power supply applications. Both established and emerging markets demand low-cost reliable hydrogen sensors [7].

To ensure the availability of hydrogen sensors to meet end-user needs, both the Office of Energy Efficiency and Renewable Energy (EERE) within the U.S. Department of Energy (DOE) [8] and the European Commission Joint Research Centre (JRC) established sensor test facilities [9,10]. One common mission of the DOE and the JRC sensor laboratories is to educate the hydrogen community on the proper use of hydrogen sensors; this includes providing an unbiased assessment of performance and limitations associated with different sensor designs [11]. As part of its commitment to hydrogen safety, DOE organized several hydrogen sensor workshops to identify specific sensor specifications required for hydrogen infrastructure [12,13]. Participants in each workshop included a range of stakeholders in the hydrogen community, including end-users, sensor developers, and safety, code and standard officials. Cost and response time were identified as critical gaps for hydrogen sensors. As an outcome of the workshops, the DOE assigned a target specification of a 1 s response time for low-cost sensors/sensing elements [14]. To a significant extent these two requirements have guided hydrogen sensor development since 2005. One strategy employed by sensor developers to improve response time so as to meet the DOE target is to miniaturize geometric dimensions of the sensing element. Similarly, low-cost manufacturing methods relying on economy of scale production are being implemented to lower sensing element unit cost. Both response time improvements via miniaturization and economy of scale production can be potentially achieved using micro-machining manufacturing techniques. Indeed micro-machined hydrogen sensing elements for numerous platform types are now commercially available (e.g., catalytic – CAT, thermal conductivity – TC, metal oxide – MOX).

Micro-machined hydrogen sensing elements for each of these platform types have shown dramatic improvements in response times, although achievement of DOE response time target of 1 s remains elusive. Further, cost reductions can be expected as the market grows so as to properly exploit economy of scale production. However, some manufacturers of commercial devices seemed to have overly focused on response time, paying less attention to other critical sensor metrics. Many commercial hydrogen micro-machined sensing elements suffer severe degradations in some critical metrics relative to their conventional analogs, including long- and short-term stability, dynamic range, robustness to harsh environments, and repeatability. Through a comparison of conventional and micro-machined hydrogen sensor performance as measured in the NREL and JRC sensor test facilities, this study examines the impact of miniaturization on the performance metrics of representative commercial micro-machined sensing elements. The specific aims of this study are to:

- Provide end-users a resource to make better informed decisions on the selection of a sensing technology for their application,
- Inform and guide sensor manufacturers and developers on design modifications that improve one performance metric but may have unintended and unacceptable degradations in other metrics,
- Provide guidance on allocation of limited resources for R&D support.

This paper will use the nomenclature presented in ISO 26142 [15] to distinguish between sensor and sensing element. The sensing element is the component (electrochemical, thermal conductivity, etc.) that reacts with or responds to the analyte gas (e.g., hydrogen) to generate a response that can then be processed into an electrical signal. The control circuitry and user interface allow practical use of this signal. Developers of sensing technology often use the word sensor to describe the sensing element; however, in this report, sensor will refer to an instrumented system composed of a sensing element, control circuitry, and a user interface that provides analytically useful information to the end-user.

2. Micro-machined hydrogen sensing elements

2.1. Definition

A micro-machined device is a three-dimensional structure with micrometer-scale dimensions typically manufactured using silicon micro-fabrication techniques. Occasionally, sensor developers use the term *microelectromechanical systems* (MEMS) to describe their sensor structure because fabrication protocols to produce MEMS devices and non-MEMS micro-fabricated devices are similar. MEMS devices are mechanical devices fabricated at micrometer scale using a micro-machining process on a substrate. However, MEMS devices incorporate some form of actual mechanical motion or vibrations [16]. Thus, a critical distinction is that MEMS devices

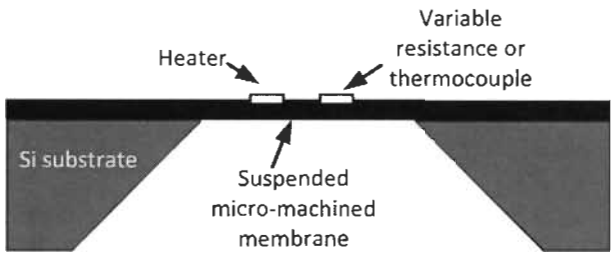

Fig. 1 – The structure of a commercial micro-machined TC sensing element for hydrogen.

contain a mechanical moving part that can be actuated, for example, by the introduction of a target gas that induces changes in mechanical motion, such as the mechanical resonance frequency of the sensing element, in a MEMS gas sensor. In the absence of a mechanical component, the term *micro-machined* is more appropriate. Although there are commercial micro-machined hydrogen sensors, no MEMS hydrogen sensor is commercially available to the authors' knowledge. However, recent research shows the possibility of hydrogen detection using MEMS mechanical resonators [17].

2.2. *Overview of common micro-machined hydrogen detection platforms*

A literature and market survey indicated that most commercial micro-machined hydrogen safety sensing elements were based on the TC, MOX, and CAT platforms.

2.2.1. *Thermal conductivity sensor*

TC sensors rely on a temperature-induced change of resistance in a heated sensing element following exposure to the analyte. The TC sensing element is heated slightly above ambient temperature. In addition to the input power, which is electronically controlled, the TC coefficient (λ) of the surrounding gas affects the device temperature. A higher λ leads to a greater transfer of heat to the surrounding environment. The λ for hydrogen is 174 mW m^{-1} K^{-1}, the highest of any known gas. TC sensors exploit this property to detect and monitor hydrogen in air or in other gas matrices. Although often marketed as a hydrogen sensor, the TC sensor is actually sensitive to a broad range of chemical vapors. The TC sensor is, in fact, often deployed as a nonspecific detector in a gas chromatograph. However, the sensitivity to changes in hydrogen concentration is significantly greater than for any other gas or vapor. For comparison, λ for helium is 142 mW m^{-1} K^{-1}, 30.0 mW m^{-1} K^{-1} for methane, and 24.3 mW m^{-1} K^{-1} for nitrogen. It should be noted that in the TC sensor, the transduction mechanism is associated with a change of a physical property (i.e., a change in the temperature of the sensing element induced by a change of the TC of the surrounding gas). This means that the test gas does not react chemically with the sensing element and the composition of the test gas remains unchanged. For this reason, the TC sensors tend not to be as prone to degradations induced by chemical interactions as other platforms [18].

Conventional TC sensing elements typically use a noble metal filament suspended between two mounting posts. For operation, the filament is typically heated electrically by passing current through it (e.g., Joule heating). The final packaged sensor has a dimension of approximately 1 cm^2, excluding support circuitry.

A micro-machined TC sensing element uses micron-scale features constructed either by surface or bulk micromachining (or a combination of the two) [19]. A representation of a TC microstructure sensing element is shown in Fig. 1. The sensing element is composed of a temperature-dependent resistance film or a thermocouple and a separate planar heater, both integrated onto a micro-machined membrane. The heat convection between the heater and the sensing element is altered as the composition of the surrounding gas changes; this alters the temperature of the sensing element and thereby affects its resistance or the voltage generated by the thermocouple in case of a thermocouple sensing element. The dimensions of a micro-machined TC sensing element are in the range of 10–1000 μm^2.

2.2.2. *Metal-oxide sensor*

The MOX sensor is a polycrystalline solid-state device with a wide band-gap material as the sensing element. MOX semiconductors use tin oxide (SnO_2) or other metal oxides as the sensing material. The MOX sensor is typically an insulator at room temperature but becomes conductive at elevated temperatures. The adsorption of a gas changes the electron density within the band structure of the MOX polycrystalline material, which leads to a conductivity change. The amount of that change depends on the nature and concentration of the gas and on the type of MOX material. In the presence of hydrogen, the resistance of the MOX decreases [20].

In the conventionally fabricated MOX sensing element, the active material is usually embedded in a porous sintered glass matrix and shaped as a bead around an internal heater coil. The hydrogen can diffuse inside the pores and interact with the oxide, leading to a reduction of its oxygen content, which leads to lowering the surface potential between the grains and hence the resistance of the sensing element [21].

Micro-machined MOX gas sensing elements have been extensively reported and reviewed. For example, in 2001 Simon et al. [22] discussed micro-machining processes for MOX sensing elements and sensing layer deposition techniques. The micro-machined sensing elements consisted of an insulating micro-machined membrane with the top surface coated with interdigitated electrodes on which the MOX

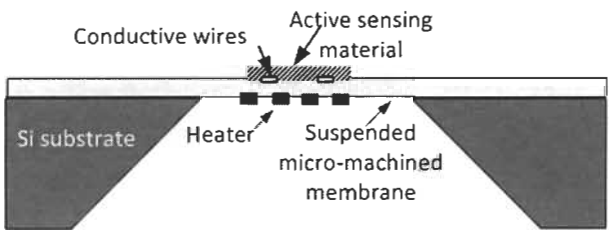

Fig. 2 – The structure for a micro-machined MOX sensing element for hydrogen.

sensing material was deposited [23]. An integrated heater was fabricated on the underside of the membrane. The membrane electrically isolated the gas sensing layer from the heater. Fig. 2 shows the structure of this MOX micro-machined sensing element design. This micro-machined sensing element design had lower power requirements than that of conventional MOX sensing elements. It was also reported that other performance metrics were improved by micro-machining, such as lower detection limit (LDL) and dynamic range. It is important to note that there are many varieties of micro-machined MOX sensors and the cited structure is only a representative design [24]. Experimental evaluations, as discussed below, show that not all micro-machined MOX sensing elements exhibit improved performance metrics relative to conventional designs.

2.2.3. *Catalytic sensor*

CAT sensing elements are based on the generation of heat induced by the thermal oxidation (e.g., combustion) of hydrogen or other combustible gases on a catalytic surface. Conventional CAT sensing elements typically have a platinum wire embedded in a ceramic bead (pellistor). Heating of the catalytic bead by surface combustion increases the temperature of the bead, thereby inducing an increase in the resistance of the embedded wire. CAT sensing elements often include a reference isolated pellistor that does not react with the analyte. Both the active and isolated pellistors are mounted on a Wheatstone bridge. Exposure of the active pellistor to a combustible gas changes the resistance of the platinum wire, which creates an imbalance in the Wheatstone bridge. The combustible gas concentration is related to the change in the resistance of the heated platinum wire [25]. Micro-fabrication techniques have been used to construct hydrogen CAT sensing elements [26,27]. Fig. 3 shows a generic structure. One of the earliest micro-machined CAT sensing elements was based on surface silicon micro-machining technology [28] and had dimensions of approximately 850 μm^2.

3. Experimental

This study was initiated to assess general sensor performance behavior associated with different design features. Typically three sensors of a specific model type were assessed per test. It was not an assessment of a specific technology or product, and for this reason, no sensor or sensing element model, manufacturer, or part number has been identified as per the respective policies of the sensor testing laboratories.

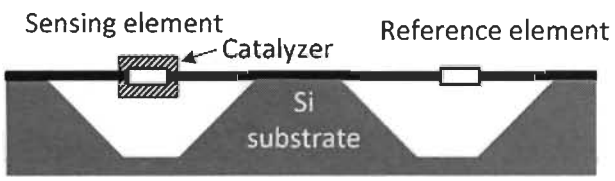

Fig. 3 – The structure for a micro-machined CAT sensing element for hydrogen.

3.1. *Sensor platforms*

A market survey was performed to identify commercial-off-the-shelf hydrogen sensors and sensing elements available in both micro-machined and conventional formats. TC sensors with conventional and micro-machined sensing elements were purchased and tested (i.e., the sensing elements were instrumented into a sensor package by the manufacturer). The commercial TC sensors had an electronic output that was readily converted to volume percent of hydrogen (vol % H_2) using the calibration procedure provided by the manufacturer, thereby allowing direct quantitation of hydrogen in the test gas. MOX sensing elements without commercial control circuitry were also purchased and tested. The MOX sensing elements (conventional & micro-machined) had a resistive output that was transduced to a voltage using in-house circuitry built according to manufacturer recommendations. A commercial micro-fabricated CAT sensing element was previously evaluated [29]. In the previous study it was found that following repetitive exposures to hydrogen, there was both degradation in performance and a change in the microstructure of the CAT sensing material. Furthermore, the tested device tended to fail prematurely due to a lack of physical robustness. The results from this study indicated that this particular CAT sensing element did not meet the minimum performance requirements to be included in the current study. However, the use of TC and MOX platforms was sufficient to illustrate the potential positive and negative impacts associated with sensing element miniaturization, which is the primary goal of this paper.

3.2. *Sensor test apparatus*

The evaluation of hydrogen safety sensors and sensing elements is an ongoing activity within the sensor test facilities at the JRC-Institute for Energy and Transport and at the U.S. Department of Energy's (DOE's) National Renewable Energy Laboratory (NREL) [30]. The sensor test apparatus in each facility was designed with advanced capabilities, including parallel testing of multiple gas sensors or sensing elements, sub-ambient to elevated temperature, sub-ambient to elevated pressure, and humidity control from dry to 95%. Each sensor test apparatus was instrumented with temperature, pressure, humidity and mass flow probes certified to national standards. Control of gas parameters was achieved with multiple precision mass flow controllers operating in parallel. Test gas composition was thus dynamically controlled via regulation of the mass flow controller set points. It was also possible to continuously verify gas composition using gas analyzers (mass spectrometer or gas chromatograph) to provide independent and near real-time analysis of the test gas composition and concentration. Inter-laboratory testing of identical sensors confirmed that the NREL and JRC facilities provide quantitatively identical sensor performance assessments [11]. Testing of the sensors was performed using test protocols developed by and routinely used in both the JRC and NREL sensor test facilities. The test protocols were analogous to those recommended in international standards and included linear/dynamic range and short-term stability/repeatability measurements. In addition, sensor response and

recovery time measurements were performed using a dedicated test fixture and validated test method (flow-method) described previously [31]. The response time, t_{90}, is defined as the interval between the time when an instantaneous variation from clean air to the test gas is produced at the inlet of the hydrogen sensor and the time when the response reaches 90% of the maximum indication. The recovery time, t_{10}, is defined as the interval between the time when an instantaneous variation from the test gas to clean air is produced at the inlet of the hydrogen sensor and the time when the response reaches 10% of the preceding maximum indication. During these tests, the impact of gas flow rate on sensor response kinetics was also evaluated.

Typically, sensor evaluations were performed at 25 °C, 1 bar pressure, and 50% relative humidity. Test gas concentrations ranged from 0 to 2 vol% H_2 in air, with specific concentrations and exposure sequences indicated for each test. Test gas mixtures were generated from cylinders of air and 2 vol% H_2 in air. Laboratory protocol allowed for the hydrogen to be within 10% of its nominal value (e.g., 1.8–2.2 vol% H_2), but the actual concentration was certified to 1.0%. For each test condition, the sensor response was taken as the "final indication" as per the criteria defined in ISO 26142; this is essentially the steady-state sensor response, but may accommodate sensors with slowly drifting signals.

All sensors and sensing elements were operated following the recommendations provided by the manufacturer and within their specified operating conditions.

4. Results and discussion

In an earlier investigation, poor short-term stability and a lack of robustness were observed on a specific commercial CAT micro-machined hydrogen sensing element model [29], whereas conventionally designed CAT sensors are routinely and reliably used. This indicated that the transformation of sensing element platforms from conventional to micro-machined designs might not be straight forward. Since a CAT platform was evaluated previously, this study focused on other platforms, namely TC and MOX.

This section compares the results of the performance tests done on the MOX and TC micro-machined hydrogen gas sensing elements and their conventional analogs.

4.1. *Thermal conductivity hydrogen sensors*

Conventional and micro-machined TC sensing elements were obtained. The performance comparisons described in this paper were restricted to one model each for the conventional and the micro-machined sensing elements. In part this was due to a limited availability of moderately priced commercially available micro-machined TC sensing elements (e.g., the unit price in small quantity can be <1000 euros each, while in large quantities, the price can drop to <10 euros each). Numerous conventional TC platforms were previously tested in separate but unpublished studies by the NREL and JRC laboratories. The various conventional TC sensing element models exhibited comparable performance behavior for many critical metrics, including those specifically evaluated in this study.

4.1.1. *Response and recovery times*

The response time, t_{90}, and the recovery time, t_{10}, were measured for sensors instrumented with micro-machined and conventional TC sensing elements under gas flow rates ranging from 50 to 200 standard cubic centimeters per minute (sccm). The test gas was 0.5 vol% H_2 in air.

Fig. 4 compares the response and recovery times between a micro-machined TC sensing element relative to a conventional TC sensing element, and clearly indicates the improvement in response and recovery times that can be achieved with TC sensing element miniaturization. The response time for the micro-machined TC sensing element was 6.7 ± 0.6 s while the response time of the conventional sensing element was 26.1 ± 1.16 s. The response time of the conventional TC sensing element exhibited a flow-rate dependence systematically decreasing from 29 s at 50 sccm to 24 s at 200 sccm. In contrast, the flow-rate dependence on the response time for the micro-machined TC sensing element was negligible over the flow rate range tested. The micro-machined TC sensing element also

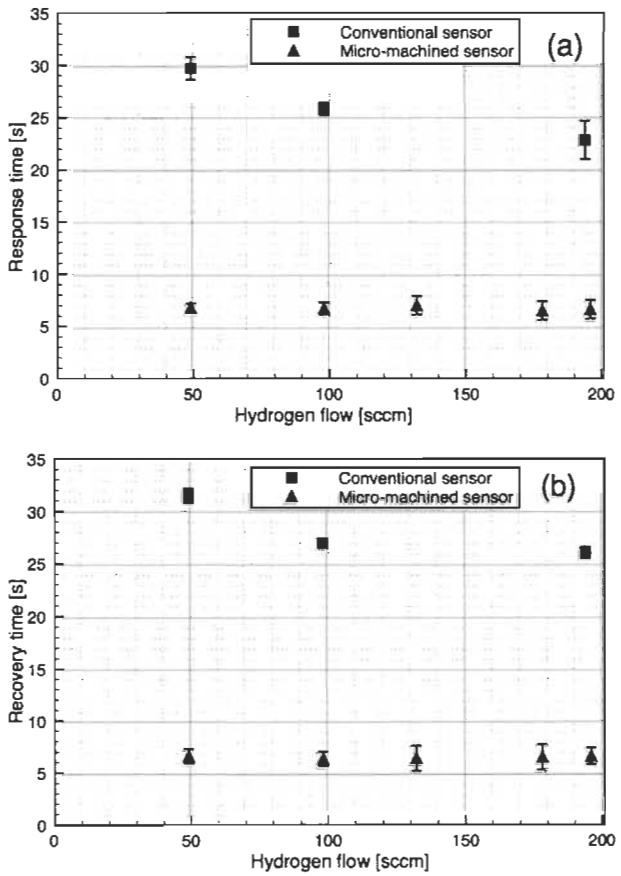

Fig. 4 – (a) Response time and (b) recovery time as a function of the gas flow rate for micro-machined and conventional TC sensing elements. Measurements were made in 0.5 vol% H_2 in air. The error bars represent the standard deviation for four and five independent measurements.

showed faster recovery kinetics. The recovery time of the conventional sensing element ranged from 32 s to 26 s, depending on flow rate, while the recovery time of micro-machined sensing element was 6.7 ± 0.5 s for all flow rates. This is nearly 5 times faster than the conventional sensing element response. The micro-machined TC sensing element showed no flow-rate dependence for response and recovery times over the flow-rate range tested. In contrast, the response and recovery times for conventional TC sensing elements were flow-rate dependent. It is noted that for both the conventional and micro-machined TC sensing elements the respective recovery and response times were nearly identical. This is because the TC transduction mechanism is controlled by physical rather than chemical interactions with the environment.

Miniaturization of the TC sensing element through micro-machining improved the response and recovery times by nearly a factor of 5. Although not yet achieving the DOE's target of a 1 s response time, miniaturization dramatically improved device kinetics.

4.1.2. *The influence of the gas flow rate on the final indication*

The final indications of the TC sensing element were measured at a fixed concentration of 0.5 vol% H_2 at gas flow rates ranging from 50 to 200 sccm. The final indications for the micro-machined and conventional TC sensing elements are shown in Fig. 5. As the figure shows, the gas flow rate had a greater impact on the sensor with the conventional TC sensing element than the sensor with the micro-machined sensing element.

One reason for this effect is the small dimension of the micro-machined TC sensing element where the heater and the sensing elements are co-integrated on the suspended membrane on the same substrate (see Fig. 1). In addition, the heat transfer mechanism in the micro-machined TC sensing element is convective whereas it is a Joule-heated filament in conventional sensors. These differences between the micro-machined and conventional TC sensing element designs can explain the influence of the gas flow rate on the stability of the sensing element readings. Variations in the gas flow rate may change the temperature of the filament, especially at higher gas flow rates where additional cooling of the heated sensing element may occur, resulting in more variation in the final sensing element indication.

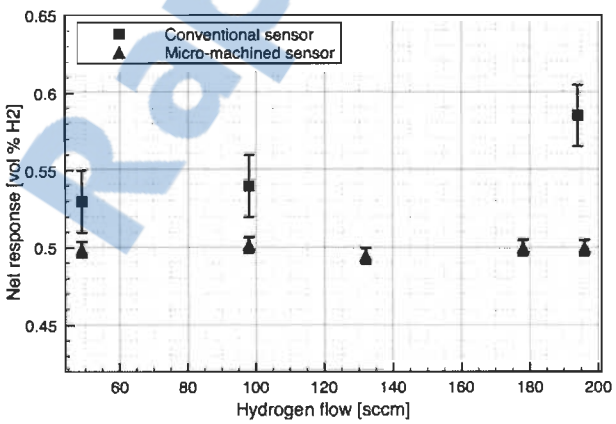

Fig. 5 – The response of the TC sensors elements as a function of the flow in 0.5 vol% H_2 in air.

4.1.3. *Linearity and accuracy*

The responses of sensors with micro-machined and conventional TC sensing elements to different hydrogen concentrations (0.5 vol%, 1 vol%, and 2 vol%) were measured. The vendor-supplied control circuitry transformed the output of each sensing element from a resistance change to a voltage change, which was then converted into vol% H_2 using the calibration procedures supplied by the respective manufacturers. The results are shown in Fig. 6. Both the conventional and micro-machined TC sensing elements showed good linearity over the hydrogen concentration range investigated. The repeatability of both sensors was very good at all concentrations as indicated by the narrow error bars, which represent the standard deviation over nine measurements. Based on a comparison of the final indication to the actual test gas concentration, a better accuracy was observed for the sensor with the micro-machined TC sensing element relative to the conventional type. However, the final indication of both sensors was usually within ±10% of the actual test gas concentration.

4.2. *Micro-machined MOX hydrogen sensing element performance*

This section compares the performance of commercial micro-machined and conventional MOX sensing elements. Micro-machined MOX sensors have been commercialized for several years by various venders. Assessments of some model types were previously performed at the NREL sensor laboratory [32]. It was found that some of the models exhibited such poor performance that further assessments were unwarranted. Specifically the response of some micro-machined sensing elements saturated at a small fraction of the manufacturer specified dynamic range. Saturation sometimes even occurred at less than 10% of the specified range. Other models of micro-machined MOX sensing elements showed a broader dynamic

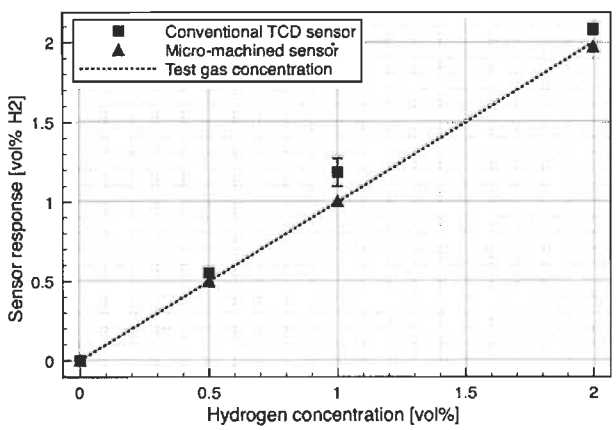

Fig. 6 – The response (final indication) of sensors with micro-machined and conventional TC sensing elements compared to the actual test gas concentration. Plotted is the average final indication obtained for a specific test gas concentration at all flow rates.

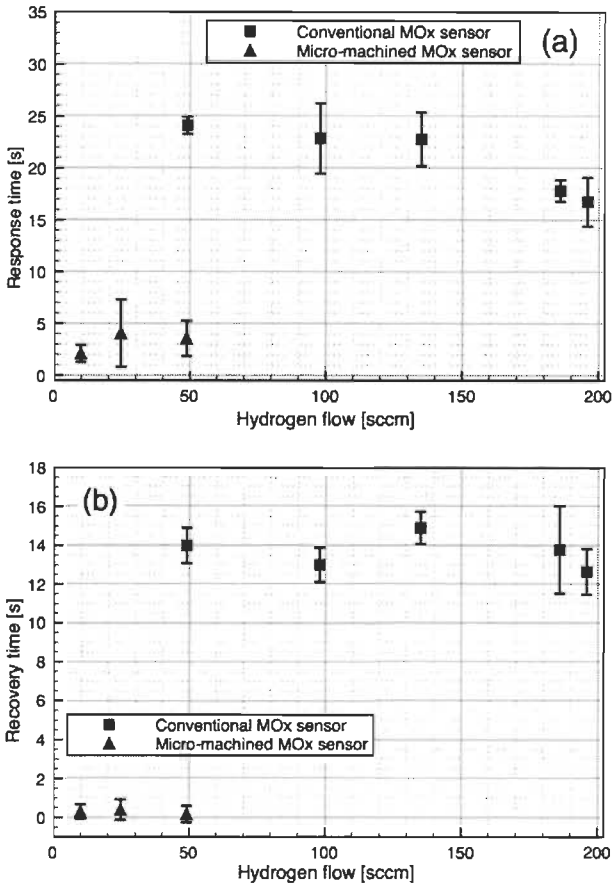

Fig. 7 – Comparison between the response and recovery times of the MOX micro-machined and conventional sensing elements. The test gas was 0.1 vol% H_2 in air. The data represent the average of five or six replicate measurements.

range, but not as broad as that typically obtained with conventional commercially available MOX sensing elements. Results in this study are presented for one micro-machined MOX sensing element representative of those that exhibited intermediate performance. For the evaluations presented in this paper, the MOX sensing elements were operated using electronic circuitry that was built in-house based on manufacturer recommendations. The electronic circuitry transduced the resistance of the sensing element to a voltage, which was logged by the data acquisition system into an electronic data file. Sensing element operation included a fixed voltage for the heater. Owing to the nonlinear sensor response of the MOX sensing element to changes in the analyte concentration, in-house calibrations and accuracy assessments were not performed. Instead, an assessment of the dynamic range and repeatability of micro-machined and conventional MOX sensing elements was performed.

4.2.1. *Response and recovery times*

The response and recovery times of micro-machined and conventional MOX sensing elements were measured under different gas flow-rate ranges, namely, 10–50 sccm for the micro-machined sensing element and 50–250 sccm for the conventional sensing element. The flow rate ranges were chosen following the recommendation of the sensor manufacturers. The measurements were performed using test gas concentrations of 0.1 vol% H_2, which was within the dynamic measuring range of both sensor platforms. The kinetics of the two platforms are compared in Fig. 7(a) and (b). This test confirmed that the MOX sensing elements' response time, t_{90}, and the recovery time, t_{10}, improved with miniaturization. The response and recovery times at 50 sccm are 3.6 ± 1.7 s and 1.4 ± 0.6 s, respectively; in comparison, the response and recovery times of the conventional sensing elements are 33.6 ± 6.7 s and 13.6 ± 0.7 s, respectively. The micro-machined MOX sensing element's response and recovery times were nearly 10 times faster than the corresponding conventional sensing element. Furthermore, the results for the conventional MOX sensing element design were not as repeatable as the results for the micro-machined sensing elements as indicated by the larger error bars (standard deviation of repetitive measurements). Although the MOX sensing elements exhibited faster kinetics than the corresponding TC sensing element, a comparison of Fig. 7(a, b) indicates that both MOX sensing element platforms are noisier (larger error bars) than either TC sensing element. Unlike the TC sensor, the response time and recovery time of the MOX sensors were not symmetric. This indicates different kinetic rates for the chemical processes controlling the sensor response and recovery.

4.2.2. *Influence of gas flow rate on final indication*

Along with response and recovery time, the influence of the gas flow rate on the final indication of the conventional and micro-machined MOX sensing elements was also investigated. 0.1 vol% H_2 was used as the test gas. The results are presented in Fig. 8, where the final indication in voltage is plotted as a function of the gas flow rates. There was negligible impact on the final indication for either platform by variations in gas flow rate. At 50 sccm, the response of the micro-machined sensing element was 1.6 ± 0.4 V versus 5.6 ± 0.1 V for the conventional sensing element. The micro-machined sensing element measurements exhibited less repeatability than the conventional platform, as indicated by the error bars shown in Fig. 8. The error bars associated with the micro-

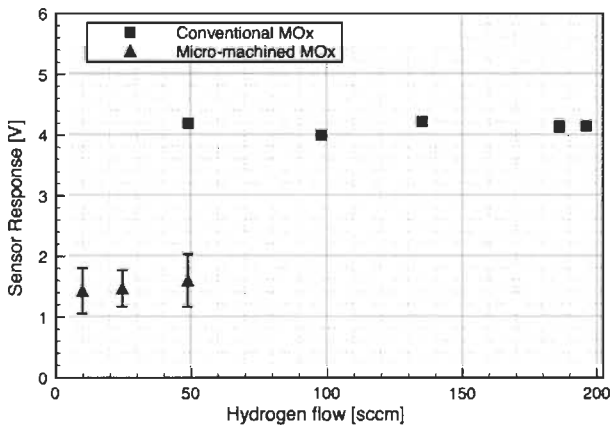

Fig. 8 – Impact of gas flow rate on the final indication for conventional and micro-machined MOX sensing elements. The test gas was 0.1 vol% H_2 in air.

machined sensing element represented approximately 25% of the final indication. On the other hand, the conventional MOX sensing element has a larger packaging requirement and a higher heating power requirement (over 650 mW for the conventional sensing element versus less than 125 mW for the micro-machined sensing element). Thus, depending upon the requirements for a specific application, an end-user may decide that a lower power requirement is critical and offsets the difference in accuracy between the two platform types.

4.2.3. *Dynamic range and sensor response repeatability*

The dynamic range of the MOX micro-machined sensing element was evaluated using test gas concentrations ranging from 0.005 to 2.0 vol% H_2. The sensor response is shown in Fig. 9. These assessments confirmed that micro-machined MOX sensing elements were capable of responding to low concentrations of hydrogen, with an LDL of <0.005 vol% H_2, which was the lowest test gas concentration used in the evaluation of the micro-machined MOX sensing element. The net response of the micro-machined sensing element to 0.005 vol% H_2 was 1.559 ± 0.0001 V, which corresponds to a calculated LDL of approximately 1×10^{-6} vol% H_2 based on the sensing element response equivalent to 3 times the net noise (standard deviation) associated with the sensor response in air. It is noted that the response for the micro-machined sensing element tended to be unstable and prone to significant drift when exposed to hydrogen, so that the LDL calculated on sensor noise levels is probably overly optimistic and the actual LDL would be an order of magnitude higher (1×10^{-5} vol% H_2), although this would still be a very good LDL for hydrogen detection. However, the dynamic range of this micro-machined sensing element was very narrow, with the device saturating at test gas concentrations of 0.05 vol% H_2. The saturation point defines the upper limit of the dynamic range of the sensing element. Thus, the sensing element would not be able to differentiate between, let alone accurately quantify, hydrogen concentrations above 0.05 vol%. Signal saturation at low hydrogen concentrations would preclude deployment in applications where some quantitative monitoring of hydrogen levels is desired. Such a requirement is usually mandated for industrial uses, but may be optional for home monitors. The lower flammability limit of hydrogen is 4 vol%. The typical alarm set points for hydrogen safety applications are at either 0.4 vol% or 1.0 vol% H_2, which represents 10% or 25% of the lower flammability limit, respectively. Both alarm levels are routinely used for industrial or laboratory safety systems with multiple alarm levels; in this case, each alarm level would activate different actions (e.g., increased facility ventilation at the 0.4 vol% alarm, but activate system shutdown and facility evacuation at the 1 vol% alarm). The saturation point of micro-machined MOX sensing elements occurred at a hydrogen concentration well below either alarm set point, which could result in false or premature alarms. While such low-level saturation behavior may not preclude the use of this sensing element for applications that need to only indicate the presence of hydrogen, this sensing element would not be able to differentiate between typical hydrogen alarm levels or if the prevailing hydrogen concentration was increasing to extremely dangerous levels above the lower flammability limit.

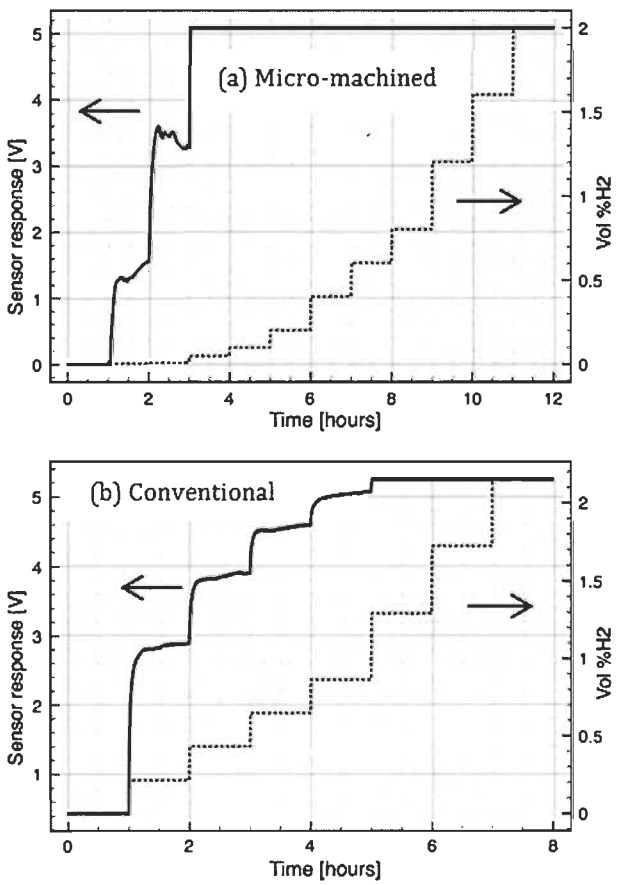

Fig. 9 – Response of the MOX sensing elements to different test gas concentrations illustrating the dynamic range of commercial (a) micro-machined and (b) conventional MOX sensing elements.

Fig. 9 also compares the dynamic range of the micro-machined sensing element with that of a conventional MOX sensing element. A range of 0.2–2 vol% H_2 was used for the conventional sensing element. This range is actually the standard concentration range used by NREL and JRC for sensor/sensing element evaluations [11]. The lower concentrations used for evaluation of the micro-machined sensing element was because of the proclivity of this device to saturate at concentrations below 0.2 vol% H_2. The net response of the conventional MOX sensing element at 0.2 vol% H_2 was 2.462 ± 0.0018 V, indicating a calculated LDL of 4×10^{-4} vol% H_2, which is more than adequate for most safety applications. Although the micro-machined sensing element had a calculated LDL somewhat better than the conventional analog, the conventional analog had a significantly better upper limit for its dynamic range. The conventional sensing element did not saturate until exposed to 2 vol% H_2; thus, this platform could be used to differentiate between the two major hydrogen alarm set points. It is noted that both sensing element platforms were operated in a manner consistent with the manufacturer's recommendations.

Saturation of commercial MOX sensors at modest hydrogen concentrations in air has been observed previously

[32]. Both the micro-machined and conventional sensing element designs tested here tended to saturate at lower hydrogen concentrations than the upper measurement range specified by the manufacturer; this discrepancy emphasizes the importance of independent verification of sensor performance before deployment.

5. Conclusion

This work presents a comparison of the performance of commercially available hydrogen sensors with micro-machined sensing elements to that of their conventional analogs. The TC and MOX platforms were used to illustrate promises and potential pitfalls associated with sensing element miniaturization. Although it was found that some platforms are more readily amenable to micro-machining manufacturing without compromising performance, the results presented here emphasize that advanced manufacturing techniques such as micro-machining do not always lead to improved performance. The performance of the micro-machined TC sensing element was equal or superior to its conventional counterpart on all critical analytic metrics. This was not the case for the commercial micro-machined MOX sensing elements, or as previously studied, the CAT sensing elements. This does not imply that the fabrication of MOX sensing elements (or CAT sensing elements) is fundamentally incompatible with micro-machining methodology. There is an extensive literature describing developmental micro-machined MOX devices. However, because these platforms can have complicated structures and operating requirements (e.g., layered structures with catalyst coatings operating at elevated temperatures), it is more challenging to commercially produce fully optimized micro-machined devices without compromised metrics. As shown here, the commercial-off-the-shelf micro-machined MOX devices sometimes showed degradation in performance, especially dynamic measuring range, relative to their conventional analogs. There is, however, promise in the approach of micro-machining hydrogen safety sensors. Economy-of-scale manufacturing techniques afforded by micro-machining will ultimately reduce the unit cost of the sensing element. The potential for better control of the manufacturing process is expected to improve device-to-device repeatability and overall performance.

Acknowledgments

Work described in this paper was performed as an international collaboration within the frame of the IEA HIA Task 31 on Hydrogen Safety and through H2CAN program. The JRC – Institute for Energy and Transport has been financed through the 7th Framework Programme (FP7). NREL was supported by the U.S. Department of Energy's Office of Energy Efficiency & Renewable Energy, Fuel Cell Technology Office, Safety Codes and Standards Program. The UQTR received support through the NSERC Hydrogen Canada (H2CAN) Strategic Research Network.

REFERENCES

[1] U.S. Department of Energy Office of Energy Efficiency & Renewable Energy, Alternative fuels & Advanced Vehicles Data Center. http://www.afdc.energy.gov/afdc/ [accessed 09.10.13].
[2] 2011 Toyota FCV-R concept unveiled, previews fuel-cell production car in 2015. http://www.autoevolution.com/news/2011-toyota-fcv-r-concept-unveiled-previews-fuel-cell-production-car-in-2015-40402.html [accessed 09.10.13].
[3] Burgess R, Buttner W, Rivkin C. Codes and standards requirements for deployment of emerging fuel cell technologies. NREL/TP-5600-52641, www.nrel.gov/docs/fy12osti/52641.pdf; December 2011 [accessed 09.10.13].
[4] Blanchette Jr Stephen. A hydrogen economy and its impact on the world as we know it. Energy Policy 2008;36:522–30.
[5] Dodds Paul E, Demoullin Stéphanie. Conversion of the UK gas system to transport hydrogen. Int J Hydrogen Energy 2013;38:7189–200.
[6] Najjar Yousef SH. Hydrogen safety: the road toward green technology. Int J Hydrogen Energy 2013;38:10716–28.
[7] Hübert T, Boon-Brett L, Black G, Banach U. Hydrogen sensors – a review. Sens Actuators B Chem 2011;157:329–52.
[8] US Department of Energy, Office of Energy Efficiency & Renewable Energy. http://energy.gov/eere/office-energy-efficiency-renewable-energy [accessed 08.10.13].
[9] NREL Hydrogen & Fuel Cell Research, Safety Sensor Testing Laboratory. http://www.nrel.gov/hydrogen/facilities_hsl.html [accessed 08.10.13].
[10] Boon-Brett L, Bousek J, Castello P, Salyk O, Harskamp F, Aldea L, et al. Reliability of commercially available hydrogen sensors for detection of hydrogen at critical concentrations: part I testing facility and methodologies. Int J Hydrogen Energy 2008;33:7648–57.
[11] Black G, Boon-Brett L, Harskamp F, Moretto P, Buttner W, Post M, et al. Interim report of the SINTERCOM project, EUR 24854 EN – 2011. http://iet.jrc.ec.europa.eu/sites/default/files/documents/scientific_publications/2011/ld-ne-24-854-en-n_pdf.pdf [accessed 20.12.13].
[12] Hydrogen sensor workshop. U.S. Department of Energy; April 4, 2007. See: http://www.lanl.gov/orgs/mpa/mpa11/sensors.html [accessed 08.10.13].
[13] Buttner W, Burgess R, Post M, Rivkin C. Summary and findings from the NREL/DOE hydrogen sensor workshop (June 8, 2011). Technical report, NREL/TP-5600-55645, http://www.nrel.gov/docs/fy12osti/55645.pdf; 2012 [accessed 08.10.13].
[14] Fuel Cell Technologies Office multi-year research, development and demonstration plan, technical plan – safety codes and standards. http://www1.eere.energy.gov/hydrogenandfuelcells/mypp/pdfs/safety.pdf [accessed 09.10.13].
[15] ISO 26142:2010. Hydrogen detection apparatus – stationary applications. http://www.iso.org/iso/catalogue_detail.htm?csnumber=52319 [accessed 08.10.13].
[16] Li Mo, Myers B, Tang X, Aldridge SJ, McCaig C, Whiting JJ, et al. Nanoelectromechanical resonator arrays for ultrafast, gas-phase chromatographic chemical analysis. Nano Lett 2010;10(10):3899–903.
[17] Huang XMH, Manolidis M, Chan Jun Seong, Hone J. Nanomechanical hydrogen sensing. Appl Phys Lett 2005;86:143104.
[18] Buttner WJ, Post MB, Burgess R, Rivkin C. An overview of hydrogen safety sensors and requirements. Int J Hydrogen Energy 2011;36:2462–70.
[19] Simon Isolde, Arndt Michael. Thermal and gas-sensing properties of a micromachined thermal conductivity sensor

for the detection of hydrogen in automotive applications. Sens Actuators A 2002;97:104–8.
[20] Ihokura K, Watson J. The stannic oxide gas sensor. Boca Raton: CRC Press; 1994.
[21] Korotcenkov G. Metal oxides for solid-state gas sensors: what determines our choice? Mater Sci Eng B 2007;139:1–23.
[22] Simon Isolde, Bârsan Nicolae, Bauer Michael, Weimar Udo. Micromachined metal oxide gas sensors: opportunities to improve sensor performance. Sens Actuators B 2001;73:1–26.
[23] Shukla Satyajit, Zhang Peng, Cho Hyoung J, Ludwig Lawrence, Seal Sudipta. Significance of electrode-spacing in hydrogen detection for tin oxide-based MEMS sensor. Int J Hydrogen Energy 2008;33:470–5.
[24] Aroutiounian Vladimir. Metal oxide hydrogen, oxygen, and carbon monoxide sensors for hydrogen setups and cells. Int J Hydrogen Energy 2007;37:1145–58.
[25] Boon-Brett L, Bousek J, Black G, Moretto P, Castello P, Hübert T, et al. Identifying performance gaps in hydrogen safety sensor technology for automotive and stationary applications. Int J Hydrogen Energy 2010;35:373–84.
[26] Lee Jae Suk, Park Jong Wan, Shin Sang Mo. Fabrication of a micro catalytic gas sensor using thin film process and Si anisotropic etching techniques. Sens Actuators B 1997;45:265–9.
[27] Nishibori M, Shin W, Izu N, Itoh T, Matsubara I, Yasuda S, et al. Robust hydrogen detection system with a thermoelectric hydrogen sensor for hydrogen station application. Int J Hydrogen Energy 2009;34:2834–41.
[28] Gall M. The Si planar pellistor: a low-power pellistor sensor in Si thin-film technology. Sens Actuators B Chem 1991;4:533–8.
[29] Boon-Brett LMM. Microstructural analysis of noble metal-based commercial hydrogen safety sensors to investigate why their performance deteriorates [M.Sc. dissertation]. University of Ulster; 2011.
[30] Fuel Cell Technologies Office multi-year research, development and demonstration plan, planned program activities for 2011–2020. U.S. DOE EERE Program, Table 3.7.6, http://www1.eere.energy.gov/hydrogenandfuelcells/mypp/; 2012 [accessed 09.10.13].
[31] Boon-Brett L, Black G, Moretto P, Bousek J. A comparison of test methods for the measurement of hydrogen sensor response and recovery times. Int J Hydrogen Energy 2010;35:7652–63.
[32] Burgess R, Post MB, Blake C, Rivkin C, Buttner WJ. Development and compliance to hydrogen sensor codes and standards—the NREL Hydrogen Sensor Testing Laboratory. Presented at the National Hydrogen Associate Annual Meeting, Columbia, SC, USA, March 30 to April 3, 2009.

5.3 Contribution III revue: «A Novel Chipless Identification Tag Based on a Substrate Integrated Cavity Resonator»

Cet article présente une structure RFID tag pour l'identification micro-ondes. La nouvelle structure du tag est basée sur une cavité résonante intégrée au substrat (SIW) ayant un haut facteur de qualité. Les données sont codées en introduisant une variation de la permittivité au sein de la cavité. Ce qui donne un spectre fréquentiel unique et identifiable comme étant une signature fréquentielle. Le design du tag proposé opère dans la plage fréquentielle de 10,5 à 11 GHz. La structure du tag SIW présentée a les avantages suivants : il a un faible coût de fabrication, il a une faible consommation énergétique, il est compact et peut également être transféré sur différents types de substrats, ce qui convient pour de nombreuses applications à grande échelle de production.

Dans le contexte des réseaux de capteurs sans fil, il est nécessaire d'avoir un moyen de distinguer chaque capteur dans le réseau. Un mode d'adressage intégré au substrat sera idéal pour donner une adresse à chaque capteur. Pour cela l'objectif de cette publication est d'avoir une preuve de concept et des prototypes réalisés pour vérifier la méthode d'adressage sans-fil pour les capteurs intégrés au substrat. La méthode d'adressage est basée sur des résonateurs intégrés au substrat où l'adresse est identifiée par un nombre variable de trous d'air dans les résonateurs.

La modélisation et la simulation ainsi que les dispositifs et les tests expérimentaux sont présentés dans l'article. Chaque unité d'adressage a été interrogée séparément pour

identifier sa signature. L'antenne d'interrogation et les unités d'adressage sont séparées par une distance de 1 cm. Lorsque l'antenne interrogatrice est approchée de l'une de ces unités, la fréquence de résonance de cette unité apparaît comme un pic distinct dans la signature fréquentielle. Les résultats montrent que la signature de chaque unité d'adressage correspond à sa fréquence de résonance et peut être détectée à partir du niveau du signal.

A Novel Chipless Identification Tag Based on a Substrate Integrated Cavity Resonator

Hatem El Matbouly, Naimi Boubekeur, and Frédéric Domingue

***Abstract*—This letter presents a novel tag structure for microwave identification. The new tag is based on a high quality factor ($Q = 366$) substrate integrated cavity resonator in which data are encoded by introducing a variation in the effective permittivity which gives a unique and identifiable frequency spectral signature. The proposed tag design operates in the frequency range of 10.5–11 GHz. The substrate integrated tag presented has the advantages of being low cost, zero power consumption, compact and can be also transferred to different types of substrates, making it suitable for many mass production applications.**

***Index Terms*—Cavity resonators, RFID, substrate integrated waveguide (SIW), tag.**

I. Introduction

As the wireless applications are rapidly increasing in recent years, radio frequency identification (RFID) is becoming more and more needed. Passive chipless RFID tags offer the advantage of identification at a distance with zero power consumption and unlimited lifetime [1].

Coplanar waveguide had been used to implement such tags [2] and had been demonstrated in the range of 7–10.7 GHz range. Another chipless tag based on a microstrip line and spiral resonators that can code up to 6-bits and operates at 30 GHz had been also demonstrated [3]. These solutions are based on standard planar transmission lines.

On the other hand, Substrate integrated waveguide (SIW) structures are attracting more and more attention in recent years [4]. SIW structures have many advantages such as high Q factor, low insertion loss, and high power capability; furthermore, SIW microwave components can be integrated with other planar circuit to form a compact microwave system [5]. SIW structures have been fabricated on paper based substrate using ink-jet printer [6] as well as on flexible plastic (PET) substrates [7].

This letter demonstrates the concept and the prototyping of a novel SIW structure for microwave identification. The proposed chipless tag structure is based on a single substrate integrated cavity resonator which encodes data into the magnitude of the spectrum of the interrogation signal by means of air holes introduced inside the resonator structure. Since the dielectric constant changes, the proposed structure has the advantage of encoding without increasing the resonator size. Each tag is designed to operate in the frequency band of 10.5–11 GHz and have a different frequency spectral signature in this band for tag identification.

Manuscript received August 07, 2012; accepted December 09, 2012. Date of publication January 01, 2013; date of current version January 16, 2013. This work was supported by the National Science and Engineering Research Council of Canada (NSERC), the university support through a research Chair, and the CMC Microsystems for access to test equipment.

Color versions of one or more of the figures in this paper are available online at http://ieeexplore.ieee.org.

Digital Object Identifier 10.1109/LMWC.2012.2236081

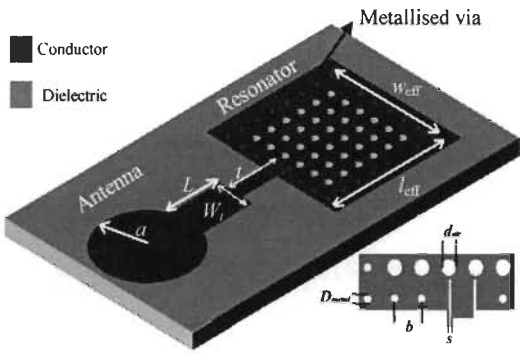

Fig. 1. 3-D structure of the substrate integrated tag.

II. Tag Operation Principle

Fig. 1 represents the basic structure of the substrate integrated cavity resonator with the interrogation antenna used to implement the tag.

The resonance frequency f_r of the substrate integrated cavity resonator operating in the TE_{10}-like mode is given by

$$f_r = \frac{c}{2\sqrt{\varepsilon_r}}\sqrt{\left(\frac{p}{w_{\text{eff}}}\right)^2 + \left(\frac{q}{l_{\text{eff}}}\right)^2} \tag{1}$$

where c is the speed of the electromagnetic wave in vacuum, ε_r is the relative permittivity of the substrate, and w_{eff} and l_{eff} are the effective width and length of the resonator cavity [8], [9]. Given that the dimensions of the resonator do not change, a variation in the dielectric constant $\Delta\varepsilon_r$ introduces a change in the resonance frequency Δf_r given by

$$\frac{\partial f_r}{\partial \varepsilon_r} \propto \frac{-1}{\varepsilon_r^{3/2}} \tag{2}$$

where the proportionality constant depends on the dimensions of the substrate integrated resonator. It is important to note that the change in resonance frequency is negative which indicates that the frequency shift will be always lower than the initial resonance frequency. To introduce a signature, a change in the effective dielectric constant of the substrate is introduced by a variable number of air via.

The basic principle of the proposed tag operation is presented in Fig. 2. The interrogator sends a broadband signal to the tag

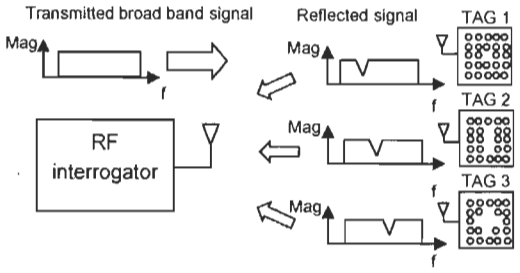

Fig. 2. Interrogation principle of the proposed tags.

TABLE I
DESIGN PARAMETERS VALUES FOR TAG

Symbol	Quantity	Value (mm)
w_{eff}	Effective width	10.5
l_{eff}	Effective length	10.5
T	Feed length	5.5
L	Antenna feed length	5.1
A	Antenna radius	4.36
d_{air}	Air via diameter	0.8
D_{metal}	Metallized via diameter	0.4
W_f	Antenna feed width	3.4
S	Feed separation	0.125
B	Pitch	1.5

and since the resonator encode the data into a form of resonance frequency, the reflected signal will have all the transmitted frequencies except the resonance frequency of the tag which represents the signature.

III. SIMULATION AND EXPERIMENTAL RESULTS

A. Simulation Results

The resonator has been simulated and optimized by finite element electromagnetic tool using the design parameters shown in Table I. These parameters have been used for RO3004C Roger substrate ($\varepsilon_r = 3.55, h = 1.524$ mm, $\tan\delta = 0.002$). The dielectric constant of this substrate is stable in the temperature rang (25–60°C) with small drifts at higher temperatures reducing the temperature dependency of the proposed device.

Four configurations have been proposed representing four different encoded data in the frequency spectrum. The four configurations are shown in Fig. 3. The simulation results are shown in Fig. 4 for TE_{10} resonance mode of each configuration. The electric field is maximum at the vertical center plane along the propagation direction. In this case, introducing dielectric modifications near the center will have a significant impact on the resonance frequency for encoding the data. The resonance frequencies are in the frequency band of 10.5–11.1 GHz. This mode exhibit a quality factor (Q) of 373.3 and the frequency is decreased by 0.1 GHz for each missing air via inside the substrate integrated cavity resonator. The circular patch antenna has been designed to resonate at 10.7 GHz which is a central frequency in the frequency band of the tags.

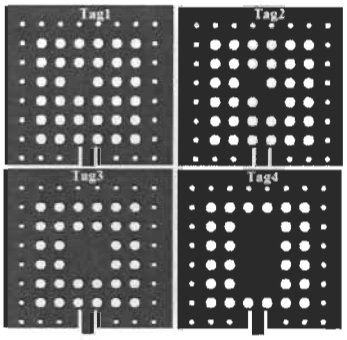

Fig. 3. Layout of the four proposed resonators.

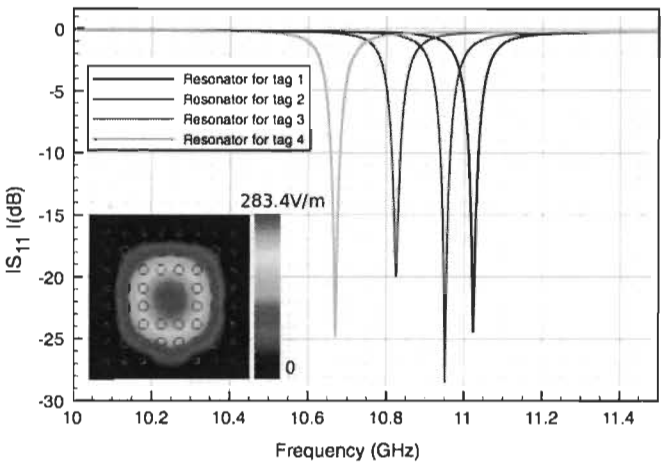

Fig. 4. Simulation results for the proposed configurations.

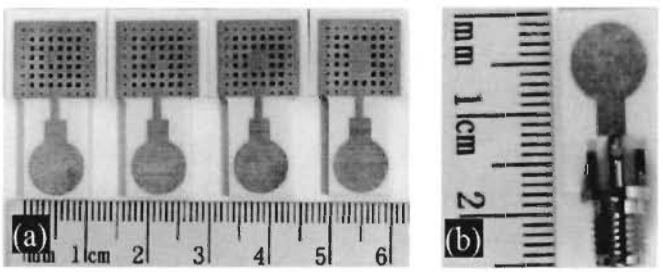

Fig. 5. (a) Fabricated substrate integrated tags (b) circular patch antenna for interrogation.

B. Experimental Results

Fig. 5 shows a picture of the fabricated tags measuring (1.5×3.0) cm^2 including the antenna.

The first validation consists of the measurement of the four resonators separately as shown in Fig. 6. The measurement results match the simulation with a measured quality factor of 366.

Each tag has been interrogated separately to identify its signature. The interrogator antenna and the tags were separated by a distance of 1 cm. The results show that the signature of each tag coincides with its resonance frequency and can be detected from the signal level. Fig. 7 shows the results of wireless test

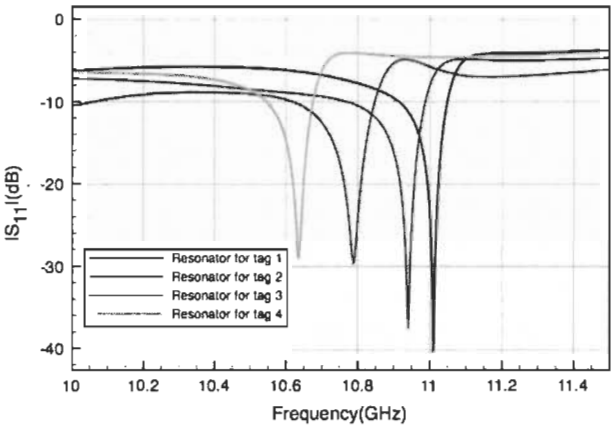

Fig. 6. Measured results of each substrate integrated cavity resonator.

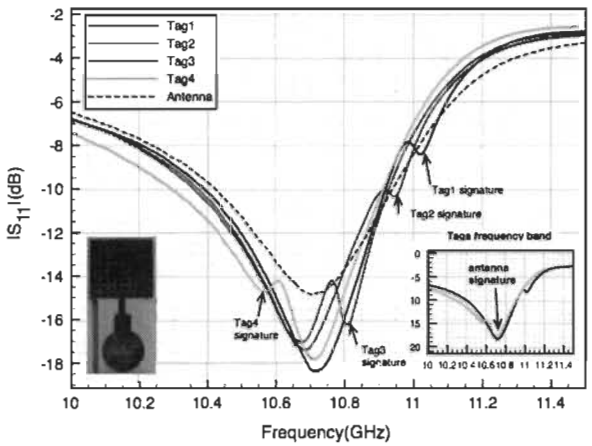

Fig. 7. Measured interrogated signal for each tag.

conducted on each tag separately. The S_{11} parameter of the antenna is shown by the dotted curve. When the interrogator antenna is approached to one of the tags, the resonance frequency of that tag appears as a distinguishable peak in the frequency signature.

Table II presents a comparison between different encoding tag structures [10]–[12]. The proposed structure can encode the signature without increasing the size of the resonator since the resonance frequency can be modified by modifying the effective dielectric constant inside the resonator instead of the resonator dimensions.

IV. Conclusion

In this work, a novel microwave identification tag based on substrate integrated cavity resonator has been demonstrated. The tag encodes the data by changing the effective permittivity of the substrate integrated resonator which gives a unique frequency signature. The tag is designed to operate in the frequency band of 10.5–11 GHz which can be easily modified by changing the resonator dimensions. The new tag has the advantage of having a high quality factor ($Q = 366$) as well as compact size (4 cm^2). The proposed tag design can be transferred to other types of technology such as flexible substrates or paper which is suitable for low cost mass production applications. The structure has the advantages of being low cost, passive and compact.

TABLE II
Different Tag Encoding Units in Literature

Tag encoding structure	Area of encoding unit	Principle of operation	Frequency band	REF
Metallic strip scatters	2.5×25mm^2	Encoding by back scattering signal	2-4GHz	[10]
Split ring resonator	3.5×3.5 mm^2	Encoding by the EM characteristic of SRR	8.5-12.4GHz	[11]
Antenna with diode	157×15 mm^2	Harmonic tag with Doppler shift	2.4 GHz	[12]
Spiral resonator	7.7×12 mm^2	Encoding in frequency and phase	2 GHz	[3]
Substrate integrate resonator	10×10 mm^2	Encoding by air via	10.5-11GHz	This work

References

[1] R. Want, "An introduction to RFID technology," *IEEE J. Pervasive Comp. Mag.*, vol. 5, no. 1, pp. 25–33, 2006.
[2] S. Preradovic, S. Roy, and N. Karmakar, "Fully printable multi-bit chipless RFID transponder on flexible laminate," in *Proc Asia-Pacific Microw. Conf. (APMC)*, 2009, pp. 2371–2374.
[3] S. Preradovic, I. Balbin, N. C. Karmakar, and G. F. Swiegers, "Multiresonator-based chipless RFID system for low-cost item tracking," *IEEE Trans. Microw. Theory Tech.*, vol. 57, no. 5, pp. 1411–1419, May 2009.
[4] K. Wu, D. Deslandes, and Y. Cassivi, "The substrate integrated circuits—A new concept for high-frequency electronics and optoelectronics," in *Proc. TELSIKS*, Oct. 2003, pp. 3–5.
[5] W. Hong and K. Wu, "Design mechanisms and application examples of SIW structure family," in *Proc. IEEE IMS*, 2012, [CD ROM].
[6] R. Moro, S. Kim, M. Bozzi, and M. Tentzeris, "Novel inkjet-printed substrate integrated waveguide (SIW) structures on low-cost materials for wearable applications," in *Proc. 42th Eur. Microw. Conf.*, Amsterdam, The Netherlands, Oct. 28–Nov. 2 2012, [CD ROM].
[7] R. Moro, A. Collado, S. Via, A. Georgiadis, and M. Bozzi, "Plastic-based substrate integrated waveguide (SIW) components and antennas," in *Proc 42th Eur. Microw. Conf.*, Amsterdam, The Netherlands, Oct. 28–Nov. 2 2012, [CD ROM].
[8] Y. Cassivi, L. Perregrini, P. Arcioni, M. Bressan, K. Wu, and G. Conciauro, "Dispersion characteristics of substrate integrated rectangular waveguide," *IEEE Microw. Wireless Compon Lett.*, vol. 12, no. 9, pp. 333–335, Sep. 2002.
[9] X.-P. Chen, K. Wu, and W. Hong, "Electrically tunable substrate integrated waveguide reflective cavity resonator," in *Proc. Asia Pacific Microw. Conf. (APMC)*, 2009, pp. 119–122.
[10] A. Vena, E. Perret, and S. M. A. W. C. L. I. Tedjini, "A fully printable chipless RFID tag with detuning correction technique," *IEEE Microw Wireless Compon Lett.*, vol. 22, no. 4, pp. 209–211, Apr. 2012.
[11] H.-S. Jang, W.-G. Lim, K.-S. Oh, S.-M. Moon, and J.-W. Yu, "Design of low-cost chipless system using printable chipless tag with electromagnetic code," *IEEE Microw. Wireless Compon. Lett.*, vol. 20, no. 11, pp. 640–642, Nov. 2010.
[12] A. Singh and V. Lubecke, "Respiratory monitoring and Clutter rejection using a CW Doppler radar with passive RF tags," *IEEE Sensors J.*, no. 99, p. 1, 2011.

5.4 Contribution IV revue: «Passive Microwave Substrate Integrated Cavity Resonator for Humidity Sensing»

Cet article présente une réalisation d'un capteur environnemental passif qui est basé sur la technologie micro-ondes de guides d'ondes intégrés au substrat (SIW). Le capteur qui est une cavité résonante est destiné à la détection de l'humidité.

Le travail présente deux structures ayant deux différentes régions sensibles à l'intérieur de la cavité résonante ce qui donne deux fréquences d'opérations 3,6 et 4,15 GHz. Le principe de détection est basé sur un décalage de fréquence de résonance dû à la variation de la permittivité de l'air humide. Cette variation peut être détectée et utilisée en tant qu'indicateur de détection. Le décalage de fréquence a été estimé en utilisant la méthode analytique de perturbation pour les prototypes diélectriques de résonateur micro-ondes. La structure des résonateurs SIW présentée a été testée en présence de l'humidité et présente des caractéristiques sensibles dans la plage de 0 à 80% d'humidité relative (en conformité avec le modèle proposé). Une comparaison des performances de sensibilité entre la nouvelle structure et d'autres composants micro-ondes utilisés pour la détection environnementale est également présentée. Des mesures de répétabilité et de fiabilité du fonctionnement de la structure proposée sont discutées.

La modélisation et la simulation ainsi que les dispositifs et les tests expérimentaux sont présentés dans l'article. La constante diélectrique de la région sensible (air humide) du résonateur peut être affectée par les variations d'autres paramètres tels que la pression et la

température pendant l'essai. Ces variations peuvent entrainer un décalage de la fréquence de résonance du dispositif micro-ondes et par conséquent affecter par la même occasion la sensibilité de ce dernier. L'influence des variations de pression et de température sur la fréquence de résonance a été évaluée par une analyse de sensibilité et les résultats sont également présentés dans cet article.

Passive Microwave Substrate Integrated Cavity Resonator for Humidity Sensing

Hatem El Matbouly, Naimi Boubekeur, Frédéric Domingue

Abstract — **This paper presents an original passive microwave substrate integrated cavity resonator (SIW) as an environment sensor for humidity detection. The proposed structures are based on a high quality factor (*Q*~300) substrate integrated cavity resonator operating at 3.6 and 4.15 GHz. The detection principle is based on a frequency shift due to the permittivity variation of the humid air. This variation can be detected and used as the sensor indication. The frequency shift has been estimated analytically using the dielectric perturbation method for the resonator prototypes. The structure of the presented SIW resonators has been tested in the presence of humidity and shows sensitive characteristics in the range of 0 to 80% RH in accordance with the proposed model. A comparison of sensitivity performance between the new structure and other reported microwave components for environmental sensing is also presented. Measurements of repeatability and reliability for the proposed structure are discussed as well. As a new microwave component type, the proposed substrate integrated environmental sensor has the advantage of providing a new fabrication solution for RF environmental sensing and greatly simplifies the sensor's manufacturing processes and cost.**

***Index Terms*—Cavity Resonators, Passive, Microwave Detection, Substrate Integrated Waveguides (SIW), Environmental Sensor.**

I. Introduction

In recent years, many passive microwave components, including RFID technology, have been investigated for sensing applications [1]. They are expected to play an important role as environment monitoring elements for physical parameter sensing, detection of harmful agents, and non-invasive monitoring. Environmental sensors are essential devices to measure several physical quantities. Gas sensors, for example, are used to detect toxic gas leakage to avoid accidents in industrial environments, for air quality control and for monitoring in domestic environments. Recently, the need for sensors to monitor air quality (gas, humidity, dust, etc.) in vehicles and houses has gained a lot of interest [1-2].

This research was undertaken, in part, thanks to funding from the Canada Research Chairs program and from the National Science and Engineering Research Council of Canada (NSERC).

Hatem El Matbouly. Author, with the Electrical and Computer Engineering Department, Université du Québec à Trois-Rivières, Trois-Rivières, QC G9A5H7 Canada (e-mail: hatem.el.matbouly@uqtr.ca).

Naimi Boubekeur. Author, with the C2T3, Cégep de Trois-Rivières, Trois-Rivières, QC G8Z1M8 Canada (e-mail: nboubekeur@c2t3.ca).

Frédéric Domingue. Author, with the Electrical and Computer Engineering Department, Université du Québec à Trois-Rivières, Trois-Rivières, QC G9A5H7 Canada (e-mail: frederic.domingue@uqtr.ca).

Previous microwave sensing techniques focused on planar microwave components with the incorporation of dielectric sensitive materials. For example, gas sensing has been demonstrated using microwave transmission lines [3] where the dielectric response of a material in the presence of a gas under the application of a microwave signal is used as microwave transducing. Other microwave structures have been used in gas sensing. The dielectric response of carbon nanotubes (CNT) has been used as an indication of the presence of gases using an inductor-capacitor resonant microwave structure [4]. The CNT response affects the frequency spectrum of the device which can be tracked to identify the concentrations of the types. Moreover, microwave passive components have been used as detectors for other environmental parameters such as air quality. For instance, humidity detection with a group delay C-section structure has been demonstrated [5]. The structure is based on a cascaded group of micro-strip transmission line sections coupled at alternative ends. Silicon nanowires are used as a humidity sensitive layer and they are deposited on the transmission line sections [5]. An RFID antenna has been used in humidity detection [6] with polymer-based humidity sensitive material. The structure is an H-shaped slot in which the humidity reacting polymer is deposited. RFID tags have been implemented on fixable substrates for humidity sensing [7]. The tag structure was ink-jet printed onto a Kapton 500HN polymer, which is a humidity sensitive material. Most of these structures do not cover a wide humidity range, which limits them in terms of applications.

Substrate integrated waveguides (SIW) are attracting more and more attention in many areas such as microwave filters [8], RFID tags [9] and microwave resonators due to their high *Q* factor, low insertion loss, and high power capability. In addition, SIW can be integrated with other planar circuits to form a compact microwave system [10]. An SIW was demonstrated for fluid sensing [11]; the structure was tested for fluidic dispersions in which particles of high dielectric constant are dispersed in low dielectric oil. However, SIW have never been investigated for their environmental sensing capabilities.

This work proposes an original low-cost microwave component for environmental sensors. This solution is based on a new generation of substrate integrated microwave cavity resonator having a sensitive region introduced inside the resonant cavity. The structure shows sensitivity characteristics depending on the size of the sensing material inside the SIW resonator. The proposed SIW structure also shows sensitivity, in the absence of sensitive material, for humidity, comparable to other reported microwave structures. This work presents an

analytical model using the dielectric perturbation method to estimate the electromagnetic sensitivity characteristic of different prototypes. The model relates the size of the functionalized region to the fractional change of the resonance frequency. The model results were compared to the experimental values obtained from different SIW resonator prototypes.

The sensing performance of the proposed structure is compared to the performance of other microwave components and the results are discussed.

II. SENSOR STRUCTURE & OPERATION PRINCIPLE

Fig. 1 represents the proposed structure of the substrate integrated cavity resonator for a humidity sensing element.

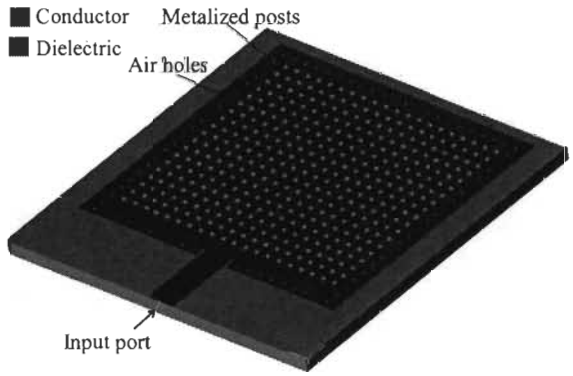

Fig. 1. The 3D structure of a microwave substrate integrated humidity sensor.

The basic principle of the proposed humidity sensor is based on the change of effective permittivity of the dielectric due to the presence of humidity inside the air holes. Moisture in the atmosphere changes air's permittivity according to the following equation [12]:

$$\varepsilon_r(RH) = 1 + \frac{211}{T}\left(P + \frac{48P_s}{T}RH\right)\times 10^{-6} \tag{1}$$

where T is the absolute temperature (in K), P is the pressure of moist air (in mmHg), P_s is the pressure of saturated water vapor (in mmHg), RH is the relative humidity (in %). Equation (1) shows that the dielectric constant of moist air is proportional to the percentage of relative humidity. Since the resonance frequency of the resonator is inversely proportional to the effective dielectric constant $f_r \propto (\varepsilon_{eff})^{-0.5}$ [9], changing the percentage of relative humidity H due to water vapor will, in turn, change the resonance frequency. This frequency shift can be exploited as an indication of the presence of moisture. The permittivity of humid air (1) is used for T = 30°C and P = 760 mmHg (atmospheric pressure) and humidity range (0 - 80%). By calculating the slope ($\Delta\varepsilon_r(RH)/\Delta RH$), the dielectric variation per relative humidity variation is found to be 0.0002/RH%. This variation can be used to estimate the frequency shift of the resonator at different humidity percentages.

III. THEORETICAL MODEL & ELECTROMAGNETIC ANALYSIS

Functionalizing a SIW resonant cavity with a sensitive dielectric implies modifying the original substrate with a different dielectric material, which can introduce a frequency shift or a change in the quality factor of the SIW resonator. In order to analyze these modifications, the cavity perturbation method can be used to estimate the frequency shift due to a functionalized region inside the cavity and a relation can be established between the functionalized region size and the range of the frequency shift. Fig. 3 shows a SIW resonator with a functionalized region. The resonance frequency of SIW cavity is given by [13]:

$$\frac{\omega_r}{2\pi} = \frac{c}{2\sqrt{\varepsilon_r}}\sqrt{\left(\frac{m}{W_{eff}}\right)^2 + \left(\frac{n}{L_{eff}}\right)^2} \tag{2}$$

Where,

$$L_{eff} = L - \frac{D^2}{0.95b}, W_{eff} = W - \frac{D^2}{0.95b} \tag{3}$$

In this case, ε_r is the relative dielectric constant of the substrate material. The conditions $D < \lambda_g/5$ and $b < 2D$ which relate to the diameter D and the pitch b of the metallic posts ensure that the radiation loss is kept at a negligible level. In this case, the SIW can be modeled using the conventional rectangular waveguide where the design equations and the theoretical framework of the rectangular waveguide are applicable to the SIW [14].

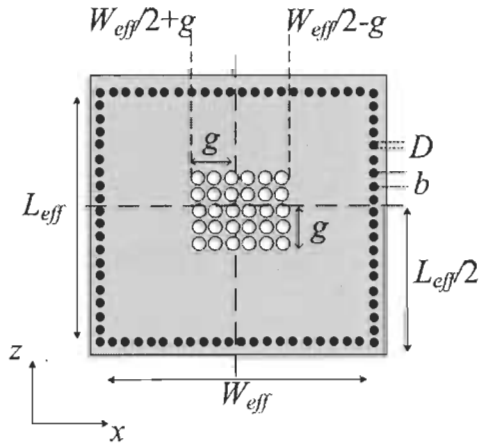

Fig. 2. Integration limits for the dielectric perturbation calculation of the functionalized resonant cavity.

For this reason, the fractional change in the resonance frequency ω_r due to dielectric perturbation $\Delta\varepsilon$ is given by

$$\frac{\omega - \omega_r}{\omega_r} \approx \frac{-\int_{V_0}\Delta\varepsilon\left|\vec{E}_0\right|^2 dV}{\int_{V_0}\left(\varepsilon\left|\vec{E}_0\right|^2 + \mu\left|\vec{H}_0\right|^2\right)dV} \tag{4}$$

where, E_0 and H_0 are the unperturbed electric and magnetic fields inside the resonator, V is the volume of the SIW

resonator and $\Delta\varepsilon=\varepsilon_{eff}(RH)-\varepsilon_r$ where $\varepsilon_{eff}(RH)$ is given by Maxwell–Garnett (MG) mixing rule [11]

$$\varepsilon_{eff}(RH)=\varepsilon_r+3f\varepsilon_r\frac{\varepsilon_r(RH)-\varepsilon_r}{\varepsilon_r(RH)+2\varepsilon_r-f(\varepsilon_r(RH)-\varepsilon_r)} \quad (5)$$

ε_r is the relative dielectric constant of the substrate, $\varepsilon_r(RH)$ is given by (1) and f is the volume fraction of the sensing region. It is important to note that the perturbation is only in the dielectric constant since the substrate has no magnetic properties, hence there is no change in the magnetic permeability $\Delta\mu=0$.

For the TE mode, the unperturbed electric field inside the resonator $E_y=A\sin\frac{\pi x}{L}\sin\frac{\pi z}{W}$ [14]. Using the geometry shown in Fig. 3, the integral in (4) has been evaluated over the volume of the resonator giving the following expression

$$-\frac{\Delta\varepsilon\left(2\pi g+L\sin\frac{2\pi g}{L}\right)\left(2\pi g+W\sin\frac{2\pi g}{W}\right)}{2WL\pi^2\varepsilon_r} \quad (6)$$

Equation (6) is a general form of resonance frequency fractional change evaluated in case the length L and the width W of SIW resonator are not equal. In case $W=L$ the fractional change in the resonance frequency will take the form

$$\frac{\omega-\omega_r}{\omega_r}\approx-\frac{\Delta\varepsilon\left(2\pi g+W\sin\frac{2\pi g}{W}\right)^2}{2W^2\pi^2\varepsilon_r} \quad (7)$$

Increasing the distance g increases the functionalized region inside the SIW resonator which will have an effect on the sensitivity. Given the dimensions W of the resonator and the size of the sensitive region g. Equation (7) gives an estimation of the frequency shift due to the variation of the dielectric constant $\Delta\varepsilon$. In order to validate the analytical expression (7), the resonator structure has been simulated using a finite element method (FEM) 3D simulator (Empro). The simulation results are compared to the analytical dielectric perturbation model. Fig. 4 shows the frequency shift obtained from (7) due to dielectric perturbation variation in the range of 1 to 3 compared to the FEM simulation. The simulated structure has dimensions of $W = L = 31.1$ mm. The difference between the simulation and the analytical perturbation model is due to the fact that the perturbation method is an approximation [15]. This comparison shows that the analytical perturbation model is a good approximation for the resonance frequency.

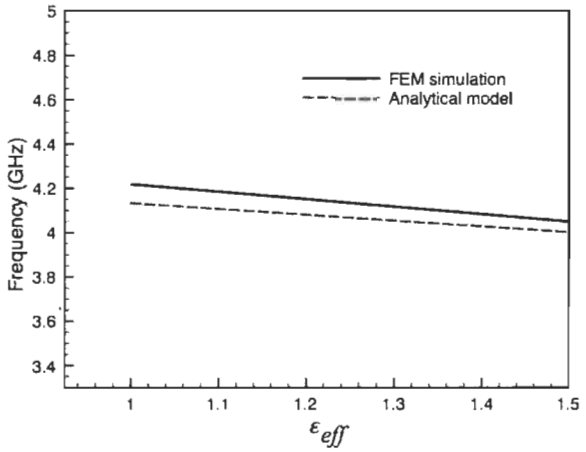

Fig. 3. Numerical results based on the analytical perturbation model and the electromagnetic FEM simulation of the SIW structure.

IV. DEVICE DESIGN AND FABRICATION

An unperturbed resonator with a resonance frequency given by (2) has been designed and simulated with the FEM tool using the design parameters shown in Fig.5 where $W = L =$ 31.1 mm, $s = 0.37$ mm and $t = 9.7$ mm. The diameter D of the metalized posts is 0.4 mm and the pitch b of the posts is 1.5 mm. These parameters have been chosen to respect the conditions ($D < \lambda_g/5$ and $b < 2D$) which ensure negligible leakage losses.

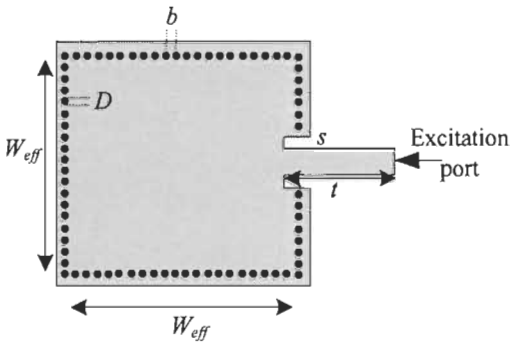

Fig. 4. The design parameter of the unperturbed SIW resonator.

In order to study the impact of the size of the functionalized region, δ, on sensitivity, two functionalized resonators have been fabricated, each with different g. The functionalized region is introduced inside the SIW resonator presented in Fig. 5 by using air holes with a diameter of 1.2 mm. The air holes have a wider diameter in order to increase the effect of humidity on the resonance frequency as they are filled with humid air. The pitch b is 1.5 mm. These parameters have been used to fabricate the resonator structure on RO4003C Roger substrate ($\varepsilon_r = 3.55$, $h = 1.524$ mm, $\tan\delta = 0.002$). The dielectric constant of this substrate is not affected by temperature variation in the range of (25 to 60°C) but a small drift can occur at higher temperatures ($T > 60$°C). Fig. 5 shows a picture of the fabricated sample resonators (SIW1 and SIW2) measuring (3.5 × 3.5) cm^2.

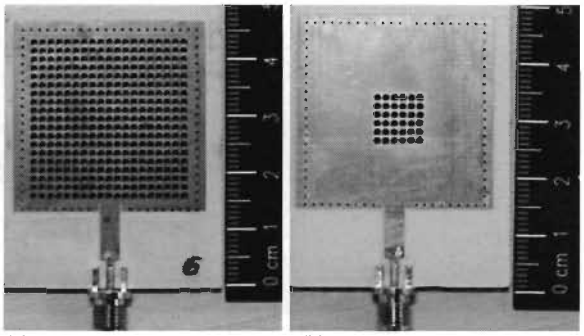

(a) (b)

Fig. 5. (a) Fabricated resonator SIW1 (b) Fabricated resonator SIW2 which has a smaller sensitive region than resonator SIW1.

The measured and simulated S_{11} parameters of the resonator structure are shown in Fig.6. The figure presents the perturbed TE10 resonance mode of resonators SIW1 and SIW2. The measured (Q) factor for SIW1 was 263.25 and 308 for SIW2. These measurements were taken at 20% humidity.

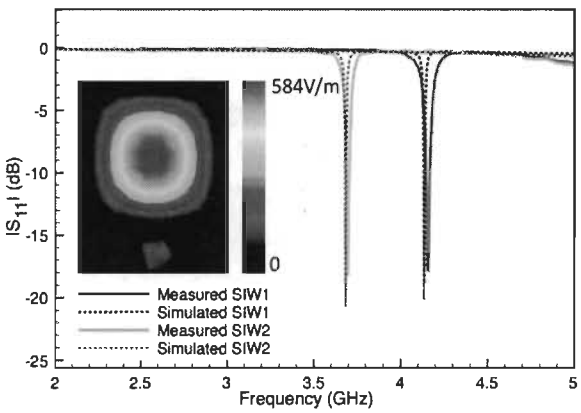

Fig. 6. Simulated and measured S_{11} for the designed substrate integrated resonators with the electric field distribution for the TE10 resonance mode.

V. EXPERIMENTAL DEMONSTRATION FOR HUMIDITY DETECTION

The humidity sensing characteristic of the proposed resonator was tested experimentally using the environmental characterization system shown in Fig. 8. Nitrogen gas was used as a carrier to deliver the humidity from the source to the chamber where the SIW resonator is placed. The gas flow was maintained at 500 sccm during the test using a mass flow controller and the gas temperature was fixed at 30°C.

The test starts by measuring the resonance frequency in a vacuum (0.03 atm) to ensure that there is no humidity in the chamber. Then, relative humidity is increased by increments of 10%RH till it reaches a maximum relative humidity value of 80%RH. The duration of each RH% step is 3 min, allowing the humidity level to stabilize at the RH% set value inside the test chamber (see Fig.7).

In order to test the repeatability of the measurement, the experiment was repeated for 5 days and the readings were taken under the same experimental conditions.

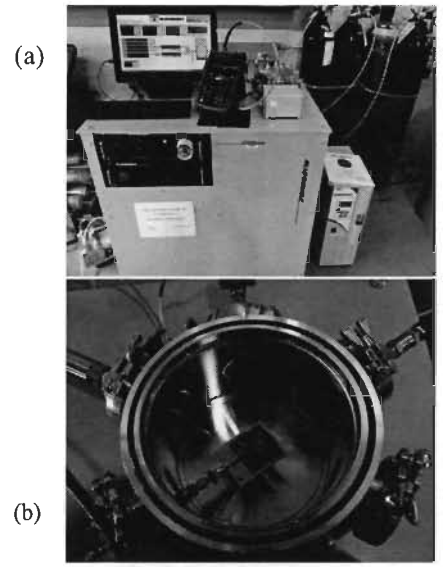

(a)

(b)

Fig. 7. (a) Measurement set-up for humidity sensing measurement using a gas sensor characterization bench, (b) the test chamber with the resonator under test.

Fig. 8 shows the measured and simulated frequency shift (left axis) with the measurement error of the proposed resonator as a function of humidity for the TE10 resonance mode.

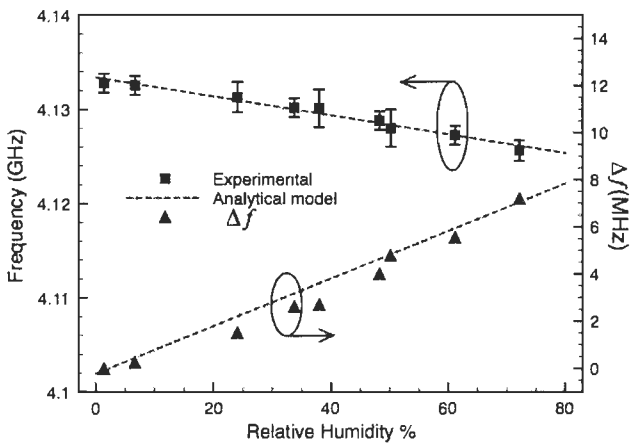

Fig. 8. TE10 resonance frequency shift of SIW1: (Left) the recorded and theoretical resonance frequency as a function of humidity variation. (Right) the resonance frequency variation.

The TE10 resonance mode exhibits a maximum frequency variation of 9 MHz at 80% RH. The measured sensitivity S of the SIW resonator is given by [17]:

$$S = \left| \frac{\Delta f_r}{\Delta \%RH} \right| \tag{7}$$

where Δf_r is the change in the resonance frequency and Δ%RH is the corresponding change of relative humidity. The measured sensitivity for SIW1 is found to be 101 kHz/RH%. The same measurement was performed on the second resonator, SIW2, for the same resonance mode; the results are shown in Fig 9. The second resonator exhibits a maximum frequency shift of 0.8 MHz at 80 RH% and a sensitivity of

9.35 kHz/RH%. The sensitivities have been calculated by linear regression of the measured resonance frequency.

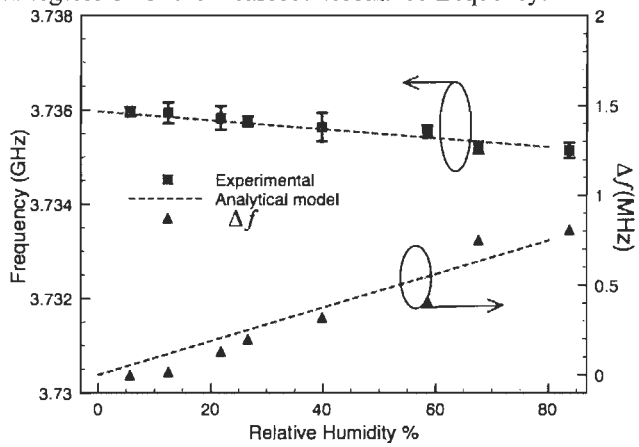

Fig. 9. TE10 resonance frequency shift of SIW2: (Left) the recorded and theoretical resonance frequency as a function of humidity variation. (Right) the resonance frequency variation.

The sensitivity of resonator sample SIW1 was higher than the second resonator sample, SIW2, due to a larger sensitive region which takes advantage of more of the electric field that occupies the interior of the resonator and, hence, has more interaction with the moisture in the air via.

VI. SENSITIVITY ANALYSIS

The dielectric constant of the sensitive region (humid air) of the resonator can be affected by the variations of other parameters such as pressure and temperature during the test. These variations can affect the resonance frequency shift of the resonator and, hence, the sensitivity. The influence of pressure and temperature variations on the resonance frequency can be evaluated by applying a sensitivity analysis on (1) which relates the dielectric constant of the humid air to the other environment parameter. The sensitivity of the dielectric constant is given by:

$$\delta\varepsilon_r = \left|\frac{\partial\varepsilon_r}{\partial P}\right|_{P_0}\delta P + \left|\frac{\partial\varepsilon_r}{\partial T}\right|_{T_0}\delta T + \left|\frac{\partial\varepsilon_r}{\partial H}\right|_{H_0}\delta H \qquad (8)$$

where, $|\partial\varepsilon_r/\partial P|$, $|\partial\varepsilon_r/\partial T|$ and $|\partial\varepsilon_r/\partial H|$ are the absolute value of partial derivatives of (1) evaluated at the nominal values of P_0, T_0 and H_0, and δP, δT and δH are the total tolerances on the environmental parameter at the measurement. The nominal values are the test condition values shown in Fig.11, which are P_0=14.7 Psi (760mmHg), T_0=30°C and H_0 has the RF measured values indicated by the arrows in Fig. 11 in the range (0-80%).

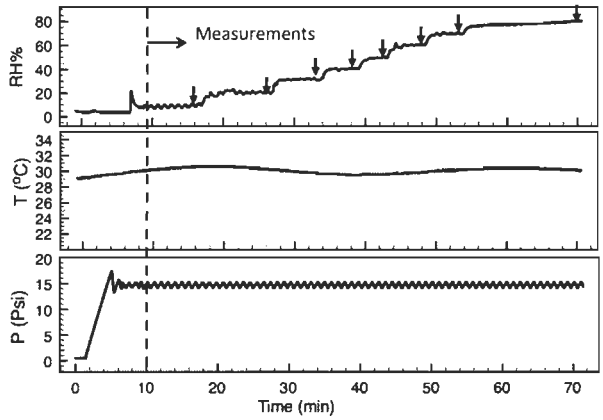

Fig. 10. Environment conditions (pressure and temperature) during humidity measurement. The arrows in the RH% curve indicate the point where measurements have been taken.

The numerical values of partial derivative terms in (8) are a measure of the sensitivity of the corresponding parameter variation. Table I lists the numerical values of $|\partial\varepsilon_r/\partial P|$, $|\partial\varepsilon_r/\partial T|$ and $|\partial\varepsilon_r/\partial H|$, the physical units are ($mmHg^{-1}$, K^{-1} and $RH\%^{-1}$)

TABLE I
SENSITIVITY ANALYSIS OF DIELECTRIC CONSTANT

	$\lvert\partial\varepsilon_r/\partial P\rvert$	$\lvert\partial\varepsilon_r/\partial T\rvert$	$\lvert\partial\varepsilon_r/\partial H\rvert$
Value	6.96×10^{-7}	5.1×10^{-5}	2×10^{-4}

From table I, the dielectric constant is more affected by the humidity variation than the rest of the parameters. A small humidity variation can be reflected in the value of the dielectric constant and hence, the measure of resonance frequency, since they are related by (2). Using the same analysis, the sensitivity of resonance frequency δf_r is related to the sensitivity of dielectric constant $\delta\varepsilon_r$ by:

$$\delta f_r = \left|\frac{\partial f_r}{\partial\varepsilon_r}\right|\delta\varepsilon_r = \left|\frac{\partial f_r}{\partial\varepsilon_r}\right|\left(\left|\frac{\partial\varepsilon_r}{\partial P}\right|_{P_0}\delta P + \left|\frac{\partial\varepsilon_r}{\partial T}\right|_{T_0}\delta T + \left|\frac{\partial\varepsilon_r}{\partial H}\right|_{H_0}\delta H\right) \qquad (9)$$

Minimizing the sensitivity of resonance frequency δf_r implies minimizing the measuring errors produced by the other parameters, which are limited by the test apparatus. Table II lists the numerical values of $|\partial f_r/\partial\varepsilon_r|$, $|\partial f_r/\partial P|$, $|\partial f_r/\partial T|$ and $|\partial f_r/\partial H|$ for both resonator prototypes, SIW1 and SIW2. Table II shows that resonator SIW1 has higher sensitivity than SIW2 in terms of the variation of dielectric constant $|\partial f_r/\partial\varepsilon_r|$, which explains the results obtained in figures Fig. 9 and Fig.10.

TABLE II
SENSITIVITY ANALYSIS OF RESONANCE FREQUENCY (GHz)

Resonator	$\lvert\partial f_r/\partial\varepsilon_r\rvert$	$\lvert\partial f_r/\partial P\rvert$	$\lvert\partial f_r/\partial T\rvert$	$\lvert\partial f_r/\partial H\rvert$
SIW1 (g=9.7mm)	0.36	2.51×10^{-7}	1.8×10^{-5}	10^{-4}
SIW2 (g=2.1mm)	0.094	0.64×10^{-7}	0.47×10^{-5}	9.35×10^{-6}

Also, the effects of pressure, temperature and humidity variations on the resonance frequency are indicated in table II. The effect of pressure and temperature variation is negligible for both SIW1 and SIW2. The measured output frequency shift for both sensors is a linear function of relative humidity as predicted by the analytical perturbation model. Table II confirms that the main factor affecting the sensitivity is the size of the sensitive region (g). In case of the first resonance mode TE101, increasing the size of the sensitive region allows more interaction between the electric field and the moist in the air holes leading to higher frequency deviation per relative humidity value.

VII. COMPARISON & DISCUSSION

The sensing performance of the proposed resonator structure has been compared to other microwave components in literature. Table III lists the microwave structures used as humidity detectors with their sensitivities.

TABLE III
COMPARISON OF MICROWAVE STRUCTURES FOR HUMIDITY SENSING

Structure	Operation principle	RH% range	Sensitive material	Sensitivity	
C-section group delay	Phase shift	53.9-94.3%	Yes	393 ns/RH%	[5]
H-slot antenna	Power level	50-100%	Yes	0.2 dB/RH%	[6]
RFID tag	Frequency shift	11.3-100%	Yes	171.4 kHz/RH%	[7]
RFID tag	Frequency shift	25-90%	Yes	108 kHz/RH%	[17]
Stepped impedance resonator	Frequency shift	65-80%	Yes	200 kHz/RH%	[18]
Substrate integrated resonator (New)	Frequency shift (1st mode)	0-80%	No	101 kHz/RH% 9.35 kHz/RH%	This work

Most of the investigated structures achieved sensitivity in the order of hundreds of kHz/RH% with the help of humidity sensitive material. On the other hand, the C-section structure [5] has higher sensitivity using doped Silicon nanowires as a sensitive material but within a small humidity range. As shown in table II, the proposed substrate integrated resonator has wider sensitivity range to humidity (0-80%) compared to other published structures which use humidity sensing materials. In addition, the proposed SIW humidity sensors show a linear response over it entire range which is convenient in passive sensing application.

VIII. CONCLUSION

In this work, a microwave substrate integrated resonator is presented as a humidity detector for the first time. The proposed structure operates without a humidity sensitive material in the humidity range from 0 to 80% RH. The humidity sensing capability of the proposed resonator is based on changing the effective permittivity inside the resonator due to the presence of moisture. The presented resonator has a sensitivity of 9.35-101 kHz/RH% depending on the size of the dielectric sensitive region introduced inside the cavity. The resonance frequency can be easily modified by changing the dimensions of the resonator to make it suitable for specific applications. The proposed structure has wider sensitivity range to humidity with linear transfer function predicted by an analytical model. As the substrate integrated technology is transferrable to different types of substrate, the proposed structure can be fabricated on flexible substrates.

REFERENCES

[1] G. Marrocco, "Pervasive electromagnetics: sensing paradigms by passive RFID technology," *IEEE Wireless Communications*, vol. 17, pp. 10 –17, Dec. 2010.

[2] Want, R, "Enabling ubiquitous sensing with RFID", *Computer*, 37, vol. 4, pp. 84–86, 2004.

[3] G. Barochi, J. Rossignol, and M. Bouvet, "Development of microwave gas sensors," *Sensors and Actuators B-Chemical*, vol. 157, pp. 374-379, Oct 20 2011.

[4] C. Occhiuzzi, A. Rida, G. Marrocco, and M. Tentzeris, "RFID Passive Gas Sensor Integrating Carbon Nanotubes," *IEEE Trans. Microw. Theory Techn*, vol. 59, pp. 2674-2684, Oct 2011.

[5] Raji Nair, Etienne Perret, Smail Tedjini, Thierry Barron, "A Humidity Sensor for Passive Chipless RFID Applications," IEEE Int Conf on RFID-Technol and Appl (RFID - TA), pp.24-33, 2012.

[6] Sabina Manzari, Cecilia Occhiuzzi, Shankar Nawale, Alexandro Catini, Corrado Di Natale, and Gaetano Marrocco, "Humidity Sensing by Polymer-Loaded UHF RFID Antennas," *IEEE Sensors J*, vol. 12, no. 9, pp. 2851-2858, Sept 2012.

[7] Juha Virtanen, Leena Ukkonen, Toni Björninen, Atef Z. Elsherbeni, Lauri Sydänheimo, "Inkjet-Printed Humidity Sensor for Passive UHF RFID Systems", *IEEE Trans. Instrum. Meas*, vol. 60, no. 8, Aug, 2011.

[8] Ding-Ding Zhang, "Novel Bandpass Filters by Using Cavity-Loaded Dielectric Resonators in a Substrate Integrated Waveguide", *IEEE Trans. Microw. Theory Techn*, vol. 62, pp. 1173-1182, 2014.

[9] El H. Matbouly, N. Boubekeur, F. Domingue, "A Novel Chipless Identification Tag Based on a Substrate Integrated Cavity Resonator," *IEEE Microw. Compon. Lett* ., vol. 23, no. 1, pp. 52-54, Jan. 2013.

[10] Wei Hong, Ke Wu, "Design Mechanisms and Application Examples of SIW Structure family," presented at IEEE IMS 2012.

[11] J. D. Barrera and G. H. Huff, "Analysis of a variable SIW resonator enabled by dielectric material perturbations and applications," *IEEE Trans. Microw. Theory Techn*, vol. 61, pp. 225-233, 2013.

[12] Jacob Fraden, "The handbook of modern sensors: Physics, Design and Application", Third edition, pp. 393-399, 2003.

[13] Y. Cassivi, L. Perregrini, P. Arcioni, M. Bressan, K. Wu, and G. Conciauro, "Dispersion Characteristics of Substrate Integrated Rectangular Waveguide," *IEEE Microw. Compon. Lett.*, vol. 12, no. 9, pp. 333-335, Sept 2002.

[14] K. Wu, D. Deslandes, and Y. Cassivi, "The substrate integrated circuits—A new concept for high-frequency electronics and optoelectronics", Proc. *TELSIKS*, pp. 3–5, Oct. 2009.

[15] D. Pozar, "Microwave Engineering," 2ed edition, 1998.

[16] E. Amin, N. Karmakar, and B. Winther-Jensen," Polyvinyl-alcohol (pva)-based RF Humidity Sensor in Microwave Frequency," *Progress in Electromagnetics Research* B, Vol. 54, 149-166, 2013.

[17] K. Chang, Y.H. Kim, Y.J. Kim and Y.J. Yoon, "Functional antenna integrated with relative humidity sensor using synthesised polyimide for passive RFID sensing, " *Electron lett*, vol. 43, no 3, 2007.

[18] Emran M. Amin, Nemai C. Karmakar," Development of a Low Cost Printable Humidity Sensor for Chipless RFID Technology," IEEE Int Conf on RFID-Technol and Appl (RFID - TA), 2012.

5.5 Contribution V brevet: «Microwave resonator sensor and associated methods of sensing»

Cet article porte sur le dépôt d'un brevet d'invention pour protéger la propriété intellectuelle. L'invention présente un résonateur passif micro-ondes intégré au substrat (SIW) fonctionnant comme un capteur environnemental. La structure du capteur proposé est basée sur l'insertion d'une région fonctionnalisée à l'intérieur de la cavité résonante SIW où le matériau de détection est choisi sur la base de la quantité physique à détecter.

En présence de la substance à analyser la permittivité de la région fonctionnalisée change, provoquant un décalage de la fréquence de résonance dans le spectre de résonance. Ce changement de fréquence peut être détecté et utilisé comme principe de détection du capteur micro-ondes. La présente invention a l'avantage de fournir une nouvelle solution de fabrication qui permet d'améliorer la sensibilité du capteur, simplifier les processus de fabrication et réduire considérablement le coût du capteur. En outre, plusieurs différents capteurs peuvent être facilement intégrés sur une seule production PCB; ce qui réduit les coûts de production. Des prototypes ont été fabriqués et testés pour confirmer les fonctionnalités de la structure du capteur SIW proposé.

L'article décrit aussi plusieurs idées associées à la structure du capteur SIW. Par exemple, cette invention inclut les capteurs passifs sans fil et les capteurs actifs intégrés au substrat. La possibilité de passer d'une technologie de capteur passif à un capteur actif intégrant le même principe de détection est également relatée dans cet article. De plus, un

élément actif comme un amplificateur RF peut être intégré avec le capteur afin d'en faire un oscillateur à boucle fermée.

NORTON ROSE FULBRIGHT

PATENT APPLICATION SPECIFICATION

Our Ref. no.	05015656-85USPR
Priority(ies)	None
Public Disclosure	None planned prior to filing of application -
Search	05015656-SRCH-03
Entity size (for US only)	small (to be confirmed by signing declaration)
Country (ies):	rights reserved worldwide for one year under Paris Convention
Illustrative figure :	TBD

Inventors :

Name	Address	Nationality
Hatem EL MATBOULY	veuillez remplir s.v.p.	-
Frederic DOMINGUE	veuillez remplir s.v.p.	-

Owner(s) (if other than inventors) :

Name	Address
GESTION VALEO S.E.C.	1155 René-Lévesque Ouest, bureau 2701 Montréal QC H3B 2K8 Canada

MICROWAVE RESONATOR SENSOR AND ASSOCIATED METHODS OF SENSING

FIELD

[0001] The improvements generally relate to the field of sensors for sensing physical properties of an environment, and more particularly to a sensor using a microwave resonator.

BACKGROUND

[0002] Sensors for sensing physical properties of an environment are well known in the art. Recently, sensors in monitoring air quality such as gas presence, humidity level, a temperature or dust level in vehicles, houses, and offices have raised a high degree of interest in science.

[0003] Although existing sensors were satisfactory to a certain degree, there remained room for improvement, particularly in terms of providing passive sensors adapted to the physical property to sense, of providing sensors that can be individually identifiable by a signature tag, of providing sensors that can be remotely interrogated and that allow these sensors to be manufactured at a competitive cost.

SUMMARY

[0004] In accordance with one aspect, there is provided a substrate-integrated waveguide (SIW) sensor reactive to a microwave signal and enabling to sense environmental physical properties such as a presence of a gas, a humidity level, a temperature, a dust level, etc.

[0005] In accordance with another aspect, there is provided a sensor having a microwave resonator in which an input microwave signal can be propagated, resonated to allow interaction with the environment, and a characteristic representative of the interaction with the environment can be measured in the output microwave signal. The microwave resonator can be characterized, for instance, by a given effective permittivity value and by a given shape. Henceforth, for the given effective permittivity value and the given shape, the microwave resonator can have a signature resonance frequency. It is known in the art that upon a physical property change around a dielectric material, the effective permittivity of the

dielectric material can change accordingly. Therefore, the sensor is adapted to sense a change of the physical property through a change in the effective permittivity value of its microwave resonator.

[0006] In other words, a microwave signal having a broad spectrum that is propagated through the microwave resonator can be transformed into a microwave output signal having a resonance frequency dip in its frequency spectrum. The resonance frequency dip can be attributed to the frequencies resonating (trapped) in the microwave resonator. Now, since the resonance frequency can depend on the effective permittivity value of the microwave resonator, any change in the environment of the microwave resonator can be sensed by a shift of the resonance frequency dip of the output microwave signal. It is readily understood that higher order resonance frequencies can also resonate within the resonator. Consequently, the shift of the resonance frequency can be measured on a first order of resonance (first mode), as it can be measured on a second order of resonance (second mode), or on a third order of resonance (third mode), and so on. As it may be understood by one skilled in the art, the shift of resonance frequency of the second order or resonance can be greater than the shift of resonance frequency of the first order for a given physical property variation, thus offering a greater sensitivity.

[0007] In accordance with another aspect, there is provided a sensor having a microwave resonator characterized by an enhanced sensitivity due to the high quality factor of its resonator (or resonant cavity). It is known in the art that quality factors can be a convenient measure for a sensor's sensitivity. Indeed, the quality factor of a resonator is as high as the width of its resonance frequency is narrow. Practically, a narrower resonance frequency can enable the measurement of a smaller increment of the physical property.

[0008] In accordance with another aspect, there is provided a sensor that has a microwave resonator having a top conductive layer, a bottom conductive layer and a dielectric substrate layer therebetween. More particularly, the top conductive layer and the substrate layer has at least one sensing portion integrated therethrough to form at least one resonance cavity, the at least one sensing portion being functionalized with a sensitive dielectric material adapted to the physical property to sense. Differently put, there is provided a sensor having a microwave resonator that can be characterized by a given effective

permittivity value, the latter being determined, for instance, at least by the dielectric constant of the substrate layer and by the sensitive dielectric constant of the dielectric material filing the at least one sensing portion. Therefore, if the sensitive dielectric material is known to vary in an enhanced manner according to a given physical property, the sensor can be more sensitive to this given physical property. For instance, the sensitive dielectric material can be air for humidity sensing, and can be tin dioxide for sensing the presence of hydrogen.

[0009] In accordance with another aspect, there is provided a sensor only having passive components therein.

[0010] In accordance with another aspect, there is provided a sensor that can be passively interrogated using electrical wires to be connected to a microwave signal port, or wirelessly interrogated using a microwave antenna connected to the microwave resonator of the sensor.

[0011] In accordance with another aspect, there is provided a sensor that has a microwave resonator having a given pattern of sensing portions disposed therethrough. Since a resonance frequency of the microwave resonator can be dependent on a given shape of the microwave resonator for instance, the microwave resonator of the sensor having the given pattern of sensing portions can have a signature resonance frequency. Therefore, a first sensor having a first pattern of sensing portions disposed through the microwave resonator can be distinguished from a second sensor having a second pattern of sensing portions disposed therethrough. Accordingly, by measuring the resonance frequency of a particular sensor, one can determine which sensor it is and consequently, determine which physical property is being sensed. Moreover, the sensor can be integrated with other systems by using radio frequency components hence increasing their compatibility and functionality.

[0012] In accordance with another aspect, there is provided a sensor for sensing at least a physical property of an environment, the sensor comprising a microwave resonator having a top conductive layer, a bottom conductive layer and a substrate layer therebetween, the substrate layer being made of a first dielectric material, a fence electrically connecting the top conductive layer to the bottom conductive layer across the substrate layer, and enclosing

at least one resonance cavity, at least one microwave signal port across the fence, at least one sensing portion of a second dielectric material functionalized to the physical property of the environment, extending in the at least one resonance cavity and being exposed to the environment by at least one of the top conductive layer and the bottom conductive layer, the microwave resonator having at least one resonance frequency being dependent of the exposure of the second dielectric material with the environment to affect a microwave signal resonating therein.

[0013] In accordance with another aspect, there is provided a method for sensing at least a physical property of an environment, the method comprising: providing a path having an input and an output; and a microwave resonator therebetween, the microwave resonator having a top conductive layer, a bottom conductive layer and a substrate layer therebetween, the top conductive layer being electrically connected to the bottom conductive layer by a conductive fence across the substrate layer, the fence enclosing at least one resonance cavity, the input being connected to the at least one resonance cavity across the fence, each of the at least one resonance cavity having at least one sensing portion of a second dielectric material functionalized to the physical property of the environment, extending in the at least one resonance cavity and being exposed to the environment across at least one of the top conductive layer and the bottom conductive layer, the microwave resonator having at least one resonance frequency; propagating an input microwave signal into the input of the path, the microwave resonator transforming the input microwave signal into an output microwave signal being characterized by the at least one resonance frequency, the at least one resonance frequency being dependent of the exposure of the second dielectric material with the environment to affect a microwave signal resonating therein; measuring the resonance frequency in the output microwave signal from the output of the path; and sensing the at least a physical property based on the resonance frequency.

[0014] In accordance with another aspect, there is provided a method of making a sensor for sensing at least a physical property of an environment, the method comprising: placing a substrate layer made of a first dielectric material; incorporating a layer of conductive material on the top of the substrate and a layer of conductive material on the bottom of the substrate; processing at least one sensing portion through the three layers thus forming a fence of

through-holes enclosing at least one resonance cavity of the three layers; processing an input channel on the layer of conductive material on the top of the substrate, the input channel protruding to one of the at least one resonance cavity of the three layers; processing, on the at least one resonance cavity, a given configuration of holes through at least the layer of conductive material on the top of the substrate and the substrate layer; applying a melted layer of conductive material on an interior surface of the through-holes thereby making an electrical link between the two layers of conductive material; and inserting a dielectric material inside the holes of at least an associated resonance cavity.

[0015] Many further features and combinations thereof concerning the present improvements will appear to those skilled in the art following a reading of the instant disclosure.

DESCRIPTION OF THE FIGURES

[0016] In the figures,

[0017] Fig. 1 is an oblique view of an example of a microwave resonator of a substrate-integrated waveguide sensor;

[0018] Fig. 2A is a bloc diagram showing an example of a substrate-integrated waveguide sensor having an antenna for remote interrogation or wireless communication with an electrical spectrum analyser while Fig. 2B is a bloc diagram showing an example of a substrate-integrated waveguide sensor used in a wired interrogation system;

[0019] Fig. 3A is a bloc diagram showing an example of a detection system involving a sensing oscillator, Fig. 3B is a bloc diagram showing an example of a detection system involving a sensing oscillator and a reference oscillator, and Fig. 3C is a bloc diagram showing an example of a detection system involving a reference oscillator connected to a high pass filter made using a functionalized substrate-integrated waveguide sensor;

[0020] Fig. 4A is a graph showing an example of the relative variation of the relative permittivity of tin dioxide as a function of frequency with and without presence of hydrogen while Fig. 4B is a graph showing an example of a resonance frequency of a substrate-

integrated waveguide sensor as a function of time when hydrogen is provided then removed in a chamber enclosing the substrate-integrated waveguide sensor;

[0021] Fig. 5 shows graphs showing an example of a simulated and measured resonance frequency of a substrate integrated sensor as a function of relative humidity percentage in an environment of the sensor for the first order of resonance in Fig. 5A and for the second order of resonance in Fig. 5B;

[0022] Fig. 6A is an oblique view of an alternate example of a substrate-integrated waveguide sensor having three resonance cavities on the top conductive layer of the sensor while Fig. 6B is a graph showing an example of the resonance frequencies associated with the three resonance cavities of the sensor of Fig. 6A;

[0023] Fig. 7A is a top view of alternate examples of substrate-integrated waveguide sensors, each sensor having a signature pattern of sensing portions, Fig. 7B shows a graph of an example of the simulated resonance frequencies associated with the signature patterns shown in Fig. 7A, and Fig. 7C shows the measured resonance frequencies associated with the signature patterns shown in Fig. 7A;

[0024] Fig. 8 shows a graph of an example of the measured resonant frequencies associated with the signature patterns of the sensors shown in the graph which has a remote interrogation system involving an antenna; and

[0025] Fig. 9 is a bloc diagram showing an example of a detection system for remote interrogation of three substrate-integrated waveguide sensors.

DETAILED DESCRIPTION

[0026] Fig. 1 shows an example of a substrate-integrated waveguide (SIW) sensor 10. The sensor 10 can have a microwave resonator that has a top conductive layer 12, a bottom conductive layer and a substrate layer 14 therebetween. The substrate layer 14 is generally made of a dielectric material while the top conductive layer 12 and the bottom conductive later can be made of a metallic material such as copper, for instance. The top conductive layer 12 can be electrically connected to the bottom conductive layer with a fence, or a fence of via holes 16 enclosing one or many resonance cavities 18. Via holes are known in the

electronic arts and are generally used to electrically connect different layers of a substrate. They typically consist of holes having their inside surface covered with a conductive material, for instance. On the other hand, it is understood that any type of fence can be used in order to electrically connect the top conductive surface 12 and the bottom conductive surface. It is important, for any design of fence, that the microwave signal can be reflected from the fence in order to resonate within the resonant cavity.

[0027] Additionally, the microwave resonator can have a microwave signal port 20 across the fence 16 and connecting the top conductive layer 12 for receiving a signal to be propagated to the resonant cavities. Particularly, each of the resonance cavities 18 can have a signature pattern of sensing portions 22 through at least the top conductive layer and the substrate layer thereunder (or through the bottom conductive surface in another embodiment). Each sensing portion can be provided in the form of a hole through either the top conductive layer and the substrate layer, or the top conductive layer, the substrate layer and the bottom conductive layer. To facilitate the manufacturing process, each sensing portion can be drilled through the microwave resonator, for instance. To obtain the sensing portions 22, the sensing portions of the resonance cavity can be filed with an associated dielectric material which is assumed particularly sensitive to a physical property to sense. It is understood that each of the resonance cavities 18 imparts an associated resonance frequency to the microwave resonator, and that the resonance frequency varies as a function of the physical property of an environment therearound.

[0028] It is understood that the sensor can have a body having any two-dimensional shape such as a circular body, a triangular body, or other polygonal bodies. Referring to Fig. 1, however, the sensor 10 can have a rectangular body 24. The dimensions of the rectangular body 24 can have an impact on the resonance frequency of the microwave resonator of the sensor 10. Henceforth, it is possible to compute the resonance frequency of the rectangular microwave resonator using the equation:

$$f_r = \frac{c}{2\sqrt{\varepsilon_r}}\sqrt{\left(\frac{n}{w_{eff}}\right)^2 + \left(\frac{m}{l_{eff}}\right)^2}, \qquad (1)$$

[0029] where f_r is the resonance frequency of the microwave resonator, c relates to the speed of an electromagnetic wave in vacuum, ε_r is the relative permittivity of the substrate layer 14, n and m indicates integers representative of the mode of the resonator, w_{eff} and l_{eff} are the effective width and length of the microwave resonator which are determined by the fence of via holes 16 enclosing the resonance cavity 18 and the microwave signal port 20. The effective dimensions are determined by the equations :

$$w_{eff} = w_i - \frac{D}{0.95b} \text{ and } l_{eff} = l_i - \frac{D}{0.95b} \quad (2)$$

[0030] where the indices *eff* indicates the effective dimensions, the indice i indicates the distance between two opposite sides of the fence of via holes, D is the diameter of the via holes of the fence of via holes 16 and b is a via hole spacing.

[0031] The microwave signal port 20 adjoining a subminiature version A (SMA) connector to the microwave resonator can be provided in the form of a microstrip transmission line adapted to the microwave resonator. Indeed, the microwave signal port 20 can propagate the microwave input signal to the microwave resonator, where the input microwave signal is transformed into an output microwave signal which can be later propagated back to the SMA connector via the microwave signal port 20.

[0032] The given pattern of sensing portions 22 introduced above can be "empty", or being filed with ambient air, i.e. a dielectric known to change its permittivity as a function of the humidity level of the environment, or it can be filed with any dielectric material that are suited for sensing a change of a physical property of the environment. It is worthy to note that the number of sensing portions inside the microwave resonator can vary depending on the dielectric constant of the sensitive dielectric material filled therein. Experiments and materials known to be particularly sensitive to the presence of a gas, or other physical property, are presented further below. In one embodiment, the sensing portions 22 can go through both the top conductive layer 12 and the substrate layer 14, while the bottom conductive layer remains plain and can be used as a circuit ground. It is readily understood that the distance s (see Fig.1), i.e. the distance between the microwave signal port 20 and the fence of via holes 16, can help in achieving a better coupling of the input microwave signal.

[0033] Fig. 2A shows an example of a bloc diagram showing the sensor 10 having an antenna 26 connected to the microwave resonator, the antenna 26 enabling remote interrogation of the sensor 10 or wireless communication with, for instance, an electrical spectrum analyser (ESA) 27 having a display 29. In this detection system, a broad microwave signal can be propagated to be received by the antenna 26 of the sensor 10. When the microwave signal is propagated through the microwave resonator of the sensor 10, a portion of the microwave signal can resonate in the resonator. Henceforth, the ESA can detect a reflected broad microwave signal having a dip representative of the portion of the microwave signal still resonating (to be subsequently attenuated) in the microwave resonator. Thus, sensing can be achieved by monitoring a spectral position of the frequency dip as a function of a physical property. Fig. 2B shows an alternate example of a detection system. In this embodiment, the sensor 10 has an input end 28 and an output end 30, where an input microwave signal can be provided to the input end 28, then transformed into an output microwave signal that can be measured with the output end 30. In another embodiment, the sensor 10 can have an amplifier 32 (or radio-frequency amplifier, RF amplifier) to form an amplification stage 34 (or loop of amplification).

[0034] Fig. 3 shows examples of detection systems which can be used to sense a physical property of an environment using one or more SIW sensors. Fig. 3A shows a detection system including a sensing oscillator 36A in which an active component such as a microwave amplifier 32A can be used as a seed to provide a base microwave signal. Since the microwave amplifier 32A of the sensing oscillator 36A is connected to a functionalized sensor 38A (sensor having a second dielectric material filing the sensing portions therein), microwave frequencies can be oscillated in the sensing oscillator 36A. A microwave power splitter 40A is used to propagate a portion of the microwave signal oscillating in the sensing oscillator 36A out of the oscillator to form an output signal. The output signal is then amplified using an output amplifier 41A and filtered using a high pass filter 42A. The output signal can later be analysed using a peak detector, a data processing computer and a display.

[0035] Fig. 3B shows an example of a detection system including a sensing oscillator 36B, and a reference oscillator 44B. The sensing oscillator has a functionalized sensor 38B,

a microwave amplifier 32B, a microwave power splitter 40B, while the reference oscillator 44B has an unfunctionalized sensor 46B (or a sensor only functionalized with air), a microwave amplifier 32B, and a microwave power splitter 40B. Output signals of both the sensing oscillator 36B and of the reference oscillator 44B are then mixed using a mixer 48B. When the two output signals have a different frequency spectrum, a frequency beat can be generated. This beat generally has higher frequency components and lower frequency components (difference of the frequencies of the two oscillators), the higher frequency components can be filtered using a low pass filter 50B. Afterwards, the lower frequency components can be amplified using a microwave output amplifier 41B, hence allowing the resulting signal to be analysed using a peak detector, a data processing computer and a display.

[0036] Fig. 3C shows an example of a detection system including a reference oscillator 44C having an unfunctionalized sensor 44C, a microwave amplifier 32C, a microwave power splitter 40C. In this detection system, a microwave signal can be amplified in the reference oscillator 44C. The microwave signal directed out of the reference oscillator 44C by the microwave power splitter 40C can be amplified using a microwave output amplifier 41C, which can then be filtered using a high pass filter 42C made using a functionalized sensor 38C. The resulting signal being subsequently analysed using a peak detector, a data processing computer and a display. A characteristic of the high pass filter 42C, such as a cut off frequency, can change due to a change of the physical property, which affects the amplitude of the output signal thus indicating the change of physical property.

[0037] These detection systems allow easy integration of the above-mentioned microwave components directly on the PCB in which the substrate-integrated waveguide sensor is integrated, henceforth providing a monitoring circuit that does not require additional packaging and assembly. It can be noted that the SIW sensors can be manufactured in many other common planar technologies such as low temperature co-fired ceramic (LTCC), thick film, thick paper printing, and the like.

[0038] The substrate-integrated waveguide sensor is designed using an electromagnetic simulation software which allows to shape the three-dimensional structure of the microwave resonator and to perform a full-wave three-dimensional analysis. Based on given

parameters, the software can estimate a signature resonance frequency, a phase thereof, and a distribution of the electric field inside the substrate-integrated microwave resonator. The effect of sensing portions inside the microwave resonator has been investigated with the software. For instance, perfect conductive material are assumed for the top conductive layer, the bottom conductive layer and the conductive material electrically connecting the top conductive layer to the bottom conductive layer in the via holes of the fence. In addition, absorbing boundary conditions were applied along the edges of the rectangular body (boundary walls of the body of the microwave resonator). For the simulation, the substrate chosen was the Roger substrate RO3004C having parameters such as an electric permittivity of ε_r = 3.55, tan δ = 0.002, a thickness of 1.524 mm and a copper thickness of 17 µm. The dimensions of the microwave resonator can be 31 mm x 31 mm, which fixes the signature resonance frequency around 3.56 GHz for a resonance of first order (fundamental frequency mode TE_{10}). This embodiment is shown in Fig 1, and the parameters *s*, *t*, *b*, w_{eff} and l_{eff} are listed in Table 1. It is readily understood by one skilled in the art that the shape and the dimensions of the substrate-integrated waveguide sensor and microwave resonator thereof can be modified to obtain resonance frequencies other than frequencies around 3.56 GHz. The dimensions shown in Table 1 are exemplary only. Indeed, dimensions facilitating the manufacturing process (using PBC techniques) can be suitable for the sensor presented herein. For instance, common diameter for via holes can range from 0.3 mm to 1.0 mm.

Table 1 – Values for parameters used to simulate the microwave cavity using the software

Parameter	w_{eff} **[mm]**	l_{eff} **[mm]**	***s*** **[mm]**	***t*** **[mm]**	**via hole diameter [mm]**	**sensing portion diameter [mm]**	***b*** **[mm]**
Value*	31	31	0.37	9.7	0.4	0.8	1.5

*Values given to the PCB prototyping machine used. The machine has a resolution of 0.5 µm and a repeatability of 0.001 mm. However, the resolution and the repeatability can vary from one prototyping machine to another.

[0039] As mentioned above, the substrate-integrated waveguide sensor described herein can have sensing portions in order to be particularly sensitive to a physical property to detect. Accordingly, Tables 2 and 3 list, respectively, sensitive dielectric materials associated to a gas to be detected and sensitive dielectric materials associated to humidity and temperature sensing. Also, it has to be noted that functionalized polymers can be used to facilitate the integration of sensitive materials in the microwave resonator using industrial PCB fabrication processes.

Table 2 – List of sensitive dielectric material that can be used for sensing the presence of a given gas

Gas to be detected	Sensitive dielectric material therefore
CO, H_2, CH_4	SnO_2 (tin dioxide)
NO_x, O_3, H_2S, SO_2	WO_3
O_2, CO	Ga_2O_3
O_3, NO_x	In_2O_3
NH_3, NO_2	MoO_3
O_2, CO, SO_2	TiO_2
CH_4, C_4H_{10}, O_3, NO_x	ZnO
H_2S, NH_3, CO, volatile organic compounds	CrTiOx
Alcohol, CH_4, NO_2	Fe_2O_3
Formaldehyde	Perovskite oxide structure: $La_{1-x}Sr_xFeO_3$ (x = 0, 0.2, 0.5); Conductive polymer PPy/EBSA
CO_2	Type electrolytic solid: $Na_{1+x}Zr_2Si_xP_{3-x}O_{12}$ (1.8 < x < 2.4); Na_2CO_3-$BaCO_3$, Na_2CO_3-$CaCO_3$, Li_2CO_3-$BaCO_3$, et Li_2CO_3-$CaCO_3$.
NO_x	WO_3, ZnO, SnO_2, In_2O_3, TiO_2
CO	WO_3, In_2O_3, MoO_3, V_2O_5
NH_3	nanofibres WO_3 polypyrrole (PPy)/$ZnSnO_3$
H_2S	SnO_2 doped by Ag ZnO nano-wires

Table 3 – List of sensitive dielectric material that can be used for sensing a given physical property

Physical property to be sensed	Sensitive dielectric material therefore
Humidity	Kapton 500HN polymer
Temperature	Epoxy/$BaTiO_3$ Composite

[0040] As listed in Table 2, tin dioxide can be used as a sensitive dielectric material to sense a presence of hydrogen in an environment. To integrate the tin dioxide into sensing portions of a given pattern of sensing portions, a tin dioxide powder having a grain size in the range of the nanometer can be used. Moreover, the grain size of the nano powder can be optimized in order to enhance the sensitivity of the material. Fig. 4A shows the relative variation of the relative permittivity of a nano powder of tin dioxide that has been grinded for 60 minutes when under a controlled environment in which hydrogen has been introduced. It is seen that the relative permittivity of the tin dioxide changes (see arrow 54) in the presence of hydrogen, which makes the tin dioxide a suitable dielectric material for sensing a presence of hydrogen in an environment. It was shown that among a nano powder that have not been grinded, a nano powder that have been grinded for 15 minutes, a nano powder that have been grinded for 30 minutes, a nano powder that have been grinded for 45 minutes and a nano powder that have been grinded for 60 minutes, the latter was the one exhibiting the largest relative variation of the relative permittivity in a given frequency range. As mentioned above, the tin dioxide tested was provided in a matrix of polymer polyvinyl alcohol (PVA), for instance, to form a composite matrix. The composite matrix facilitates the incorporation of the nano powder in the sensing portions (holes) of the resonance cavity of the substrate-integrated waveguide sensor. It is understood that other polymer matrices can be used to form a composite matrix for the dielectric material proposed in Tables 2 and 3.

[0041] Fig. 4B is a graph showing the results of an experiment using a SIW sensor functionalized with a tin dioxide nano powder grinded for 60 minutes. The experiment consisted of placing the functionalized SIW sensor in a chamber in which a constant gas

flow of hydrogen was provided while measuring the resonant frequency of the SIW sensor. Hydrogen was provided in the chamber at time zero, while it was removed around the tenth minute. It can be seen that a shift in the resonant frequency of the SIW sensor can be observed, indeed, a shift of 40 MHz was measured on the resonance of first order (first mode of resonance). All the measurements were made using an ESA. It was previously demonstrated that the frequency shift can be due to the change in the dielectric constant of the tin dioxide sensing portions of the SIW sensor. Since the resonance frequency of the microwave resonator is related to the dielectric constant of the microwave resonator by the relation $f_r \propto {\varepsilon_{eff}}^{-1/2}$, where ε_{eff} is the effective permittivity of the substrate, the variation of ε_{eff} can introduce a change in the resonance frequency of the microwave resonator, as discussed above, which can be attributed to a presence of hydrogen.

[0042] In another embodiment of the sensor, air can be used as the sensitive dielectric material filing sensing portions of a sensor in order to measure a humidity level in an environment. In this embodiment, the dielectric variation enabling a shift of resonance frequency can be due to the difference between the dielectric constant of air and the dielectric constant of moist air. Therefore, sensing portions having air therein can be used in order to sense the humidity level of the environment. It has been shown that the electric permittivity of air changes as a function of the relative humidity according to the equation:

$$\varepsilon_r(H) = 1 + \frac{211}{T}\left(P + \frac{48P_s}{T}RH\right) \times 10^{-6}; \quad (3)$$

[0043] where ε_r is the relative permittivity, *T* is the absolute temperature (in K), *P* is the pressure of moist air (in mmHg), P_s is the pressure of saturated water vapor (in mmHg), *RH* is the relative humidity (in %). Equation (3) shows that the dielectric constant of moist air is proportional to the relative humidity *RH*. Since the resonance frequency of the microwave resonator is inversely proportional to the effective dielectric constant such as $f_r \propto {\varepsilon_{eff}}^{-1/2}$, changing the relative humidity *RH* due to vapor, for instance, can consequently change the resonant frequency of the microwave resonator. Henceforth, a shift of resonance frequency can be exploited as an indication of the presence of moisture in the air surrounding the microwave resonator of the SIW sensor.

[0044] Fig. 5 shows graphs presenting the simulated and measured resonance frequencies as a function of relative humidity *RH*. In this experiment, the relative humidity *RH* was increased from 20% to 100%, and the resonance frequencies were measured using a vector network analyser (VNA). As shown in Fig. 5A, the first mode of resonance 56 of the microwave resonator, i.e. around 4.16 GHz, exhibits a maximum shift of resonance frequency of 5 MHz from a relative humidity of 20% to a relative humidity of 100%. The measured sensitivity $S=|\Delta f/\Delta RH|$ was found to be 65 kHz/*RH*, where Δf is the shift of resonance frequency measured, and ΔRH is the range of relative humidity on which the shift Δf was measured. The same measurement was performed on the second mode of resonance 58, i.e. around 6.58 GHz, and the results are shown in Fig. 5B. The resonance frequency of the second order of resonance exhibits a maximum shift of resonance frequency of 20 MHz at a relative humidity of 100%, and a sensitivity of 261 kHz/*RH* is obtained. It is noticed that the sensitivity of the second mode of resonance is higher than the sensitivity of the first order of resonance, perhaps due to the larger area of the electric field interacting with the sensing portions of the resonator in the case of the second mode of resonance. Accordingly, one can position the sensing portions of the resonance cavities at high intensity areas 56 and 58, thus increasing the interaction between the electric field (as shown in insets of Figs. 5A and 5B) of the resonance modes and the dielectric material within those strategically positioned sensing portions.

[0045] wherein the at least one sensing portion of each of the at least one resonance cavity are located on at least a given high intensity area, the at least a given high intensity area being indicative of a high electric field therearound.

[0046] In another embodiment, the substrate-integrated waveguide sensor can have more than one resonance cavity on the top conductive surface. As shown in Fig. 6A, the SIW sensor can have three resonance cavities, for instance, each having sensing portions being functionalized with a different sensitive dielectric material. Accordingly, one sensor can be used to sense three different properties of an environment by monitoring the associated signature resonance frequencies corresponding to each of the resonance cavities. For instance, the resonance cavities 60, 62 and 64 can have the resonance frequencies (simulated) 66, 68 and 70. Such an embodiment can be used as a multi gas sensor made

out of a monolithic fabrication process. It has to be noticed that to enhance the resonant phenomenon, each resonance cavity can be enclosed partially by the electrically conducting fence, as shown in Fig. 6A.

[0047] In another embodiment, the substrate-integrated waveguide sensor 10 can have a given pattern of sensing portions on the top reflective surface of the microwave resonator. Since the resonance frequency is dependent on an effective dielectric constant of the SIW sensor 10 and on a geometry of the microwave resonator, a first SIW sensor having a first given pattern 72 of sensing portions can have a different signature resonance frequency than a second SIW sensor having a second given pattern 74 of sensing portions. Therefore, the four different patterns (72, 74, 76 and 78) of sensing portions shown in Fig. 7A can have four distinct signature resonance frequencies (80, 82, 84 and 86), which can enable to distinguish a SIW sensor from another SIW sensor only by a value of its resonance frequency. For instance, as shown in Figs. 7B and 7C, the four different patterns of sensing portions presented in Fig. 7A each has a distinct simulated and measured value for their signature resonance frequency.

[0048] In another embodiment, the substrate-integrated waveguide sensor 10 can be used in a wireless interrogation system using an antenna 26 as illustrated in the substrate-integrated waveguide sensor shown in Fig. 8. In this embodiment, a broad microwave signal is propagated to the SIW sensor having a given pattern of sensing portions in a resonance cavity of the microwave resonator. Each sensor reflects a portion of the broad microwave signal to form a reflected microwave signal. Accordingly, a VNA can be used to monitor the reflected signal in order to sense a shift of a resonance frequency dip in the reflected signal. The graph shown in Fig. 8 shows an example of a microwave signal of an antenna (black dotted line) along with the microwave signals reflected by SIW sensor having the pattern of sensing portions of the SIW sensor illustrated in Fig. 7A. For each of these four SIW sensors, a different signature resonant frequency can be observed directly on the reflected microwave signal. Indeed, the four curves shown in Fig. 8 each has a particular resonance frequency that can be associated to the corresponding pattern of sensing portions 74. In other words, substrate-integrated waveguide sensors can be remotely interrogated and remotely identifiable based only on their resonance frequencies. Therefore, if a particular

SIW sensor is known to have sensing portions being filed with a nano powder of tin dioxide and that its signature resonance frequency is 10.6 GHz and another SIW sensor is known to have sensing portions being filed with air and that its signature resonance frequency is 10.9 GHz. One can send a broad microwave signal towards the two SIW sensors and measure the reflected microwave spectrum. Doing so, one can establish a shift in the resonance frequency around 10.6 GHz and another shift in the resonance frequency around 10.9 GHz in order to determine a change in one or another of the physical properties. For instance, in this situation, the resonance at 10.6 GHz can be associated to the presence of hydrogen while the resonance at 10.9 GHz can be associated with a relative humidity level. Moreover, a substrate-integrated waveguide sensor having a plurality of resonance cavities being filed each with a different dielectric material could have a different pattern (or address) of sensing portions for each of the resonance cavity. In this embodiment, a simple measurement of a reflected microwave signal can indicate a change in the physical property associated to each of the resonance cavities. Furthermore, due to the fact that the sensor structure is functioning in the microwave frequency band, this invention facilitate the possibility of wireless operation addressing applications in harsh environments.

[0049] Fig. 9 shows a bloc diagram of an example of a detection system for substrate-integrated waveguide sensors 10 having antennas mounted thereto. In this embodiment, a broad microwave generator 88 can generate a first portion of a reference microwave signal to be propagated to a data processing computer. In a parallel manner, the broad microwave generator 88 can propagate a second portion of the reference microwave signal to a microwave mixer 48D mixing the second portion of the reference microwave signal to a local oscillator signal generated by a local oscillator 92. The mixed signal is subsequently filtered with a high pass filter 42D that is amplified using a microwave amplifier 32D. This amplified signal is passed through a microwave circulator 90 having a port connected to an antenna 26 in order to communicate the signal to the substrate-integrated waveguide sensors 10. The SIW sensor 10 reflects to the antenna 26 an output microwave signal, which is propagated to a second high pass filter 42E, then to a second microwave amplifier 32E, to be subsequently mixed with the local oscillator signal by a second mixer 48E. The resulting signal can be filtered using a low pass filter 50E to form a microwave sensing signal. The data processing computer receives the first portion of the reference microwave signal and

the microwave sensing signal in order to compare the two signals to monitor a shift of resonance frequency. Therefore, sensing a physical property of the environment. It is readily understood that other detections schemes incorporating the substrate-integrated waveguide sensors can be used.

[0050] The typical sensors for detecting hydrogen, for instance, can cost from $100 to up to $1000 each. The expansiveness of these sensors limits their use where they can be needed most. However, the microwave sensor presented herein can be made using straight-forward manufacturing processes and known techniques such as PCB. Henceforth, one can make such a sensor by first placing a substrate layer made of a first dielectric material. Then, one can incorporate a layer of conductive material on the top of the substrate and a layer of conductive material on the bottom of the substrate and then process at least one sensing portion through the three layers thus forming a fence of through-holes enclosing at least one resonance cavity of the three layers, an input channel on the layer of conductive material on the top of the substrate, the input channel protruding to one of the at least one resonance cavity of the three layers, and, on the at least one resonance cavity, a given configuration of holes through at least the layer of conductive material on the top of the substrate and the substrate layer. Subsequently, one can apply a melted layer of conductive material on an interior surface of the through-holes thereby making an electrical link between the two layers of conductive material and finally insert a dielectric material inside the holes of at least an associated resonance cavity. With such straight-forward steps, cheap sensors for sensing physical properties of an environment can be made.

[0051] As can be seen therefore, the examples described above and illustrated are intended to be exemplary only. It is readily understood that the sensor can be used in industrial applications, in residential applications, in air quality monitoring applications, in vehicular applications, in energy applications, and in emerging applications. Moreover, it is understood that a width and a length of a resonance cavity having no sensing portions can be sufficient to provide a signature resonance frequency of a SIW sensor. The number of resonance cavities having no sensing portions can be one, or more, depending on the allocated bandwidth of the SIW. Also, the number of resonance cavities to be used can influence the resonance frequency and its bandwidth. Furthermore, it is understood that the

fence of via holes enclosing the resonance cavities can be replaced by a fence of conductive material thereby reflecting the microwave input signal within the microwave resonator. In addition, it is also understood that the sensor described herein can also be used with signal having radio frequencies (RF). The scope is indicated by the appended claims.

WHAT IS CLAIMED IS:

1. A sensor for sensing at least a physical property of an environment, the sensor comprising a microwave resonator having a top conductive layer, a bottom conductive layer and a substrate layer therebetween, the substrate layer being made of a first dielectric material, a fence electrically connecting the top conductive layer to the bottom conductive layer across the substrate layer, and enclosing at least one resonance cavity, at least one microwave signal port across the fence, at least one sensing portion of a second dielectric material functionalized to the physical property of the environment, extending in the at least one resonance cavity and being exposed to the environment by at least one of the top conductive layer and the bottom conductive layer, the microwave resonator having at least one resonance frequency being dependent of the exposure of the second dielectric material with the environment to affect a microwave signal resonating therein.

2. The sensor of claim 1, wherein the at least one sensing portion includes an array of sensing portions, each provided in the form of a hole filled by the second dielectric material.

3. The sensor of claim 1, wherein the fence comprises a plurality of via holes electrically connecting the top conductive layer to the bottom conductive layer.

4. The sensor of claim 1, wherein the dielectric material associated to each of the at least one resonance cavity is sensitive to a physical property to sense.

5. The sensor of claim 2, wherein the resonance frequency associated to each of the at least one resonance cavity is dependent on a signature pattern in which the array of sensing portions is disposed.

6. The sensor of claim 1, wherein the fence partially encloses each of the at least one resonance cavity individually thereby forming resonance subcavities being connected in series along the microwave resonator.

7. The sensor of claim 1, wherein the at least one microwave signal port is used as a microwave output port.

8. The sensor of claim 1, wherein the at least one microwave signal port is electrically connected to at least one of the top conductive layer and the bottom conductive layer.

9. The sensor of claim 1, wherein the at least one microwave signal port is connected to an antenna for receiving the signal in a wireless communication link.

10. The sensor of claim 9, wherein the antenna is made integral to the top conductive layer of the microwave resonator.

11. The sensor of claim 1, wherein the physical property of the environment is a presence of a gas, a relative humidity, a temperature or a dust level.

12. The sensor of claim 1, wherein the conductive layers are made of a metallic material such as copper.

13. The sensor of claim 1, wherein the second dielectric material for sensing presence of hydrogen is tin dioxide.

14. The sensor of claim 1, wherein the second dielectric material for sensing humidity is air.

15. The sensor of claim 1, where the microwave resonator has a rectangular body.

16. The sensor of claim 15, wherein the at least one microwave signal port of the microwave resonator is located in the middle of an edge of the rectangular body.

17. The sensor of claim 1 further comprising a microwave output port for at least transmitting the signal.

18. The sensor of claim 1, wherein the at least a sensing portion of each of the at least one resonance cavity are located on at least a given high intensity area, the at least a given high intensity area being indicative of a high electric field therearound.

19. A method for sensing at least a physical property of an environment, the method comprising:

providing a path having an input and an output; and a microwave resonator therebetween, the microwave resonator having a top conductive layer, a

bottom conductive layer and a substrate layer therebetween, the top conductive layer being electrically connected to the bottom conductive layer by a conductive fence across the substrate layer, the fence enclosing at least one resonance cavity, the input being connected to the at least one resonance cavity across the fence, each of the at least one resonance cavity having at least one sensing portion of a second dielectric material functionalized to the physical property of the environment, extending in the at least one resonance cavity and being exposed to the environment across at least one of the top conductive layer and the bottom conductive layer, the microwave resonator having at least one resonance frequency;

propagating an input microwave signal into the input of the path, the microwave resonator transforming the input microwave signal into an output microwave signal being characterized by the at least one resonance frequency, the at least one resonance frequency being dependent of the exposure of the second dielectric material with the environment to affect a microwave signal resonating therein;

measuring the resonance frequency in the output microwave signal from the output of the path; and

sensing the at least a physical property based on the resonance frequency.

20. The method of claim 19, wherein said providing further comprises providing a two-dimensional pattern of sensing portions in at least one resonance cavity of the microwave resonator, each of the two-dimensional pattern of sensing portions imparting a signature resonance frequency to the microwave resonator.

21. The method of claim 20 further comprising associating the signature resonance frequency to a corresponding resonance cavity.

22. The method of claim 20, wherein the resonance frequency of each of the at least one resonance cavity is recognizable based on the two-dimensional pattern of sensing portions.

23. The method of claim 19, wherein said propagating further comprises receiving the input microwave signal via an antenna connected to the input.

24. The method of claim 23, wherein said propagating further comprises transmitting the output microwave signal using an antenna connected to the output.

25. A method of making a sensor for sensing at least a physical property of an environment, the method comprising:

placing a substrate layer made of a first dielectric material;

incorporating a layer of conductive material on the top of the substrate and a layer of conductive material on the bottom of the substrate;

processing at least one sensing portion through the three layers thus forming a fence of through-holes enclosing at least one resonance cavity of the three layers;

processing an input channel on the layer of conductive material on the top of the substrate, the input channel protruding to one of the at least one resonance cavity of the three layers;

processing, on the at least one resonance cavity, a given configuration of holes through at least the layer of conductive material on the top of the substrate and the substrate layer;

applying a melted layer of conductive material on an interior surface of the through-holes thereby making an electrical link between the two layers of conductive material; and

inserting a dielectric material inside the holes of at least an associated resonance cavity.

Abstract

The sensor for sensing at least a physical property of an environment generally has a microwave resonator having a top conductive layer, a bottom conductive layer and a substrate layer therebetween, the substrate layer being made of a first dielectric material, a fence electrically connecting the top conductive layer to the bottom conductive layer across the substrate layer, and enclosing at least one resonance cavity, at least one microwave signal port across the fence, at least one sensing portion of a second dielectric material functionalized to the physical property of the environment, extending in the at least one resonance cavity and being exposed to the environment across at least one of the top conductive layer and the bottom conductive layer, the microwave resonator having at least one resonance frequency being dependent of the exposure of the second dielectric material with the environment to affect a microwave signal resonating therein.

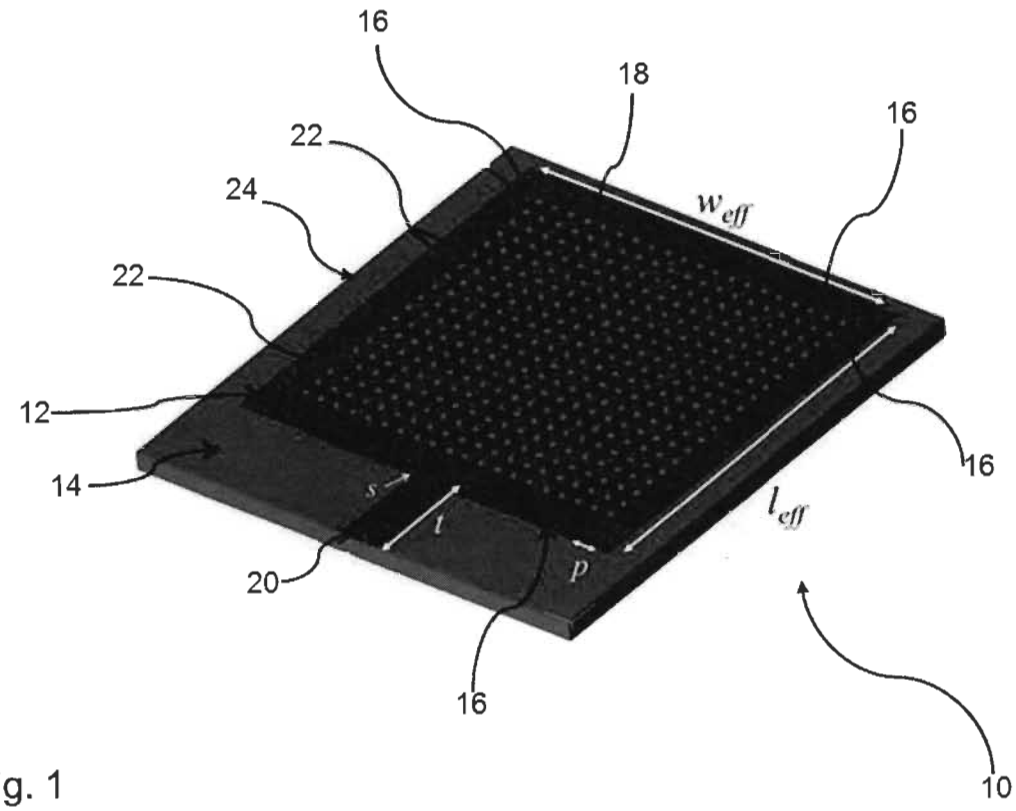

Fig. 1

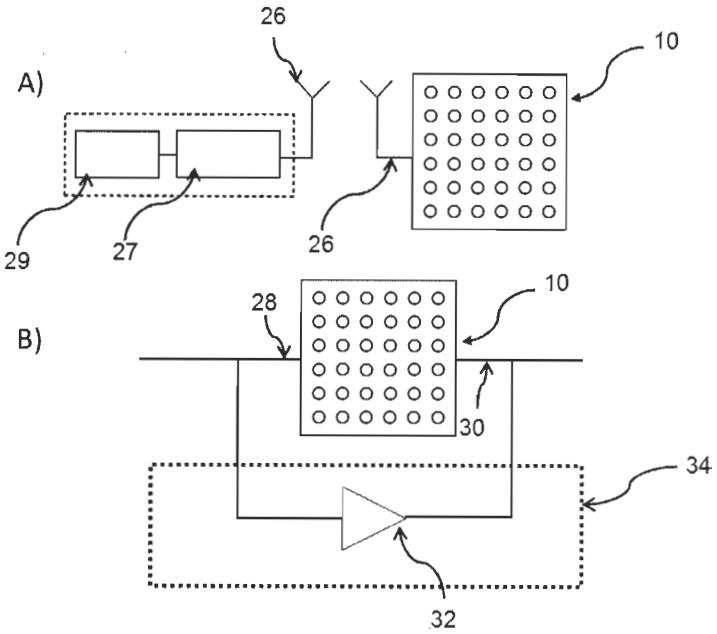

Fig. 2

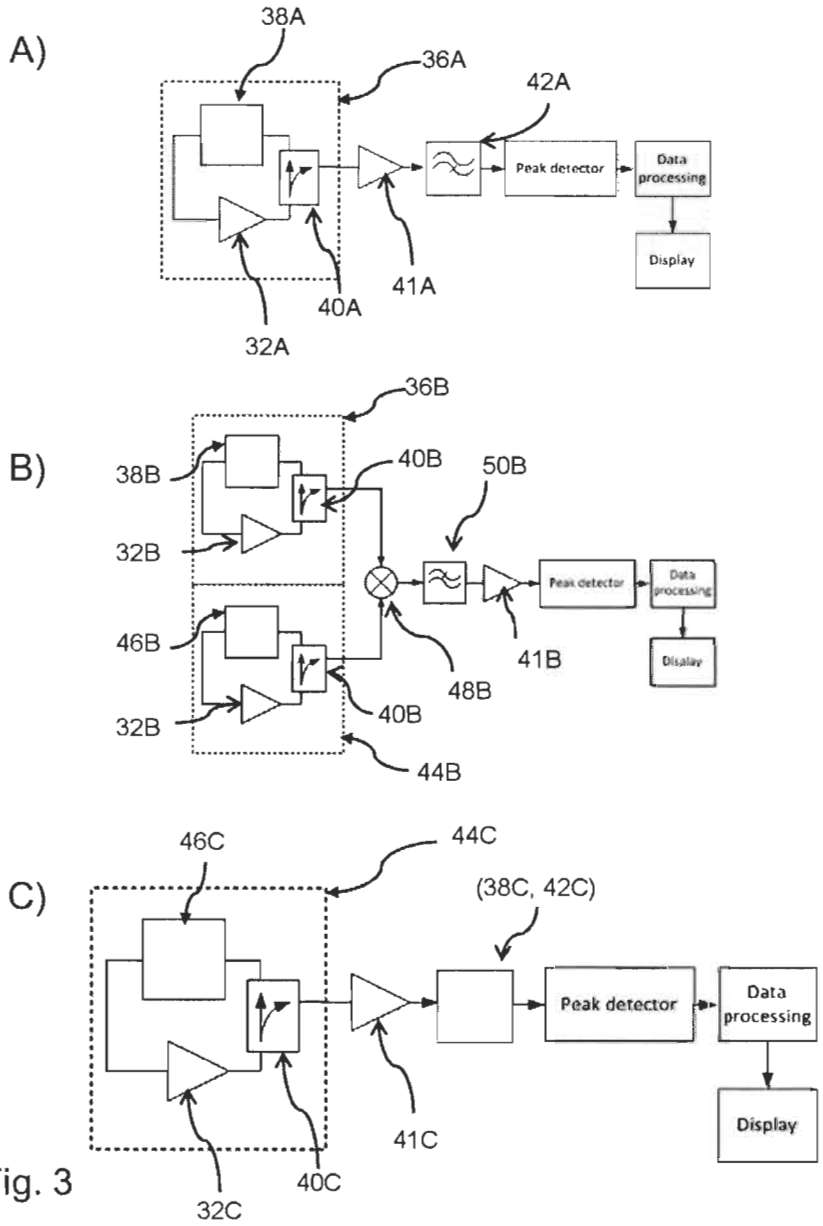
A)
38A
36A
42A
Peak detector
Data processing
Display
41A
40A
32A
B)
36B
38B
40B
50B
32B
Peak detector
Data processing
Display
46B
41B
48B
40B
32B
44B
C)
46C
44C
(38C, 42C)
Peak detector
Data processing
Display
41C
40C
32C

Fig. 3

A)

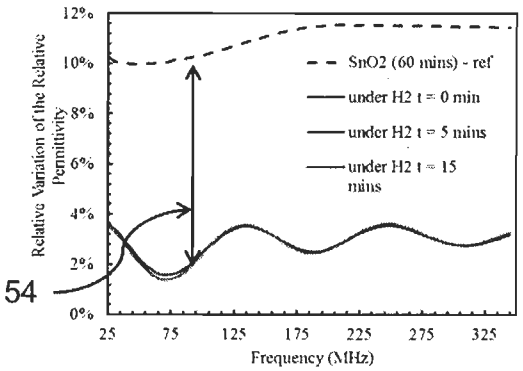

B)

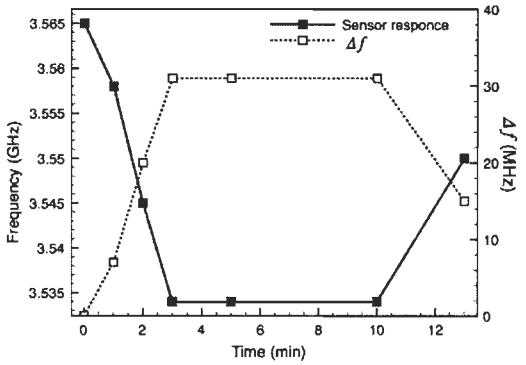

Fig. 4

A)

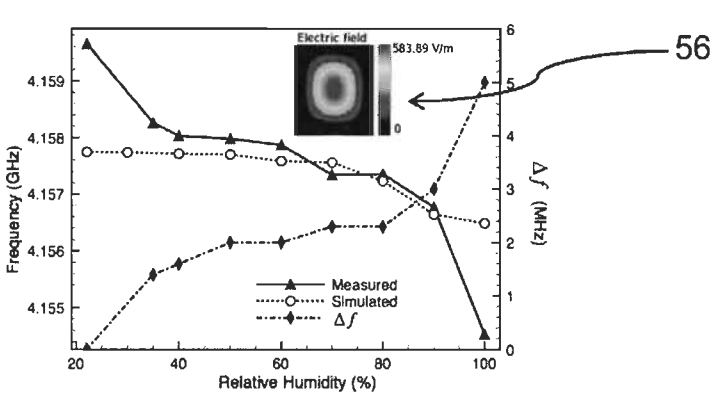

B)

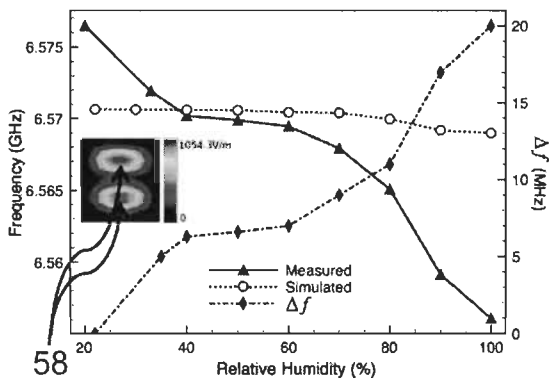

Fig. 5

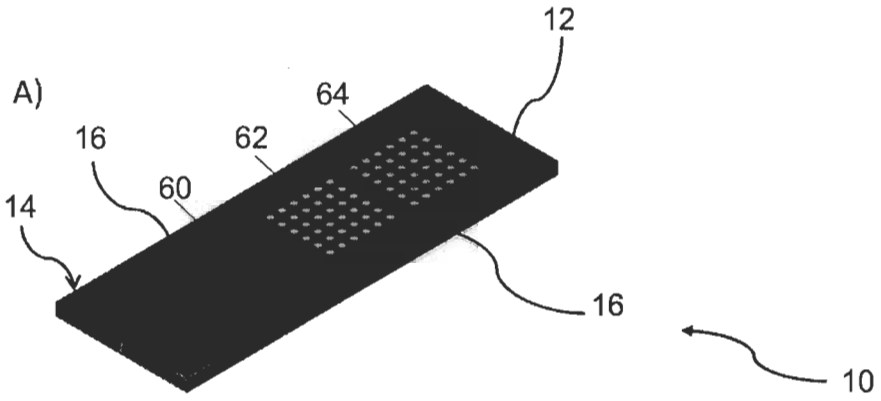
A)
12
64
16
62
60
14
16
10

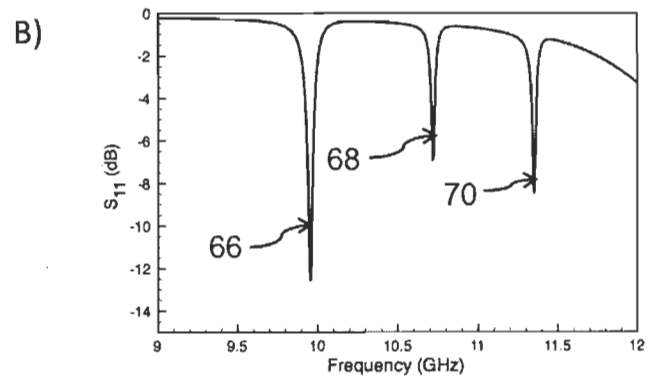
B)
0
-2
-4
-6
-8
-10
-12
-14
S_{11} (dB)
68
70
66
9
9.5
10
10.5
11
11.5
12
Frequency (GHz)

Fig. 6

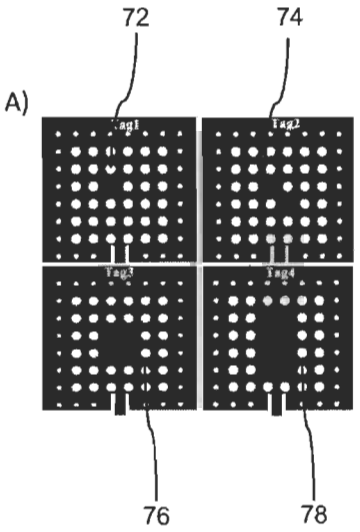
A)
72
74
Tag1
Tag2
Tag3
Tag4
76
78

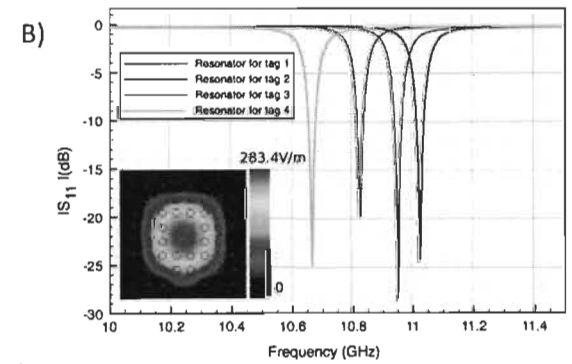
B)
Resonator for tag 1
Resonator for tag 2
Resonator for tag 3
Resonator for tag 4
283.4V/m
0
$|S_{11}|$(dB)
Frequency (GHz)

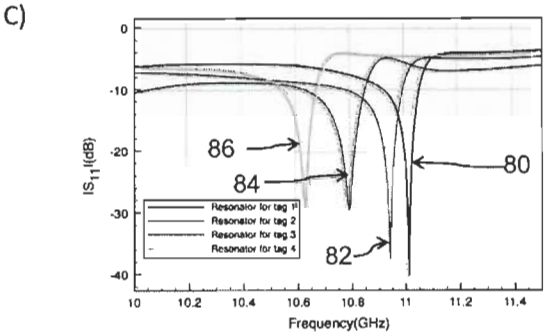
C)
86
84
80
82
Resonator for tag 1
Resonator for tag 2
Resonator for tag 3
Resonator for tag 4
$|S_{11}|$(dB)
Frequency(GHz)

Fig. 7

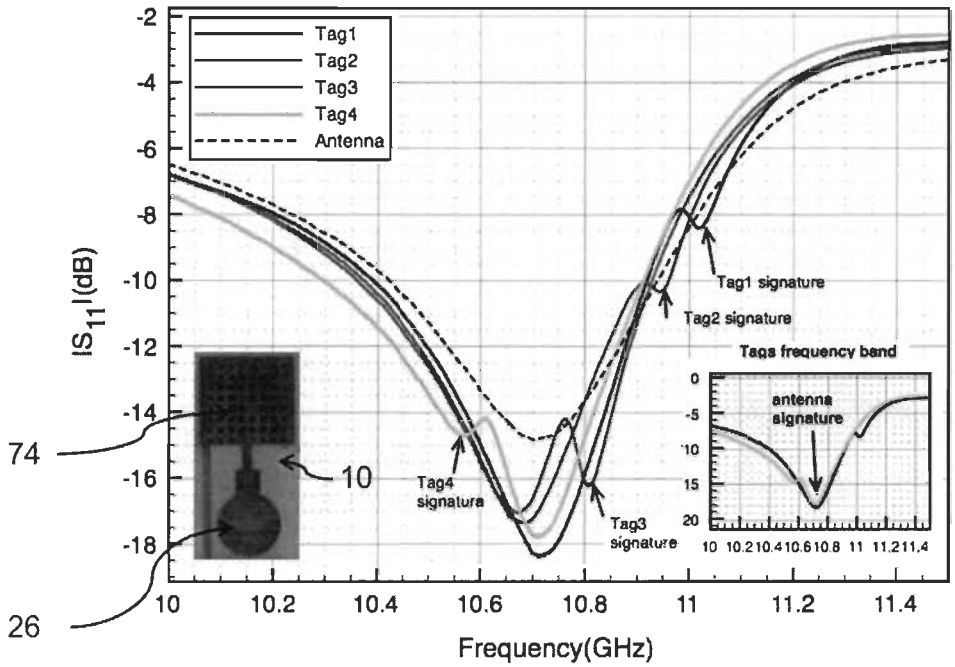
Tag1
Tag2
Tag3
Tag4
Antenna
$|S_{11}|$(dB)
Frequency(GHz)
Tag1 signature
Tag2 signature
Tags frequency band
antenna signature
Tag4 signatura
Tag3 signature
74
10
26

Fig. 8

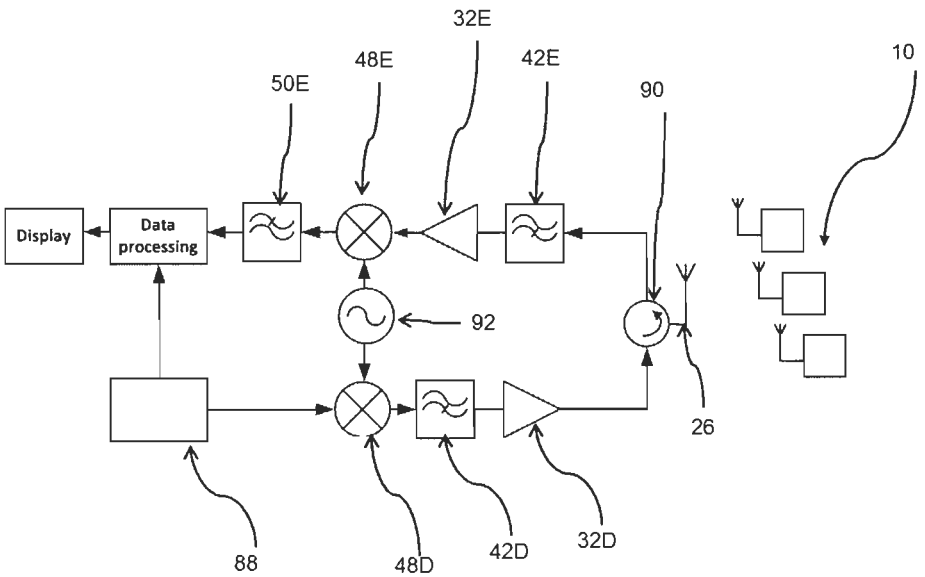
32E
48E
42E
50E
90
10
Display
Data processing
92
26
88
48D
42D
32D

Fig. 9

5.6 Contribution VI revue conference: «Modeling and Characterization of a Substrate Integrated Chip-less Tag Communication System»

Dans ce travail, un canal de communication pour les tags SIW est modélisé et caractérisé. Les tags sont basés sur un résonateur intégré au substrat où chaque résonateur est connecté à une antenne. Une adresse est attribuée à chaque variable en changeant la permittivité effective de la cavité du résonateur à substrat intégré sur la base de la présence d'un nombre variable de trous d'air à l'intérieur de la cavité.

Afin d'étudier la propagation du signal dans le canal entre les tags et l'interrogateur, la communication avec les tags est modélisée en utilisant un modèle de matrice à deux ports constitué d'un résonateur et d'une antenne. Les tags sont prototypés et testés expérimentalement; les résultats sont comparés au modèle. Des paramètres tels que la distance entre les tags et l'interrogateur, le diamètre des trous d'air et le type d'antenne de l'interrogateur ont été étudiés. De même, l'effet de tels paramètres sur la bande passante de l'interrogateur ainsi que le système de codage a été présenté. Enfin, l'architecture du circuit de l'interrogateur pour les tags SIW a été proposée.

Modeling and Characterization of a Substrate Integrated Chip-less RFID Tag Communication System

Hatem EL MATBOULY, Guy AYISSI EYEBE, Frédéric DOMINGUE

Laboratoire de Microsystèmes et Télécommunications, Département de génie électrique et génie informatique, Université du Québec à Trois-Rivières, Trois-Rivières, G9A5H7, Canada

E-mail: *hatem.el.matbouly@uqtr.ca*

Summary

In this work a communication channel for substrate-integrated RFID tags is modeled and characterized. The tags are based on a substrate integrated cavity resonators where each resonator is connected to an antenna. An address is given to each tag based on different effective permittivity of the substrate-integrated cavity resonator. In order to study the signal propagation between the tag and the reader, the communication with the tags is modeled using a two-port matrix model consisting of a resonator and antennas matrix representations. The tags are fabricated and tested experimentally; the results are compared to the model. Parameters such as the distance between the tags and the reader and the reader's antenna have been studied and their effect on the interrogation has been recorded. Finally, interrogation circuit architecture for substrate-integrated tags is proposed.

1. INTRODUCTION

Substrate integrated waveguide (SIW) structures are a promising candidate for implementing high performance and low cost communication platforms [1]. Advantages such as high quality factor, low insertion loss, and high power capability; enable the SIW microwave components to be integrated with other planar circuit as well as active circuitry components to form a compact millimeter wireless system [2-3]. In addition, SIW can be transferred to different types of substrate as paper-based substrate using ink-jet printer [4-5] as well as on flexible plastic (PET) substrates [6].

The first chip-less RFID tag structure based on a single substrate integrated cavity resonator was proposed [7]. This novel tag encodes data into the magnitude of the frequency spectrum of the interrogation signal using various configurations of the cavity resonator structure affecting the effective dielectric constant changes giving a different frequency signature [7].

In this paper a two-ports matrix representation of substrate-integrated RFID tag [7] as well as the communication between the tag and the reader is presented. The model estimates the S-parameters of the channel including the resonator and the antennas. The system is tested experimentally taken in consideration variable interrogation distances and different interrogation antennas. Based on the aforementioned characterizations of the substrate-integrated tags and their communication channel, reader circuit architecture is proposed for this new tag.

2. THEORITICAL AND EXPERIMENTAL RESULTS

The operation principle of the substrate-integrated tag is presented in Fig. 1 a. The reader sends a broadband signal to the tag through the antenna. The reflected signal will have all the transmitted frequencies except the resonance frequency of the tag which represents the signature [7].

The RFID tag communication system (Fig. 1 a) is modeled using a two-port matrix representation for each of its component as shown in Fig.1 b [6]. In this model the antenna and the resonator are modeled as a parallel *RLC* resonator with admittance $Y_{antenna}$ and $Y_{resonator}$ respectively [8]. The two admittances are coupled by an *ABCD* coupling matrix where its elements ($A_cB_cC_cD_c$) are calculated based on the measured signature of each tag. The tag is represented by a variable admittance $Y_{resonator}(C_r)$ since its resonance frequency is different for each tag. The reason the resonator admittance dependence on the capacity C_r is due to the fact that the resonance frequency is determined by different effective dielectric permittivity in the resonator. The model assumes that $R_A=R_r=50\Omega$ for the antenna and the resonator while the capacity and the inductance are given by $C=\frac{1}{(2\pi f_0)^2 L}$ and $L=\frac{R}{2\pi f_0 Q}$, where f_0 is the resonance frequency and Q is the quality factor [8]. Fig 3 (a) show four different addresses generated by changing the resonator capacitance (C_r) in the *ABCD* matrix model of the tag. The channel loss is modeled using the Free Space Path Loss (FSPL) [9]. An experimental test has been conducted

using the fabricated interrogation antenna at different distances (1-5 cm). The antenna design presented in [7] has been modified to include a matching circuit to a transmission line which results in better quality factor (Q=81). The proposed antenna has a directivity of 6.3dB and a gain of 4.2dB. Fig 2 shows the fabricated communication antenna and its radiation pattern. The measured loss is averaged out in the tag's interrogation frequency band at each distance. The experimental results are compared to the theoretical FSPL (see Fig 3 b). The difference between the theoretical and experimental losses results is due the fact that the theoretical FSPL does not include the effect of impedance miss match, polarization or loss due to propagation effect [10]. Based on these results, the S-parameters of the channel can be represented by (S_{11}=S_{22}=0, S_{21}=S_{12}=(FSPL)$^{-0.5}$). This representation does not take reflections (S_{11}=S_{22}=0) into account and assumes 50Ω channel impedance. To construct the two ports matrix representation of the channel the S-parameters are transformed into *ABCD* matrix.

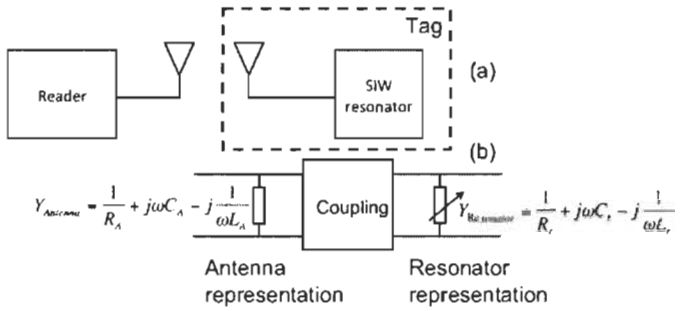

Fig 1. (a) The SIW tag communication system. (b) The two-port model of the RFID tag.

The resonators and the antennas are fabricated on RO3010 Rogers substrate (ε_r=11.2, h=1.28, tan δ = 0.0022). The choice of high dielectric substrate enables to shift the tag's interrogation band to a lower frequency while keeping a small tag dimensions.

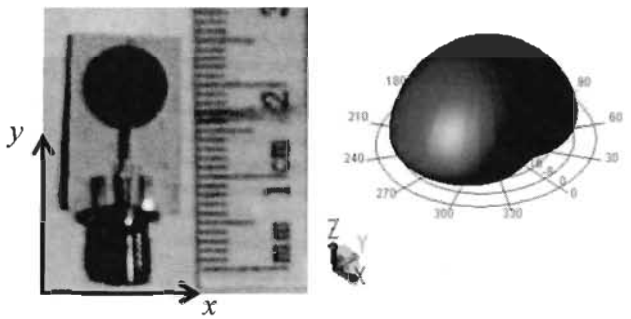

Fig 2. (a) The fabricated interrogation antenna. (b) The radiation pattern of the proposed antenna.

To verify the presented matrix model the tags are interrogated using a wide-band reference antenna. Fig 3 shows the interrogation results of the tag compared to the matrix model for the distances d of 1 and 5 cm.

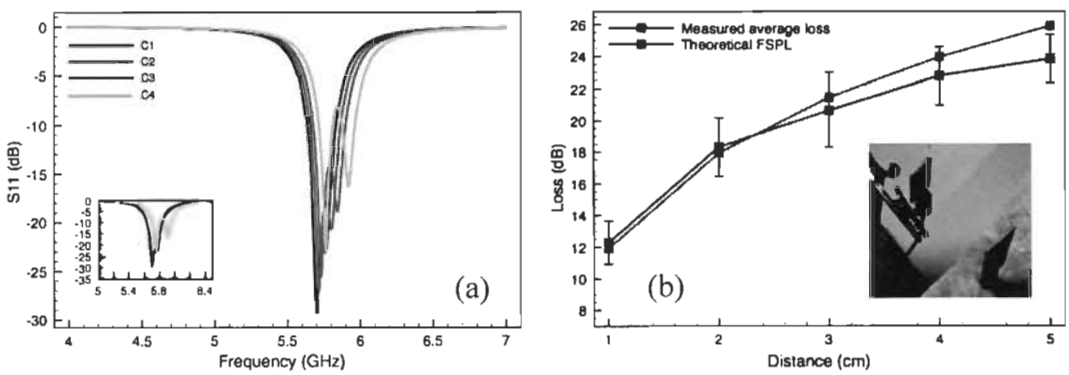

Fig 3. (a) Results of the tag matrix representation model (b) Experimental and theoretical FSPL

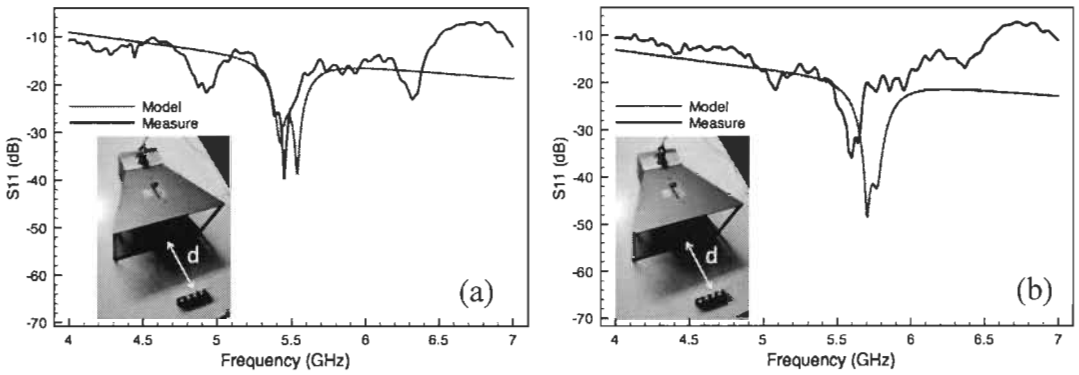

Fig. 3 Comparison between the model and the measurement for the RFID tag (a) at 1cm (b) at 5cm.

The block diagram of the reader system for the tags is shown in Fig 4. The system is composed of transmitter and receiver with data processing unit to compare the generated signal to the signal reflected from the tags. It is responsible to localize the minimums in the frequency spectrum and identify the addresses. The local oscillator frequency is chosen to be the central frequency of the tags interrogation band.

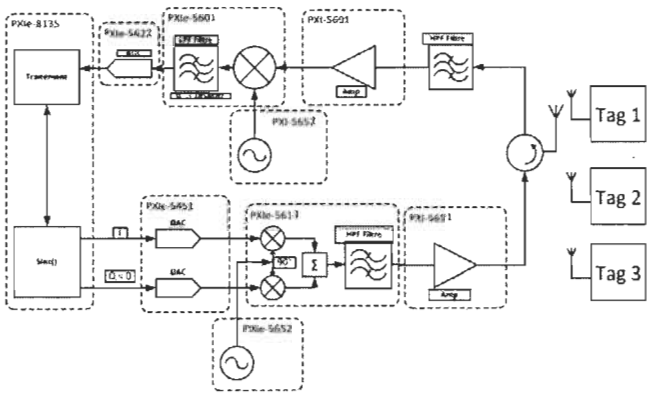

Fig. 4 The block diagram of the reader system for tag communication.

The tag's reader system was implemented using National Instrument PXI-1075 with different modules. To construct the bock diagram of the reader system, the required modules (see Fig 4) have been programmed using Labview. A user interface has been developed by which the transmitted signal power level, the central frequency and the transmitted frequency band can be adjusted. Fig 5 shows the reader system implementation and its user interface.

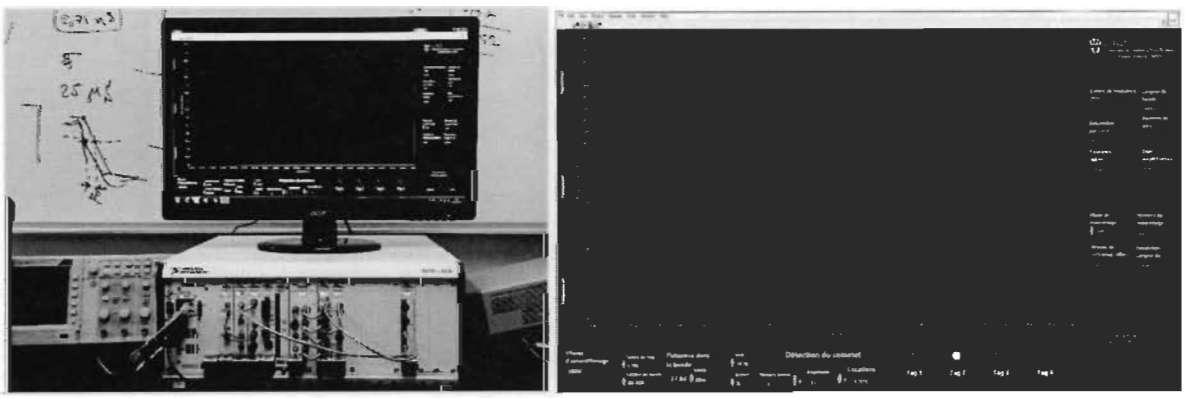

Fig. 5 The reader system implementation using National Instrument PXI-1075 with user interface.

3. CONCLUSION

In this paper a model of a SIW tag communication is presented. The tag components (antenna, resonator and coupling) are represented using *ABCD* matrixes. The channel between the reader's antenna and the tag's antenna is modeled using the Free Space Path Loss (FSPL). To verify the proposed model, tags prototypes have been fabricated and tested, the interrogated results matched the matrix model proposed. Based on the model and characterizations results of the substrate-integrated tags, reader circuit architecture is proposed and realized for this new tag. The modified antenna design has the advantage of increasing tag interrogation distance and improves the antenna's quality factor in comparison to earlier work [7]. Even though improving antenna's Q-factor improves the interrogation distance, the interrogation frequency band is reduced and hence limits the number of addresses that can be used in the band. This leads to the fewer number of tags that can be operated. In future work more antenna parameters such as the directivity and gain can be in cooperated in the channel matrix model as well as antenna orientation and/or miss match affect as other channel models [11-12] can be studied.

4. REFERENCES

[1] K. Wu, D. Deslandes, and Y. Cassivi, "The substrate integrated circuits—A new concept for high-frequency electronics and optoelectronics", *Proc. TELSIKS*, pp. 3–5, October. 2009.

[2] M. Bozzi A. Georgiadis K. Wu, "Review of substrate-integrated waveguide circuits and antennas", IET Microw. Antennas Propag, Vol. 5, Iss. 8, pp. 909–920, 2011.

[3] Djerafi, T.Wu, K, "Substrate integrated waveguide (SIW) techniques: The state-of-the-art developments and future trends", Journal of the University of Electronic Science and Technology of China, Vol. 42, Iss. 2, pp.171-192, 2013.

[4] R. Moro, S. Kim, M. Bozzi, and M. Tentzeris, "Novel inkjet-printed substrate integrated waveguide (SIW) structures on low-cost materials for wearable applications" Proc. 42th Eur. Microw. Conf., Amsterdam, The Netherlands, October. 28–Nov. 2 2012.

[5] Moro, R.Kim, S. Bozzi, M.Tentzeris, M, "Inkjet-printed paper-based substrate-integrated waveguide (SIW) components and antennas", International Journal of Microwave and Wireless Technologies, Vol. 5, Iss. 3, pp.197-204 , 2013.

[6] R. Moro, A. Collado, S. Via, A. Georgiadis, and M. Bozzi, "Plastic-based substrate integrated waveguide (SIW) components and antennas" Proc 42th Eur. Microw. Conf., Amsterdam, The Netherlands, Oct. 28–Nov. 2 2012.

[7] Hatem El Matbouly, Naimi Boubekeur, and Frédéric Domingue, "A Novel Chipless Identification Tag Based on a Substrate Integrated Cavity Resonator", IEEE Microw. Wireless Compon Lett, Vol. 23, No. 1, January 2013.

[8] David M. Pozar, *Microwave Engineering*, John Wiley, 1998.

[9] Andreas F. Molisch, Kannan Balakrishnan, Dajana Cassioli, Chia-Chin Chong, Shahriar Emami, Andrew Fort,Johan Karedal, Juergen Kunisch, Hans Schantz, Ulrich Schuster, Kai Siwiak, *IEEE 802.15.4a channel model - final report*, Technology, work and learning. Australian Government Printing Service, 2004.

[10] Balanis, *Antenna Theory Analysis and Design*, 3ed Edition, John Wiley, 2005.

[11] Y. Duroc, "On the system modeling of antennas", Progress In Electromagnetics Research B, Vol. 21, pp. 69-85, 2010.

[12] Teguh Prakoso, Razali Ngah, and Tharek Abdul Rahman, "Representation of Antenna in Two-Port Network S-Parameter", Proc, IEEE International RF and Microwave Conference, pp. 293-297, 2008.

Chapitre 6 - Conclusion

Aujourd'hui, il existe un besoin croissant en réseau de capteurs autonomes et aux communications sans fil. Le travail présenté dans cette thèse porte sur cette dynamique en se focalisant sur la conception, la réalisation et la caractérisation d'un nouveau capteur de gaz passif et à transduction RF. L'approche du capteur environnemental à base d'un résonateur micro-ondes intégré au substrat (SIW) est particulièrement innovante, par rapport aux technologies existantes.

Dans cette thèse, nous avons présenté notre travail en faisant tout d'abord une revue de littérature sur les technologies actuelles de détections de gaz. Ensuite, nous avons proposé une solution originale d'une transduction RF pour la détection de gaz qui est basée sur la fonctionnalisation d'un résonateur SIW avec un matériau diélectrique sensible aux gaz. Le changement de la permittivité du diélectrique dans la région fonctionnalisée en présence de gaz se traduit par un décalage de la fréquence de résonance.

Ensuite, pour concevoir le capteur à base de résonateur SIW et déterminer la région fonctionnalisée, un modèle analytique basé sur la méthode de perturbation de cavité résonante a été développé en s'appuyant sur le principe d'introduction de région fonctionnalisée dans un résonateur. Ce modèle permet d'étudier l'effet de la taille de la région fonctionnalisée sur la sensibilité. Le mode d'excitation choisi est TE101 où le champ électrique est maximum au centre du résonateur.

Avant toute conception, le modèle numérique du dispositif a été simulé sur un outil de simulation électromagnétique 3D (EMPro) afin de déterminer la fréquence de résonance simulée de ce dernier qui dépend particulièrement des dimensions de la structure. Dans un premier temps, l'effet de l'introduction des tous d'air a été simulé pour trouver l'influence d'une région fonctionnalisée sur la fréquence de résonance du capteur et le couplage avec une ligne micro-ruban. Dans le cas où le résonateur SIW présenté est un tag RFID l'effet de la variation de nombre de trous d'air sur l'adressage a été simulé pour déterminer la bande de fréquence d'opération des tags.

Une fois le dispositif réalisé, des tests ont été réalisés avec deux types de gaz (l'humidité et l'hydrogène). Tout d'abord, deux résonateurs SIW ont été réalisés avec deux différentes régions fonctionnalisées (tailles différentes) pour la détection de l'humidité. Cela permet d'étudier l'impact de la taille de la région fonctionnalisée sur la sensibilité du dispositif ainsi que confronter les résultats au modèle théorique fondé sur la méthode des perturbations. Dans le cas de la détection de l'humidité, l'introduction d'un matériau sensible n'était pas nécessaire parce que l'air pouvant être considéré comme un diélectrique, la variation de l'humidité ambiante affecte la valeur de la constante diélectrique de ce dernier. Des évaluations visant à déterminer la performance du capteur SIW en fonction des variations de la température, du taux d'humidité et de la pression ont été effectuées. Aussi leurs effets sur la sensibilité ont été étudiés.

Pour la détection de l'hydrogène une étude bibliographique a été faite sur les matériaux potentiels qui pourraient être intégrés dans la structure du résonateur SIW en s'intéressant à leurs propriétés diélectriques et les techniques utilisées pour leur élaboration. Le dioxyde d'étain SnO2 a été choisi pour fonctionnaliser les trous dans le résonateur et le rendre sensible à la présence de l'hydrogène. Le SnO2 étant un oxyde métallique, il apporte des pertes diélectriques qui diminuent le facteur de qualité du résonateur SIW ainsi que ses performances. Ainsi, la région sensible a été choisie la plus petite possible pour le capteur de l'hydrogène afin de réduire l'effet des pertes et ainsi permettre une validation préalable de la détection de l'hydrogène. La technique de broyage a été utilisée pour amener les grains de la poudre SnO2 à des tailles nano métriques, ce qui a augmenté leur adsorption de l'hydrogène et ainsi la sensibilité de détection. L'effet de dopage de SnO2 avec la nano poudre de Palladium qui est un bon catalyseur à l'adsorption de l'hydrogène a été étudié, les résultats montrent qu'en mélangeant la nano poudre de SnO2 avec 1% (pourcentage massique) de nano poudre de Palladium le décalage fréquentiel dû à la présence de l'hydrogène augmente d'un facteur dix. Par contre, l'introduction de nano poudre métallique augmente davantage les pertes, ce qui affecte le facteur de qualité du résonateur SIW.

Un travail futur sur la même structure de capteur proposée dans cette thèse peut être poursuivi dans le but d'amener le capteur proposé à la maturité industrielle. D'autres idées et tests peuvent être explorées et effectués pour améliorer la performance du capteur; par exemple, l'incorporation d'autres matériaux sensibles afin de fonctionnaliser le résonateur SIW pour la détection d'autres gaz ou même d'autres grandeurs physiques ou chimiques.

Les tests effectués dans cette thèse montrent que le résonateur SIW fonctionnalisé peut fonctionner comme un capteur. Comme mentionné dans les sections (5.1 et 5.2) le résonateur a été testé pour la détection de l'humidité et de l'hydrogène. La technique de broyage pour la nano poudre (SnO2) peut être exploitée pour d'autres types d'oxydes métalliques capables de détecter des gaz autres que l'hydrogène. La production de matériaux composites pour les applications variées (à base de nano poudre ou polymère) sera investiguée. Différentes concentrations de nano poudre sensible dans le polymère seront testées pour la sensibilité aux gaz selon la poudre choisie pour la détection.

D'autres types de structure à technologie SIW peuvent être étudiés afin de réaliser des capteurs. Par exemple, on peut étudier des guides SIW diélectriques ou SIW coplanaire grâce à l'exploitation de leur principe de fonctionnement électronique. L'évaluation des métriques standardisées de performance de capteur peut être ajoutée aux tests actuels (SIW). Des protocoles de tests analogues à ceux qui sont recommandés dans les normes internationales [6, 39-41] comme, la réponse des capteurs t(90) et des mesures de temps de recouvrement t(10) pourraient être effectuées en utilisant une méthode d'essai dédiée aux tests et validations de performances [42]. Au cours de ces tests, l'impact du débit de gaz sur la performance du capteur serait également évalué. Finalement, une optimisation portant sur les matériaux sensibles et la géométrie de la structure SIW choisie peut être envisagée. Les résultats d'évaluation approfondie effectuée (voir contribution IV) ainsi que des tests sur d'autres matériaux sensibles peuvent être utilisés pour optimiser la performance du capteur SIW proposé. Étant donné que chaque matériau sensible a une constante diélectrique et des pertes qui lui sont propres, la structure de résonateur SIW et la région

fonctionnalisée doivent être conçues pour minimiser l'effet négatif de l'insertion d'un diélectrique sur la qualité du résonateur (substrat hôte de propriétés diélectriques différentes). Les points suivants résument les travaux futurs proposés pour améliorer la performance, par exemple le seuil de détection du capteur SIW proposé :

- Optimisation de la poudre dans une matrice de polymère. Les paramètres comme la concentration de la poudre intégrée dans la matrice de polymère seront optimisés pour assurer la détection du dispositif tout en facilitant les techniques d'intégration industrielles…

- Optimisation de la structure géométrique du capteur SIW. L'adaptation électromagnétique du dispositif SIW pour minimiser la dégradation du facteur de qualité due au remplacement d'une région de substrat par un autre diélectrique, sera investiguée. D'autres types de substrats comme les LTCC peuvent être utilisés pour atteindre des fréquences d'opération plus élevées ou avoir une meilleure intégration avec les diélectriques sensibles.

- Optimisation du processus d'intégration applicable à l'échelle industrielle. Ce processus a pour but de faciliter la fonctionnalisation de résonateur SIW. Étant donné que la forme actuelle du matériau diélectrique sensible (poudre) ne permet pas d'avoir un dispositif robuste, la matrice de nano poudre dans un polymère perméable aux gaz sera utilisée dans un processus de fabrication avec une méthode de sérigraphie. Cela nécessite la fabrication d'un masque additionnel pour l'intégrer dans le processus de sérigraphie.

Références

[1] "MNT Gas Sensor Road Map," MNT Gas Sensor Forum, descember 2006.

[2] S. C. Xiao Liu , Hong Liu , Sha Hu , Daqiang Zhang and Huansheng Ning, "A Survey on Gas Sensing Technology," Sensors, vol. 12, pp. 9635-9665, 2012.

[3] N. Yamazoe, "Toward innovations of gas sensor technology," Sensors and Actuators B vol. 108, pp. 2-14, 2005.

[4] "Looking to the future of gas sensing – a new galaxy of possibilities, Industrial fire journal," Industrial fire journal, 2010.

[5] T. Shigemori, "Gas Sensors Status and Future Trends for Safety Applications," The 14th International Meeting on Chemical Sensors IMCS, 2012.

[6] L. Boon-Brett, J. Bousek, G. Black, P. Moretto, P. Castello, T. Hubert, et al., "Identifying performance gaps in hydrogen safety sensor technology for automotive and stationary applications," International Journal of Hydrogen Energy, vol. 35, pp. 373-384, Jan 2010.

[7] H. Hallil, F. Chebila, P. Menini, P. Pons, and H. Aubert, "Feasibility of Wireless Gas Detection with an FMCW RADAR Interrogation of Passive RF Gas Sensor," 2010 Ieee Sensors, pp. 759-762, 2010.

[8] H. Aubert, F. Chebila, M. Jatlaoui, T. Thai, H. Hallil, A. Traille, et al., "Wireless Sensing and Identification of Passive Electromagnetic Sensors based on Millimetre-wave FMCW RADAR," 2012 Ieee International Conference on Rfid-Technologies and Applications (Rfid-Ta), 2012.

[9] H. Aubert, F. Chebila, M. Jatlaoui, T. Thai, H. Hallil, A. Traille, et al., "Wireless sensing and identification based on radar cross section variability measurement of passive electromagnetic sensors," Annals of Telecommunications-Annales Des Telecommunications, vol. 68, pp. 425-435, Aug 2013.

[10] M. Bozzi, "Substrate integrated waveguide (SIW): An emerging technology for wireless systems," Kaohsiung, 2012, pp. 788-790.

[11] K. Wu, "Substrate integrated circuits (SICs) for low-cost high-density integration of millimeter-wave wireless systems," Orlando, FL, 2008, pp. 683-686.

[12] G. Romo and A. C. Scogna, "Substrate integrated waveguide (SIW) filter: Design methodology and performance study," Guadalajara, 2009, pp. 23-26.

[13] M. Bozzi, L. Perregrini, K. Wu, and P. Arcioni, "Current and future research trends in substrate integrated waveguide technology," Radioengineering, vol. 18, pp. 201-209, // 2009.

[14] A. Suntives and R. Abhari, "Transition structures for 3-D integration of substrate integrated waveguide interconnects," IEEE Microwave and Wireless Components Letters, vol. 17, pp. 697-699, // 2007.

[15] K. Wu, "Multi-dimensional and multi-functional substrate integrated waveguide antennas and arrays for GHz and THz applications: An emerging disruptive technology," Gothenburg, 2013, pp. 11-15.

[16] T. Djerafi and K. Wu, "Substrate integrated waveguide (SIW) techniques: The state-of-the-art developments and future trends," Dianzi Keji Daxue Xuebao/Journal of the University of Electronic Science and Technology of China, vol. 42, pp. 171-192, // 2013.

[17] J. Chen, W. Hong, Z. Hao, P. Yan, X. Zhu, J. Zhou, et al., "Development of a single board microwave sub-system based on substrate integrated waveguide (SIW) technology," Montreal, QC, 2012.

[18] J. Rossignol, G. Barochi, B. de Fonseca, J. Brunet, M. Bouvet, A. Pauly, et al., "Development of gas sensors by microwave transduction with phthalocyanine film," 26th European Conference on Solid-State Transducers, Eurosensor 2012, vol. 47, pp. 1191-1194, 2012.

[19] G. Barochi, J. Rossignol, and M. Bouvet, "Development of microwave gas sensors," Sensors and Actuators B-Chemical, vol. 157, pp. 374-379, Oct 20 2011.

[20] J. D. Barrera and G. H. Huff, "Analysis of a variable SIW resonator enabled by dielectric material perturbations and applications," IEEE Transactions on Microwave Theory and Techniques, vol. 61, pp. 225-233, // 2013.

[21] H. Lobato-Morales, A. Corona-Chavez, D. V. B. Murthy, J. Martinez-Brito, and L. G. Guerrero-Ojeda, "Experimental dielectric sensing of materials using Epsilon-Near-Zero tunnel in SIW technology," Anaheim, CA, 2010, pp. 1644-1647.

[22] H. Hallil, P. Menini, and H. Aubert, "New microwave gas detector using dielectric resonator based on a Whispering-Gallery-Mode," 2009 European Microwave Conference, Vols 1-3, pp. 1097-1100, 2009.

[23] H. Hallil, P. Menini, and H. Aubert, "Novel Microwave Gas Sensor using Dielectric Resonator With SnO(2) Sensitive Layer," Proceedings of the Eurosensors Xxiii Conference, vol. 1, pp. 935-938, 2009.

[24] H. Hallil, P. Menini, and H. Aubert, "Novel millimeter-wave gas sensor using dielectric resonator with sensitive layer on TiO2," 2009 Ieee Sensors, Vols 1-3, pp. 226-228, 2009.

[25] L. Dai, K. Cheng, Z. Wang, and J. Cheng, "The application of SIW in LTCC," Shanghai, 2007.

[26] Q. PinJie, Z. Yong, and Y. Bo, "A novel millimeter-wave substrate integrated waveguide (SIW) filter buried in LTCC," Hong Kong, 2008.

[27] Q. F. Wei, Z. F. Li, L. S. Wu, and L. Li, "A novel multilayered cross-coupled substrate-integrated waveguide (SIW) circular cavity filter in LTCC," Microwave and Optical Technology Letters, vol. 51, pp. 1686-1689, // 2009.

[28] L. S. Wu, J. Mao, W. Y. Yin, and X. L. Zhou, "Broadband filter based on stub-loaded ridge substrate integrated waveguide (SIW) in low temperature cofired ceramic (LTCC)," Hanzhou, 2011.

[29] A. C. Bunea, M. Lahti, D. Neculoiu, A. Stefanescu, and T. Vaha-Heikkila, "Investigation of substrate integrated waveguide in LTCC technology for mm-wave applications," Melbourne, VIC, 2011, pp. 395-398.

[30] F. D. L. Peters, T. A. Denidni, and S. O. Tatu, "Two layer LTCC substrate integrated to rectangular waveguide transition and its application for millimeter-wave LTCC characterization," Microwave and Optical Technology Letters, vol. 54, pp. 2675-2679, // 2012.

[31] S. Kim, M. Riccardo, M. Bozzi, S. Nikolaou, and M. M. Tentzeris, "Inkjet-printed wearable microwave components for biomedical applications," Gothenburg, 2013, pp. 1926-1929.

[32] R. Moro, S. Kim, M. Bozzi, and M. Tentzeris, "Inkjet-printed paper-based substrate-integrated waveguide (SIW) components and antennas," International Journal of Microwave and Wireless Technologies, vol. 5, pp. 197-204, // 2013.

[33] R. Moro, M. Bozzi, A. Collado, A. Georgiadis, and S. Via, "Plastic-based Substrate Integrated Waveguide (SIW) components and antennas," Amsterdam, 2012, pp. 1007-1010.

[34] R. Moro, M. Bozzi, S. Kim, and M. Tentzeris, "Novel inkjet-printed substrate integrated waveguide (SIW) structures on low-cost materials for wearable applications," Amsterdam, 2012, pp. 72-75.

[35] R. Torres-Torres, G. Romo, B. Horine, A. Sánchez, and H. Heck, "Full characterization of substrate integrated waveguides from S-parameter measurements," Scottsdale, AZ, 2006, pp. 277-280.

[36] D. Deslandes, M. Bozzi, P. Arcioni, and K. Wu, "Substrate integrated slab waveguide (SISW) for wideband microwave applications," Philadelphia, PA, 2003, pp. 1103-1106.

[37] J. Fraden, "The handbook of modern sensors: Physics, Design and Application," pp. 393-399, 2003.

[38] H. El Matbouly, N. Boubekeur, and F. Domingue, "A novel chipless identification tag based on a substrate integrated cavity resonator," IEEE Microwave and Wireless Components Letters, vol. 23, pp. 52-54, // 2013.

[39] L. Boon-Brett, J. Bousek, P. Castello, O. Salyk, F. Harskamp, L. Aldea, et al., "Reliability of commercially available hydrogen sensors for detection of hydrogen at critical concentrations: Part I - Testing facility and methodologies," International Journal of Hydrogen Energy, vol. 33, pp. 7648-7657, Dec 2008.

[40] L. Boon-Brett, J. Bousek, and P. Moretto, "Reliability of commercially available hydrogen sensors for detection of hydrogen at critical concentrations: Part II - selected sensor test results," International Journal of Hydrogen Energy, vol. 34, pp. 562-571, Jan 2009.

[41] W. J. Buttner, R. Burgess, C. Rivkin, M. B. Post, L. Boon-Brett, G. Black, et al., "Inter-laboratory assessment of hydrogen safety sensors performance under anaerobic conditions," International Journal of Hydrogen Energy, vol. 37, pp. 17540-17548, Nov 2012.

[42] L. Boon-Brett, G. Black, P. Moretto, and J. Bousek, "A comparison of test methods for the measurement of hydrogen sensor response and recovery times," International Journal of Hydrogen Energy, vol. 35, pp. 7652-7663, Jul 2010.